Chapter 1

Sound fields

1.1 Introduction

This opening chapter looks at aspects of sound fields that are particularly relevant to sound insulation; the reader will also find that it has general applications to room acoustics.

The audible frequency range for human hearing is typically 20 to 20 000 Hz, but we generally consider the building acoustics frequency range to be defined by one-third-octave-bands from 50 to 5000 Hz. Airborne sound insulation tends to be lowest in the low-frequency range and highest in the high-frequency range. Hence significant transmission of airborne sound above 5000 Hz is not usually an issue. However, low-frequency airborne sound insulation is of particular importance because domestic audio equipment is often capable of generating high levels below 100 Hz. In addition, there are issues with low-frequency impact sound insulation from footsteps and other impacts on floors. Low frequencies are also relevant to façade sound insulation because road traffic is often the dominant external noise source in the urban environment. Despite the importance of sound insulation in the low-frequency range it is harder to achieve the desired measurement repeatability and reproducibility. In addition, the statistical assumptions used in some measurements and prediction models are no longer valid. There are some situations such as in recording studios or industrial buildings where it is necessary to consider frequencies below 50 Hz and/or above 5000 Hz. In most cases it should be clear from the text what will need to be considered at frequencies outside the building acoustics frequency range.

1.2 Rooms

Sound fields in rooms are of primary importance in the study of sound insulation. This section starts with the basic principles needed to discuss the more detailed aspects of sound fields that are relevant to measurement and prediction. In the laboratory there is some degree of control over the sound field in rooms due to the validation procedures that are used to commission them. Hence for at least part of the building acoustics frequency range, the sound field in laboratories can often be considered as a diffuse sound field; a very useful idealized model. Outside of the laboratory there are a wide variety of rooms with different sound fields. These can usually be interpreted with reference to two idealized models: the modal sound field and the diffuse sound field.

1.2.1 Sound in air

Sound in air can be described as compressional in character due to the compressions and rarefactions that the air undergoes during wave propagation (see Fig. 1.1). Air particles move to and fro in the direction of propagation, hence sound waves are referred to as longitudinal waves. The compressions and rarefactions cause temporal variation of the air density compared to the

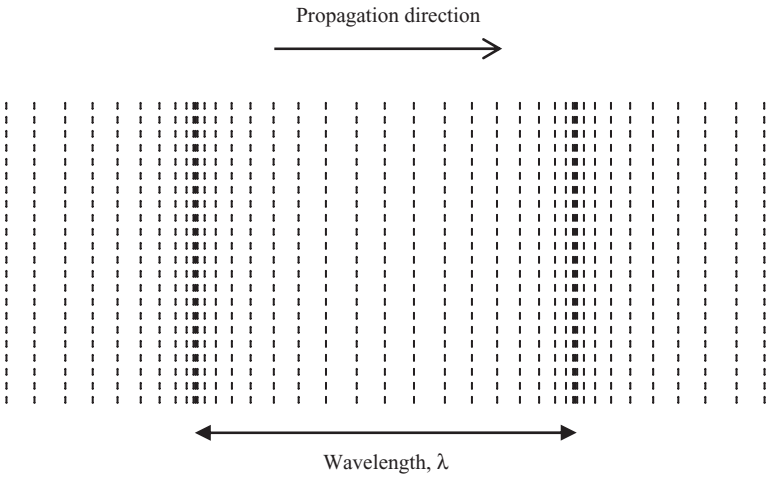

Figure 1.1

Longitudinal wave – compression and rarefaction of air particles.

density at equilibrium. The result is temporal variation of the air pressure compared to the static air pressure. Sound pressure is therefore defined by the difference between the instantaneous pressure and the static pressure.

The phase velocity for sound in air, c_0 (or as it is more commonly referred to, the speed of sound) is dependent upon the temperature, T, in °C and for most practical purposes can be calculated using

$$c_0 = 331 + 0.6T \tag{1.1}$$

for temperatures between 15°C and 30°C and at atmospheric pressure.

The density of air at equilibrium, ρ_0, is also temperature dependent and can be calculated from

$$\rho_0 = \frac{353.2}{273 + T} \tag{1.2}$$

For calculations in buildings it is often assumed that the temperature is 20°C, for which the speed of sound is 343 m/s and the density of air is 1.21 kg/m^3. This will be assumed throughout the book.

The fundamental relationship between the phase velocity, the frequency, f, and the wavelength, λ, is

$$c_0 = f\lambda \tag{1.3}$$

The wavelength is the distance from peak to peak (or trough to trough) of a sinusoidal wave; this equals the distance between identical points of compression (see Fig. 1.1) or rarefaction. For the building acoustics frequency range, the wavelength in air at 20°C is shown in Fig. 1.2. If we consider these wavelengths relative to typical room dimensions, it is clear that we are dealing with a very wide range. For this reason it is useful to describe various aspects of sound fields by referring to low-, mid-, and high-frequency ranges; corresponding to 50 to 200 Hz, 250 to 1000 Hz, and 1250 to 5000 Hz respectively.

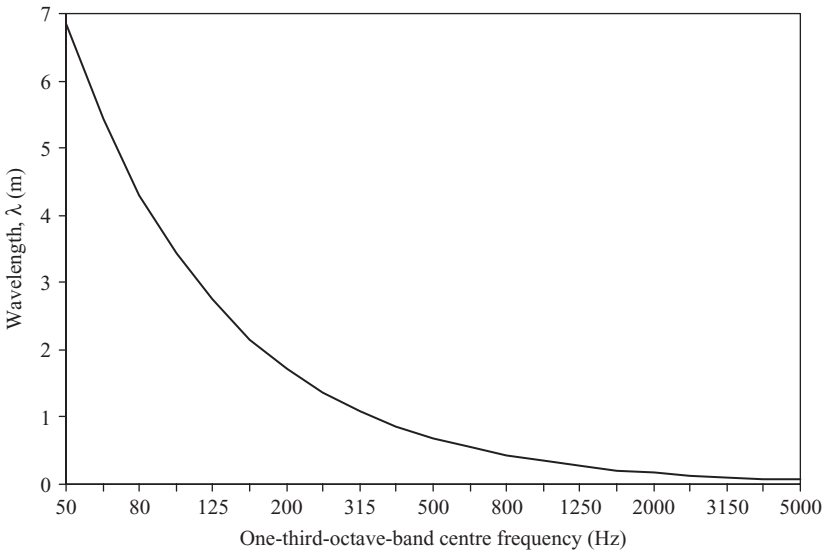

Figure 1.2

Wavelength of sound in air at 20°C.

As we need to describe the spatial variation of sound pressure as well as the temporal variation, it is necessary to use the wavenumber, k, which is defined as

$$k = \frac{\omega}{c_0} = \frac{2\pi}{\lambda} \tag{1.4}$$

where the angular frequency, ω, is

$$\omega = 2\pi f \tag{1.5}$$

and the period, T, of the wave is

$$T = \frac{2\pi}{\omega} = \frac{1}{f} \tag{1.6}$$

The wavenumber is useful for discussing aspects relating to spatial variation in both sound and vibration fields in terms of kd, where d is the distance between two points.

Two types of wave need to be considered both inside and outside of buildings: plane waves and spherical waves. Before reviewing these waves we will briefly review the use of complex notation that simplifies many derivations for sound and structure-borne sound waves.

1.2.1.1 Complex notation

For both sound and vibration, it is useful to look at wave motion or signals at single frequencies; these are defined using harmonic sine and cosine functions, e.g. $p(x,t) = \cos(\omega t - kx)$. It is usually more convenient to describe these simple harmonic waves using complex exponential notation, where

$$\exp(iX) = \cos X + i \sin X \tag{1.7}$$

Equations using complex notation are often easier to manipulate than sines and cosines, and can be written in a more compact form. A brief review of complex notation is given here as this is covered in general acoustic textbooks (e.g. see Fahy, 2001).

The most commonly used complex exponentials are those that describe the temporal and spatial variation of harmonic waves. For the convention used in this book, these are

$$\exp(i\omega t) = \cos(\omega t) + i\sin(\omega t) \tag{1.8}$$

and

$$\exp(-kx) = \cos(kx) - i\sin(kx)$$

Complex notation also simplifies differentiation and integration. For example, differentiation or integration with respect to time becomes equivalent to multiplication or division by $i\omega$ respectively.

Whilst it can be convenient to work with complex notation, the final result that corresponds to a physical quantity (sound pressure, velocity, etc.) must be real, rather than imaginary. In general, it is the real part of the solution that represents the physical quantity.

The time-average of harmonic waves is frequently needed for practical purposes and is denoted by $\langle\ \rangle_t$. The following time-averages often occur in derivations,

$$\lim_{T\to\infty}\frac{1}{T}\int_0^T \cos^2(\omega t)\mathrm{d}t = \lim_{T\to\infty}\frac{1}{T}\int_0^T \sin^2(\omega t)\mathrm{d}t = 0.5 \tag{1.9}$$

and

$$\lim_{T\to\infty}\frac{1}{T}\int_0^T \sin(\omega t)\mathrm{d}t = \lim_{T\to\infty}\frac{1}{T}\int_0^T \cos(\omega t)\mathrm{d}t = \lim_{T\to\infty}\frac{1}{T}\int_0^T \sin(\omega t)\cos(\omega t)\mathrm{d}t = 0 \tag{1.10}$$

where T is the averaging time.

The time-average of the product of two waves, $p_1(t)$ and $p_2(t)$, that are written in complex exponential notation can be calculated using

$$\langle p_1 p_2\rangle_t = \frac{1}{2}\mathrm{Re}\{p_1 p_2^*\} \tag{1.11}$$

where * denotes the complex conjugate.

1.2.1.2 Plane waves

To gain an insight into the sound field in rooms we often assume that it is comprised of plane waves; so called, because in any plane that is perpendicular to the propagation direction, the sound pressure and the particle velocity are uniform with constant phase. These planes are referred to as wavefronts. In practice, plane waves can be realized (approximately) in a long hollow cylinder which has rigid walls. A sound source is placed at one end of the cylinder that generates sound with a wavelength that is larger than the diameter of the cylinder. This results in a plane wave propagating in the direction away from the source. The longitudinal wave shown in Fig. 1.1 can also be seen as representing a plane wave in this cylinder. This one-dimensional scenario may seem somewhat removed from real sound fields in typical rooms. However, the plane wave model can often be used to provide a perfectly adequate description of the complex sound fields that are encountered in practice.

Using a Cartesian coordinate system, the wave equation that governs the propagation of sound through three-dimensional space is

$$\frac{\partial^2 p}{\partial x^2} + \frac{\partial^2 p}{\partial y^2} + \frac{\partial^2 p}{\partial z^2} - \frac{1}{c_0^2}\frac{\partial^2 p}{\partial t^2} = 0 \tag{1.12}$$

where p is the sound pressure.

For a plane wave that is propagating in the positive x, y, and z-direction across this space, the sound pressure is described by an equation of the form

$$p(x, y, z, t) = \hat{p} \exp(-ik_x x) \exp(-ik_y y) \exp(-ik_z z) \exp(i\omega t) \tag{1.13}$$

where $\hat{p}$ is an arbitrary constant for the peak value, and k_x, k_y, and k_z are constants relating to the wavenumber.

As we are using harmonic time dependence, $\exp(i\omega t)$, the wave equation can now be written in terms of the wavenumber as

$$\frac{\partial^2 p}{\partial x^2} + \frac{\partial^2 p}{\partial y^2} + \frac{\partial^2 p}{\partial z^2} + k^2 p = 0 \tag{1.14}$$

The relationship between the wavenumber and the constants, k_x, k_y, and k_z is found by inserting Eq. 1.13 into the wave equation, which gives

$$k^2 = k_x^2 + k_y^2 + k_z^2 \tag{1.15}$$

We will need to make use of this relationship to describe the sound field in rooms. However, the wave equation only governs sound propagation across three-dimensional space. It does not describe the sound field in a room because it does not take account of the waves impinging upon the room surfaces. In other words, this equation does not take account of boundary conditions. Hence the constants, k_x, k_y, and k_z can only be determined once we have defined these boundary conditions.

The particle motion gives rise to sound pressure; hence we can relate the sound particle velocities, u_x, u_y, and u_z (in the x, y, and z directions respectively) to the sound pressure by using the following equations of motion,

$$\frac{\partial p}{\partial x} = -\rho_0 \frac{\partial u_x}{\partial t} \qquad \frac{\partial p}{\partial y} = -\rho_0 \frac{\partial u_y}{\partial t} \qquad \frac{\partial p}{\partial z} = -\rho_0 \frac{\partial u_z}{\partial t} \tag{1.16}$$

and therefore the particle velocities are

$$u_x = \frac{k_x}{\omega \rho_0} p \qquad u_y = \frac{k_y}{\omega \rho_0} p \qquad u_z = \frac{k_z}{\omega \rho_0} p \tag{1.17}$$

The ratio of the complex sound pressure to the complex sound particle velocity at a single point is the specific acoustic impedance, Z_a. For a plane wave propagating in a single direction (we will choose the x-direction, so that $k = k_x$ and $u = u_x$), this impedance is referred to as the characteristic impedance of air, Z_0, and is defined as

$$Z_0 = \frac{p}{u} = \rho_0 c_0 = \sqrt{\frac{\rho_0}{\kappa}} \tag{1.18}$$

where κ is the gas compressibility (adiabatic).

The particle velocity is related to the sound pressure by a real constant that is independent of frequency. Therefore, the sound pressure and the particle velocity always have the same phase on the plane that lies perpendicular to the direction of propagation.

In order to predict or measure sound transmission we will need to quantify the sound intensity, I; the energy that flows through unit surface area in unit time. The sound intensity is the time-averaged value of the product of sound pressure and particle velocity,

$$I = \langle pu \rangle_t = \frac{\langle p^2 \rangle_t}{\rho_0 c_0} \tag{1.19}$$

where $\langle p^2 \rangle_t$ is the temporal average mean-square sound pressure given by

$$\langle p^2 \rangle_t = \frac{1}{T} \int_0^T p^2 \, dt \tag{1.20}$$

and T is the averaging time. Note that $\sqrt{\langle p^2 \rangle_t}$ is described as the root-mean-square (rms) sound pressure.

1.2.1.3 Spherical waves

For spherical waves the sound pressure and the particle velocity over a spherical surface are uniform with constant phase; these surfaces are referred to as wavefronts (see Fig. 1.3). For a sound source such as a loudspeaker used in sound insulation measurements, a useful idealized model is to treat the loudspeaker as a point source that generates spherical waves. A point source is one for which the physical dimensions are much smaller than the wavelength of the sound, and the sound radiation is omnidirectional.

We now need to make use of a spherical coordinate system defined by a distance, r, from the origin at $r = 0$. For spherically symmetrical waves, the wave equation that governs the propagation of sound through three-dimensional space is

$$\frac{\partial^2 p}{\partial r^2} + \frac{2}{r} \frac{\partial p}{\partial r} - \frac{1}{c_0^2} \frac{\partial^2 p}{\partial t^2} = 0 \tag{1.21}$$

For a spherical wave propagating across this space, the sound pressure can be described by an equation of the form

$$p(r, t) = \frac{\hat{p}}{r} \exp(-ikr) \exp(i\omega t) \tag{1.22}$$

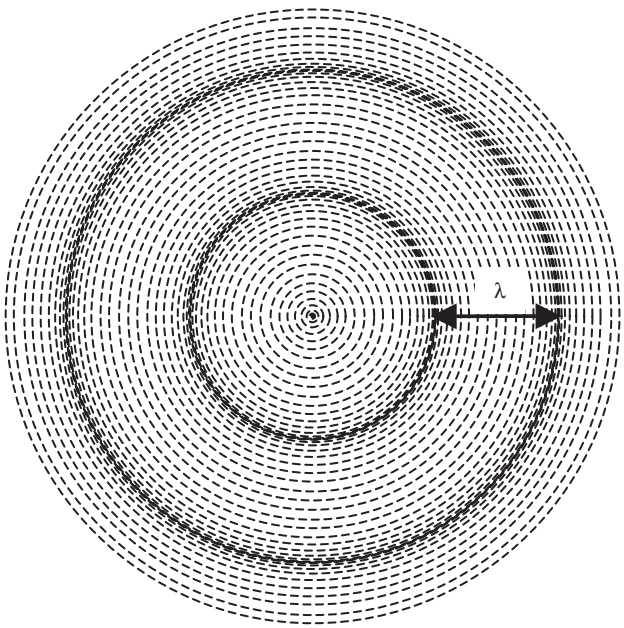

Figure 1.3

Spherical wavefronts produced by a point source.

where $\hat{p}$ is an arbitrary constant for the peak value and r is the distance from a spherical wavefront to the origin.

Substitution of Eq. 1.22 into the following equation of motion,

$$\frac{\partial p}{\partial r} = -\rho_0 \frac{\partial u_r}{\partial t} \tag{1.23}$$

gives the radial particle velocity, u_r, as

$$u_r = \frac{p}{\rho_0 c_0}\left(1 - \frac{i}{kr}\right) = \frac{p}{\rho_0 c_0}\left(1 - i\frac{c_0}{2\pi fr}\right) \tag{1.24}$$

This gives the acoustic impedance, Z_a, as

$$Z_a = \frac{p}{u_r} = \frac{\rho_0 c_0}{\left(1 - \frac{i}{kr}\right)} = \frac{\rho_0 c_0 k^2 r^2}{1 + k^2 r^2} + i\frac{\rho_0 c_0 kr}{1 + k^2 r^2} \tag{1.25}$$

In contrast to plane waves, the particle velocity is related to the sound pressure by a complex variable that is dependent on both the wavenumber and distance. So although the phase of the sound pressure and the phase of the particle velocity are constant over a spherical surface at a specific frequency, they do not have the same phase over this surface.

The time-averaged sound intensity for a harmonic spherical wave is

$$I = \frac{1}{2\rho_0 c_0}\left(\frac{\hat{p}}{r}\right)^2 = \frac{\langle p^2 \rangle_t}{\rho_0 c_0} \tag{1.26}$$

For spherical waves, the intensity is seen to be proportional to $1/r^2$; this feature is often referred to as spherical divergence. The sound power associated with a point source producing spherical waves can now be calculated from the intensity using

$$W = 4\pi r^2 I = \frac{2\pi \hat{p}^2}{\rho_0 c_0} \tag{1.27}$$

Rather than use $\hat{p}$ in Eqs 1.26 and 1.27, a point source can be described using a peak volume velocity, $\hat{Q}$, given by

$$\hat{Q} = \frac{4\pi \hat{p}}{\omega \rho_0} \tag{1.28}$$

When $kr \gg 1$ (i.e. at high frequencies and/or large distances) the imaginary part of Z_a is small, therefore the particle velocity has almost the same phase as the sound pressure and Z_a tends towards Z_0. The time-averaged sound intensity for the harmonic spherical wave then tends towards the value for a plane wave (Eq. 1.19). These links between plane waves and spherical waves indicate why we are able to use the simpler plane wave model in many of the derivations involved in sound insulation. Any errors incurred through the assumption of plane waves are often negligible or insignificant compared to those that are accumulated from other assumptions.

1.2.1.4 Acoustic surface impedance and admittance

As rooms are formed by the surfaces at the boundaries of the space we need to know the acoustic impedance of a room surface as seen by an impinging sound wave. The normal

acoustic surface impedance, $Z_{a,n}$, is defined as the ratio of the complex sound pressure at a surface, to the component of the complex sound particle velocity that is normal to this surface,

$$Z_{a,n} = \frac{p}{u_n} \tag{1.29}$$

Although we are mainly interested in plates (representing walls or floors) that form the room boundaries, the above definition applies to any surface, including sheets of porous materials such as mineral wool or foam.

The specific acoustic impedance, $Z_{a,s}$, is defined using the characteristic impedance of air,

$$Z_{a,s} = \frac{Z_{a,n}}{\rho_0 c_0} \tag{1.30}$$

In some calculations it is more appropriate or convenient to use the specific acoustic admittance, $\beta_{a,s}$, rather than the specific acoustic impedance, where

$$\beta_{a,s} = \frac{1}{Z_{a,s}} \tag{1.31}$$

When calculating sound fields in rooms it is often convenient to assume that the room surfaces are rigid. This is reasonable for many hard surfaces in buildings. At a rigid surface, the particle velocity that is normal to this surface is zero; hence $Z_{a,n}$ and $Z_{a,s}$ become infinitely large and $\beta_{a,s}$ is taken to be zero.

1.2.1.5 Decibels and reference quantities

The human ear can detect a wide range of sound intensities. The decibel scale (dB) is commonly used to deal with the wide range in pressure, intensity, power, and energy that are encountered in acoustics. Levels in decibels are defined using the preferred SI reference quantities for acoustics in Table 1.1 (ISO 1683); these reference quantities are used for all figures in the book.

Table 1.1. Sound – definitions of levels in decibels

Level	Definition	Reference quantity
Sound pressure	$L_p = 20 \lg \left(\frac{p}{p_0}\right)$	$p_0 = 20 \times 10^{-6}$ Pa
	where p is the rms pressure	NB only for sound in air
Energy	$L_E = 10 \lg \left(\frac{E}{E_0}\right)$	$E_0 = 10^{-12}$ J
Intensity	$L_I = 10 \lg \left(\frac{I}{I_0}\right)$	$I_0 = 10^{-12}$ W/m^2
Sound power	$L_W = 10 \lg \left(\frac{W}{W_0}\right)$	$W_0 = 10^{-12}$ W
Loss factors (Internal, Coupling, Total)	$L_{ILF}/L_{CLF}/L_{TLF} = 10 \lg \left(\frac{\eta}{\eta_0}\right)$	$\eta_0 = 10^{-12}$

1.2.1.6 A-weighting

A-weighting is used to combine sound pressure levels from a range of frequencies into a single value. This is the A-weighted sound pressure level, $L_{p,A}$. It is intended to represent the frequency response of human hearing and is often used to try and make a simple link between the objective and subjective assessment of a sound. A-weighting accounts for the fact that with the same sound pressure level, we do not perceive all frequencies as being equally loud. In terms of the building acoustics frequency range it weights the low-frequency range as being less significant than the mid- and high-frequency range. This does not mean that the low-frequency range is unimportant for sound insulation, usually quite the opposite is true; the A-weighted level depends upon the spectrum of the sound pressure level. Although it is common to measure and predict sound insulation in frequency bands, assessment of the sound pressure level in the receiving room is often made in terms of the A-weighted level.

For N frequency bands, the sound pressure level $L_p(n)$ in each frequency band, n, is combined to give an A-weighted level using

$$L_{p,A} = 10 \lg \left(\sum_{n=1}^{N} 10^{(L_p(n)+A(n))/10} \right) \tag{1.32}$$

where the A-weighting values, A(n), are shown in Fig. 1.4 for one-third-octave-bands (IEC 61672-1).

For regulatory and practical purposes, the airborne sound insulation is often described using a single-number quantity that corresponds to the difference between the A-weighted level in the source room and the A-weighted level in the receiving room for a specific sound spectrum (e.g. pink noise) in the source room (ISO 717 Part 1). Use of this A-weighted level difference

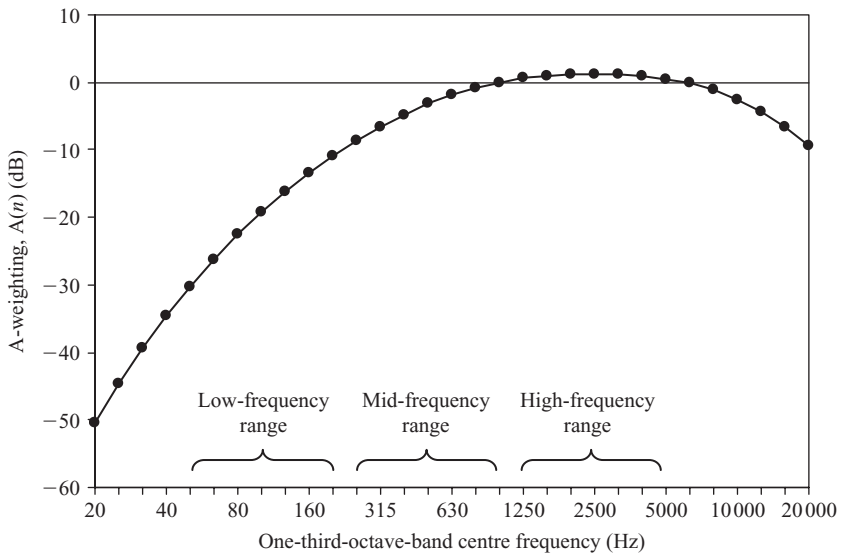

Figure 1.4

A-weighting values over the range of human hearing indicating the low-, mid-, and high-frequency ranges for the building acoustics frequency range.

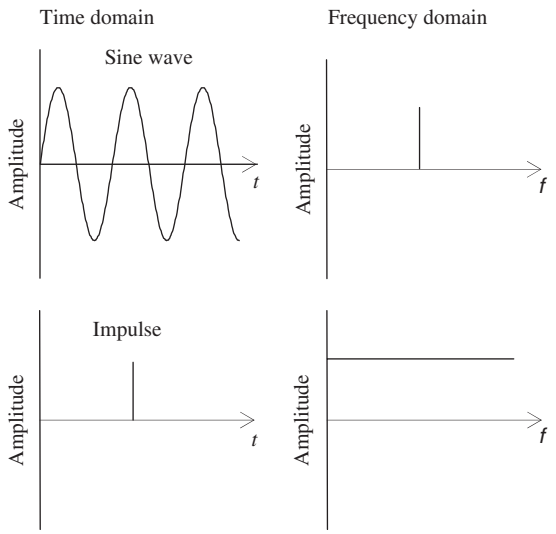

Figure 1.5

Illustration of a sine wave and an impulse in the time and frequency domains.

simplifies calculation of the A-weighted level in the receiving room. It can also be used to make a link to subjective annoyance (Vian *et al.*, 1983).

1.2.2 Impulse response

In sound insulation as well as in room acoustics, we need to make use of the impulse response in both measurement and theory. The frequency spectrum of an impulse is flat. It therefore contains energy at all frequencies, whereas a sine wave only has energy at a single frequency (see Fig. 1.5).

The general principle for an impulse response applies to any acoustic system, whether it is sound pressure in a room or a cavity, or the vibration of a plate or a beam. It is based upon the response of an acoustic system to a Dirac delta function, $\delta(t)$, sometimes called a unit impulse. The delta function is infinite at $t = 0$ and infinitely narrow, such that $\delta(t) = 0$ when $t \neq 0$, and it has the property

$$\int_{-\infty}^{\infty} \delta(t)\mathrm{d}t = 1 \tag{1.33}$$

Excitation of a linear time-invariant (LTI) acoustic system with a delta function results in the impulse response of the system, $h(t)$. The delta function is important because any kind of signal can be described by using a train of impulses that have been appropriately scaled and shifted in time. Hence, the impulse response completely describes the response of an LTI system to any input signal, $x(t)$. The output signal, $y(t)$, can then be found from the convolution integral

$$y(t) = \int_{-\infty}^{\infty} h(u)x(t-u)\mathrm{d}u = \int_{-\infty}^{\infty} h(t-u)x(u)\mathrm{d}u \tag{1.34}$$

where u is a dummy time variable.

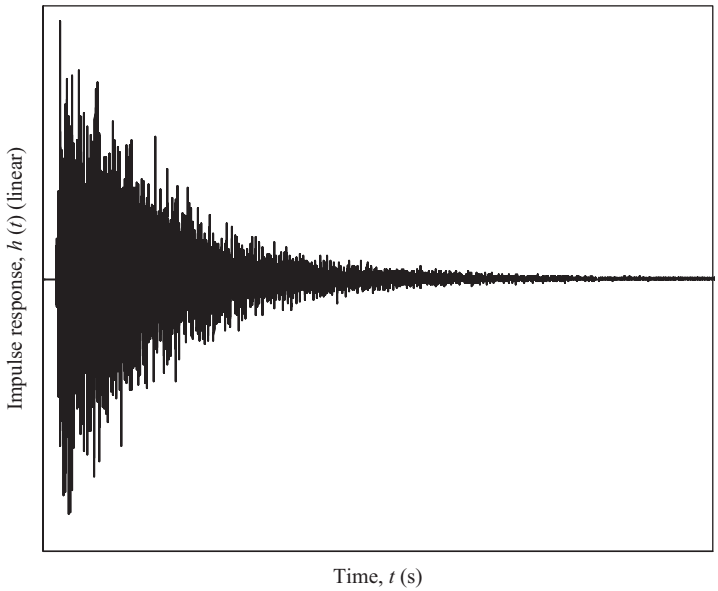

Figure 1.6

Example of a measured impulse response in a room.

For brevity, convolution is often written as $y(t) = x(t) * h(t)$. The convolution integral uses the dummy time variable to multiply the time-reversed input signal by the impulse response (or the time-reversed impulse response by the input signal), and integrate over all possible values of t to give the output signal.

An example of a measured impulse response for sound pressure in a room is shown in Fig. 1.6.

1.2.3 Diffuse field

One of the assumptions commonly made in the measurement and prediction of sound insulation is that the sound field in rooms can be considered as being diffuse. A diffuse sound field can be considered as one in which the sound energy density is uniform throughout the space (i.e. the sound field can be considered to be homogeneous), and, if we choose any point in the space, sound waves arriving at this point will have random phase, and there will be equal probability of a sound wave arriving from any direction. The diffuse field is a concept; in practice there must be dissipation of energy, so there cannot be equal energy flow in all directions, there must be net energy flow from a sound source towards part(s) of the space where sound is absorbed.

In diffuse fields it is common to refer to diffuse reflections; this means that the relationship between the angle of incidence and the angle of reflection is random. This is in contrast to specular reflection, where the angle of incidence equals the angle of reflection. Walls and floors commonly found in buildings (excluding spaces specially designed for music performance such as studios or concert halls) tend to be flat and smooth, from which one might assume that specular reflections were the norm, and that diffuse reflections were the exception. However, walls commonly have objects placed near them that partially obscure the wall from the incident sound wave, such as tables, chairs, bookcases, filing cabinets, and cupboards. These can

cause the incident wave to be scattered in non-specular directions. Non-specular reflection also occurs when the acoustic impedance varies across the surface; for example a wall where the majority of the surface area is concrete but with areas of glazing, wooden doors, or recessed cupboards, each of which have different impedances. Hence there will usually be a degree of non-specular reflection, such that some of the incident energy is specularly reflected and some is diffusely reflected.

The diffuse field is a very useful concept. It allows many simplifications to be made in the measurement and prediction of sound insulation, as well as in other room acoustics calculations. These make use of the mean free path that will be defined in the following section. In the laboratory we can create close approximations to a diffuse field in the central zone of a room. However, the sound field does not always bare a close resemblance to a diffuse field over the entire building acoustics frequency range. In the low-frequency range this is primarily due to the fact that sound waves arriving at any point come from a limited number of directions. In the mid- and high-frequency ranges, waves arriving at any point tend to come from many different directions. In the central zone of typical rooms it is often reasonable to assume that there is a diffuse field in the mid- and high-frequency ranges. However it is not always appropriate to assume that there is a diffuse field when: (a) there are regular room shapes without diffusing elements, (b) there are non-diffuse reflections from room surfaces, and (c) there is non-uniform distribution of absorption over the room surfaces. For the above reasons, we need to note the limitations in applying diffuse field theory to the real world.

1.2.3.1 Mean free path

The mean free path, d_{mfp}, is the average distance travelled by a sound wave between two successive diffuse reflections from the room surfaces. From the basic relationship, $c_0 = d_{\mathrm{mfp}}/t$, we can calculate the time, t, taken to travel this distance. Upon each reflection, a fraction of the sound energy is absorbed; hence the mean free path allows us to calculate the build-up or decay of sound energy in a room over time. It will therefore be needed later on when we derive the reverberation time in diffuse fields as well as when calculating the power incident upon walls or floors that face into a room with a diffuse sound field. The following derivation is taken from Kosten (1960) and starts by deriving the mean free path in a two-dimensional space before extending it to three dimensions. This two-dimensional space has an area, S, and a perimeter length, U. An arbitrary two-dimensional space can be defined by a closed curve as shown in Fig. 1.7; note that although the space is defined by curved lines we assume that all reflections are diffuse. The dashed lines within this curve represent free paths in a single direction, where each free path has a length, l.

Projective geometry is now used to transform points along the perimeter of the space onto a projection plane. Each of the free paths lies perpendicular to a projection plane that defines the apparent length of the surface, L_{a}. When the space is uniformly filled with free paths, the surface area of the space can be written in terms of the free path lengths using

$$S = \int_{L_{\mathrm{a}}} l \mathrm{d}L_{\mathrm{a}} = L_{\mathrm{a}} \bar{l} \tag{1.35}$$

where $\bar{l}$ is the mean free path in one direction.

The number of paths in a single direction is proportional to the apparent length, so using a fixed number of paths per unit of the projection length, and accounting for all N possible directions

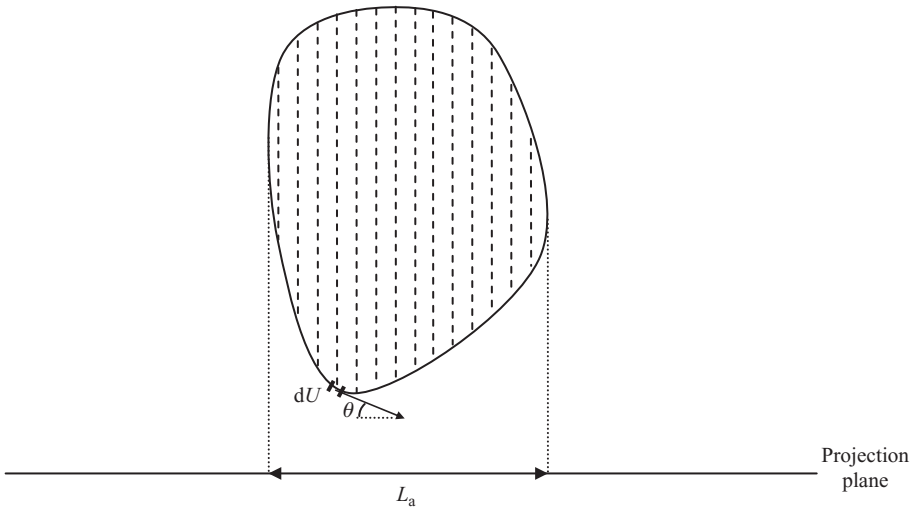

Figure 1.7

Two-dimensional space showing some of the free paths (dashed lines) in a single direction that lie perpendicular to the projection plane. The apparent length, L_a, is calculated by using a line integral to sum the projection of the small perimeter length, dU, onto the projection plane.

gives the mean free path, d_{mfp}, as

$$d_{mfp} = \frac{\lim\limits_{N\to\infty} \sum_{n=1}^{N} L_{a,n}\bar{l}_n}{\lim\limits_{N\to\infty} \sum_{n=1}^{N} L_{a,n}} \tag{1.36}$$

From Eq. 1.35, $S = L_{a,n}\bar{l}_n$ in each direction, n, so Eq. 1.36 can be rewritten as

$$d_{mfp} = \frac{S}{\overline{L_a}} \tag{1.37}$$

where $\overline{L_a}$ is the average apparent length.

The next step is to determine this average apparent length, but first we just look at a single direction and calculate the apparent length. This is done by using a line integral for the closed curve. At each point along the closed curve, the vector in the direction of the curve makes an angle, θ, with the projection plane (see Fig. 1.7). The projection of each small perimeter length, dU, onto the projection plane is a positive value, $|\cos\theta|$dU. By integrating around the entire closed curve, the integral is effectively counting each free path twice, so a multiplier of one-half is needed. The apparent length is therefore given by

$$L_a = \frac{1}{2}\oint_C |\cos\theta| \mathrm{d}U \tag{1.38}$$

To find the average apparent length, it is necessary to average over all possible directions. This results in an average cosine term,

$$\overline{|\cos\theta|} = \frac{1}{\pi}\int_0^{\pi} |\cos\theta| \mathrm{d}\theta = \frac{2}{\pi} \tag{1.39}$$

which gives the average apparent length as

$$\bar{L}_a = \frac{1}{2}\oint_C \overline{|\cos\theta|}\mathrm{d}U = \frac{U}{\pi} \tag{1.40}$$

The mean free path for a two-dimensional space can now be found from Eqs 1.37 and 1.40, giving

$$d_{mfp} = \frac{\pi S}{U} \tag{1.41}$$

We now consider a three-dimensional space with a volume, V, and a total surface area, S_T. Moving to three dimensions means that the projection plane becomes a surface (rather than a line) onto which small parts of the surface area, $\mathrm{d}S_T$, are projected (rather than small perimeter lengths). Hence we need to define an apparent surface area, S_a.

The volume of the space can be written in terms of the free path lengths using

$$V = \int_{S_a} l\mathrm{d}S_a = S_a\bar{l} \tag{1.42}$$

where $\bar{l}$ is the mean free path in one direction.

The number of paths in a single direction is proportional to the apparent surface area, so using a fixed number of paths per unit area of the projection surface, and accounting for all N possible directions gives the mean free path, d_{mfp}, as

$$d_{mfp} = \frac{\lim\limits_{N\to\infty}\sum_{n=1}^{N} S_{a,n}\bar{l}_n}{\lim\limits_{N\to\infty}\sum_{n=1}^{N} S_{a,n}} \tag{1.43}$$

From Eq. 1.42, $V = S_{a,n}\bar{l}_n$ in each direction, n, so Eq. 1.43 can be rewritten as

$$d_{mfp} = \frac{V}{\overline{S}_a} \tag{1.44}$$

where $\overline{S}_a$ is the average apparent surface area.

The average apparent surface area is found from the surface integral,

$$S_a = \frac{1}{2}\oint_S |\cos\theta|\mathrm{d}S_T \tag{1.45}$$

Averaging over all possible directions gives the average cosine term. For any enclosed volume with convex surfaces, the average apparent surface area is given by

$$\overline{S}_a = \frac{S_T}{4} \tag{1.46}$$

The assumption that the volume effectively forms a convex solid does not limit its applicability to real rooms as long as the surface area associated with any concave surfaces within the volume are included in the calculation of S_T (Kosten, 1960). Note once again that it is assumed that all of these curved surfaces result in diffuse reflections.

For any shape of room in which all room surfaces diffusely reflect sound waves, the mean free path for a three-dimensional space is given by Eqs 1.44 and 1.46, hence

$$d_{\text{mfp}} = \frac{4V}{S_{\text{T}}} \tag{1.47}$$

where S_{T} is the total area of the room surfaces and V is the room volume.

It is important to note that Eq. 1.47 gives the mean value; as with any random process, there will be a spread of results. The mean free path applies to any shape of room with diffusely reflecting surfaces. However, the statistical distribution of the mean free path in rooms with diffusely reflecting surfaces depends upon the room shape and its dimensions as well as the presence of scattering objects within the room (Kuttruff, 1979).

1.2.4 Image sources

A geometrical approach to room acoustics allows calculation of the room response using image sources. It is briefly described here to introduce the concept of image sources for specular reflections from surfaces. This will be needed in later sections to describe sound fields within rooms, as well as sound incident upon a building façade from outside.

This approach assumes that the wavelength is small compared with the dimensions of the surface that the wave hits. In the study of room acoustics in large rooms and/or at high frequencies this allows sound to be considered in terms of rays rather than waves. Using rays means that diffraction and phase information that causes interference patterns is ignored. In a similar way to the study of optics, a ray can be followed from a point source to the boundary where it undergoes specular reflection, such that the angle of incidence equals the angle of reflection.

Image sources are defined by treating every boundary (e.g. wall, floor, ground) as mirrors in which the actual source can be reflected (see Fig. 1.8). The length of the propagation path from source to receiver is then equal to the distance along the straight line from the image source to the receiver. As we are considering spherical waves from a point source it is necessary to use this distance to take account of spherical divergence when calculating the intensity (Eq. 1.26).

For certain receiver positions in rooms with shapes that are much more complex than a simple box, some of the image sources generated by the reflection process will correspond to paths that cannot physically exist in practice. Hence for rooms other than box-shaped rooms, it is necessary to check the validity of each image source for each receiver position.

1.2.4.1 Temporal density of reflections

For a box-shaped room containing a single point source, the image source approach that was described above can be used to create an infinitely large number of image rooms each containing a single image source. A small portion of this infinite matrix of image rooms in two-dimensional space is shown in Fig. 1.9. Assuming that the point source generates an impulse at $t = 0$, each image source must also generate an identical impulse at $t = 0$. This ensures that all propagation paths have the correct time lag/gain relative to each other. A circle of radius, $c_0 t$, with its origin in the centre of the source room will therefore enclose image sources (i.e. propagation paths with reflections) with propagation times less than t. Moving on to consider

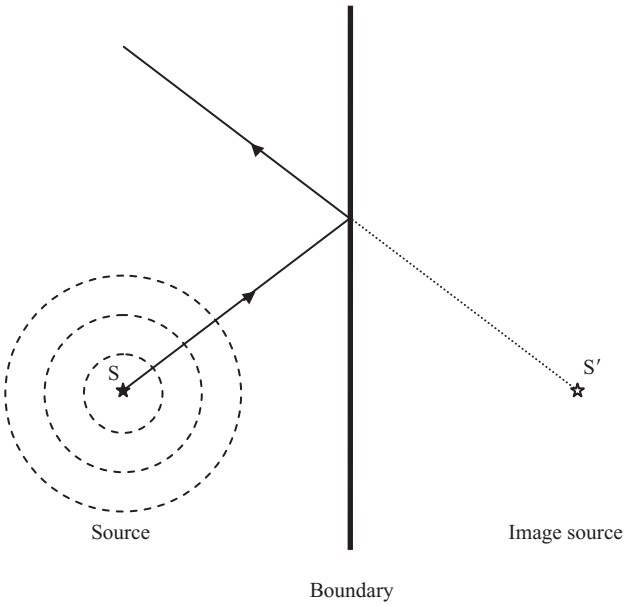

Figure 1.8

Source and image source.

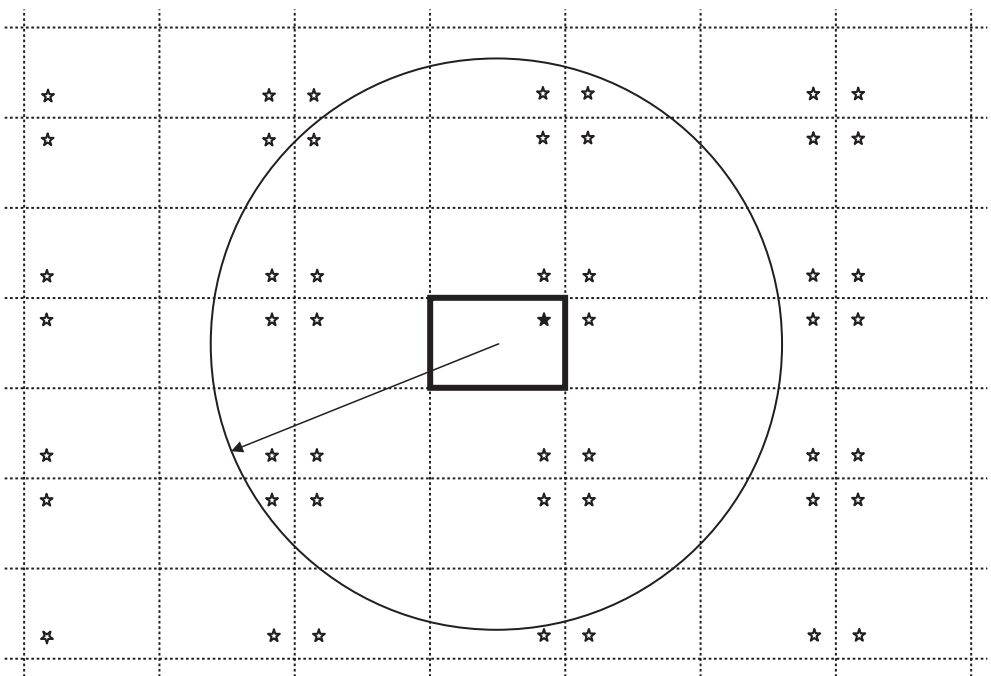

Figure 1.9

Source (★) and image sources (☆) for a box-shaped room (dark solid lines) and some of its image rooms (dotted lines).

three-dimensional space, it follows that the volume of a sphere of radius, $c_0 t$, divided by the volume associated with each image source (i.e. the room volume, V) will equal the number of reflections, N, arriving at a point in the room within time, t. Hence,

$$N = \frac{4\pi(c_0 t)^3}{3V} \tag{1.48}$$

and the temporal density of reflections, $\mathrm{d}N/\mathrm{d}t$ (i.e. the number of reflections arriving per second at time, t) is

$$\frac{\mathrm{d}N}{\mathrm{d}t} = \frac{4\pi c_0^3 t^2}{V} \tag{1.49}$$

This equation applies to any shape of room with a diffuse field; the derivation simply uses a box-shaped room to simplify use of the image source approach.

1.2.5 Local modes

Having looked at the diffuse field, we will now look at the other idealized model, the modal sound field. We start by defining room modes. To do this we can follow the journey of a plane wave as it travels around a box-shaped room. To simplify matters we assume that all the room surfaces are perfectly reflecting and rigid. Therefore the incident and reflected waves have the same magnitude and the sound pressure is reflected from the surface without any change in phase. A rigid wall or floor is defined as one which is not caused to vibrate when a sound wave impinges upon it; hence the particle velocity normal to the surface is zero. In practice, walls and floors do vibrate because this is the mechanism that is responsible for sound transmission; however, this assumption avoids having to consider the wide range of acoustic surface impedances that are associated with real surfaces.

We now follow the path that is travelled by a sound wave as it travels across a box-shaped room (see Fig. 1.10). At some point in time it will hit one of the room boundaries from which it will be reflected before continuing on its journey to be reflected from other room boundaries.

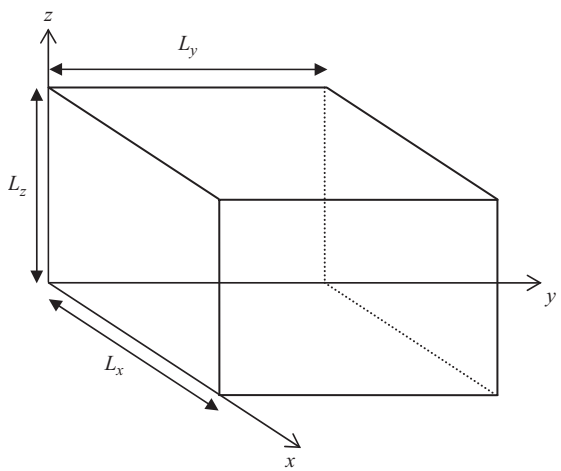

Figure 1.10

Box-shaped room.

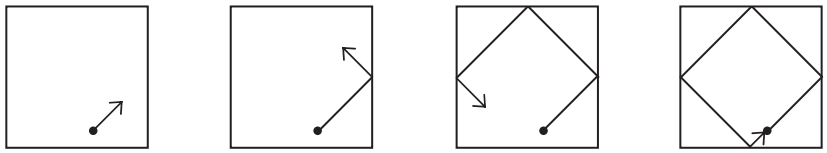

Figure 1.11

Room modes. Plan view of a box-shaped room showing one possible journey taken by a plane wave. A room mode occurs when the wave travels through the same starting point (•) travelling in exactly the same direction as when it first left, whilst achieving phase closure.

These reflections are assumed to be specular as would occur with smooth walls and floors that have uniform acoustic surface impedance over their surface. We can also follow the journeys taken by other sound waves travelling in other directions. Some of these waves will return to the starting point travelling in exactly the same direction as when they first left. In some instances the length of their journey, in terms of phase, will correspond to an integer multiple of 2π such that there will be continuity of phase; we will refer to this as phase closure. Each journey that returns to the same starting point travelling in the same direction whilst achieving phase closure defines a mode with a specific frequency (see Fig. 1.11).

The term 'local mode' is used because the modes are 'local' to a space that is defined by its boundaries; in a similar way we will define local modes of vibration for structure-borne sound on plates and beams in Chapter 2. For rooms this definition assumes that there is no interaction between the sound waves in the room and the structure-borne sound waves on the walls and floors that face into that room. The walls and floors are only considered as boundaries that determine the fraction of wave energy that is reflected and the phase change that occurs upon reflection. It is also assumed that there is no sound source exciting these modes; we have simply followed the journey of a plane wave without considering how it was generated. Hence it is important to note that local modes of spaces and structures (e.g. rooms, walls, and floors) are a concept; they do not actually exist in real buildings where the spaces and structures are coupled together. Although the definition of local modes is slightly removed from reality, the concept is very useful in studying certain features of sound or vibration fields, as well as the interaction between these fields using methods such as Statistical Energy Analysis. Local modes are also referred to as natural modes or pure standing waves; they are a property of the space, rather than a combined function of the space and the excitation. The latter is referred to as a resonance. The term local mode is sometimes abbreviated to mode; only using the full name where it is necessary to distinguish it from a global mode.

To calculate the frequencies of the room modes in this box-shaped room it is necessary to calculate the wavenumbers. Hence we refer back to our discussion in Section 1.2.1.2 on plane waves and the wave equation where the relationship between the wavenumber and the constants, k_x, k_y, and k_z, was given by Eq. 1.15. These constants are calculated by using the equation for sound pressure in a plane wave which must satisfy both the wave equation (Eq. 1.14) and the boundary conditions. For a box-shaped room with dimensions L_x, L_y, and L_z, the following boundary conditions are required to ensure that the particle velocity normal to the rigid room surfaces is zero,

$$\frac{\partial p}{\partial x} = 0 \text{ at } x = 0 \text{ and } x = L_x \quad \frac{\partial p}{\partial y} = 0 \text{ at } y = 0 \text{ and } y = L_y \quad \frac{\partial p}{\partial z} = 0 \text{ at } z = 0 \text{ and } z = L_z. \tag{1.50}$$

By taking the real part of Eq. 1.13 that describes the sound pressure for a plane wave and ignoring time dependence we have the following solution

$$p(x, y, z) = \hat{p}\cos(k_x x)\cos(k_y y)\cos(k_z z) \tag{1.51}$$

This will only satisfy the boundary conditions when $\sin(k_x L_x) = \sin(k_y L_y) = \sin(k_z L_z) = 0$, hence

$$k_x = \frac{p\pi}{L_x} \qquad k_y = \frac{q\pi}{L_y} \qquad k_z = \frac{r\pi}{L_z} \tag{1.52}$$

where the variables p, q, and r can take zero or positive integer values.

Each combination of values for p, q, and r describes a room mode for which the mode wavenumber, $k_{p,q,r}$, (also called an eigenvalue) is found from Eqs 1.15 and 1.52 to be

$$k_{p,q,r} = \pi\sqrt{\left(\frac{p}{L_x}\right)^2 + \left(\frac{q}{L_y}\right)^2 + \left(\frac{r}{L_z}\right)^2} \tag{1.53}$$

Therefore the mode frequency, $f_{p,q,r}$ (also called an eigenfrequency) is

$$f_{p,q,r} = \frac{c_0}{2}\sqrt{\left(\frac{p}{L_x}\right)^2 + \left(\frac{q}{L_y}\right)^2 + \left(\frac{r}{L_z}\right)^2} \tag{1.54}$$

where p, q, and r take zero or positive integer values.

In a box-shaped room there are three different types of room mode: axial, tangential, and oblique modes.

Axial modes describe the situation where wave propagation is parallel to the x, y, or z axis. They have one non-zero value for p, q, or r, and zero values for the other two variables (e.g. $f_{1,0,0}, f_{0,3,0}, f_{0,0,2}$).

Tangential modes can be described by defining a 'pair of surfaces' as two surfaces that lie opposite each other, where each pair of surfaces partially defines the box-shaped room. Hence, tangential modes describe wave propagation at an angle that is oblique to two pairs of surfaces, and is tangential to the other pair of surfaces. They have non-zero values for two of the variables p, q, or r, and a zero value for the other variable (e.g. $f_{1,2,0}$, $f_{3,0,1}$, $f_{0,2,2}$).

Oblique modes describe the situation where wave propagation occurs at an angle that is oblique to all surfaces; hence they have non-zero values for p, q, and r (e.g. $f_{2,3,1}$).

We have assumed that all the room surfaces are perfectly reflecting and rigid, in practice there is interaction between the sound pressure in the room and the vibration of the walls and floors facing into that room. However, the assumption of rigid walls and floors is reasonable in many rooms because this interaction results in relatively minor shifts in the eigenfrequencies.

1.2.5.1 Modal density

It is often useful to calculate the first 10 or so modes to gain an insight into their distribution between the frequency bands in the low-frequency range. However, in a room of approximately 50 m^3 there are almost one-million modes in the building acoustics frequency range. Fortunately there is no need to calculate all of these modes because we can adopt a statistical viewpoint. A statistical approach also helps us to deal with the fact that very few rooms are

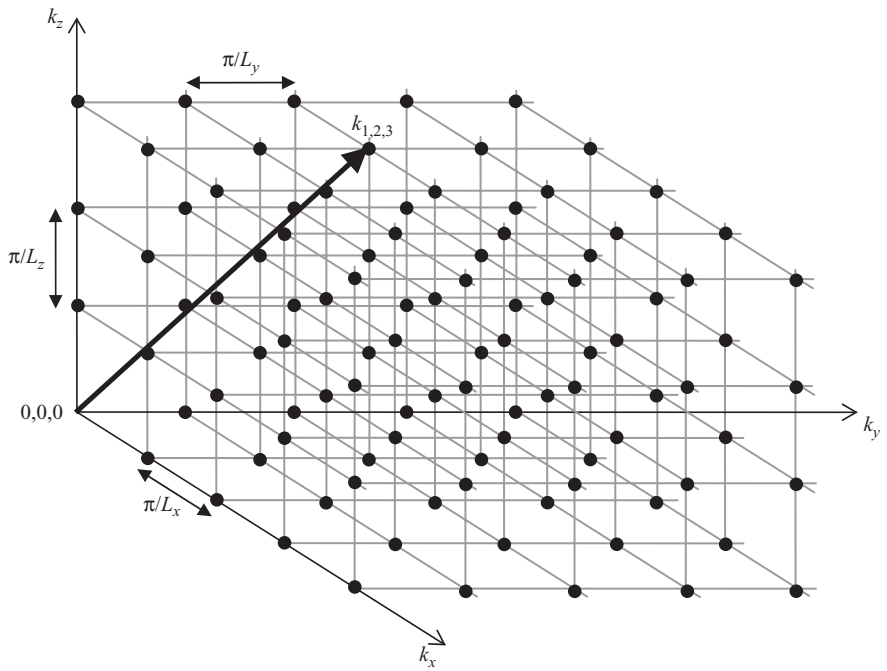

Figure 1.12

Mode lattice for a three-dimensional space. The vector corresponding to eigenvalue, $k_{1,2,3}$, is shown as an example.

perfectly box-shaped with rigid boundaries. For this reason the calculation of any individual mode frequency will rarely be accurate when the wavelength is smaller than any of the room dimensions. We can usually expect to estimate the one-third-octave-band in which a mode frequency will fall to an accuracy of plus or minus one-third-octave-band.

The statistical descriptor for modes is the statistical modal density, $n(f)$, the number of modes per Hertz. To calculate the modal density it is necessary to arrange the eigenvalues in such a way that facilitates counting the modes in a chosen frequency range. It is implicit in the form of Eq. 1.15 that this can be achieved by creating a lattice in Cartesian coordinates where the x, y, and z axes represent k_x, k_y, and k_z (Kuttruff, 1979). This lattice of eigenvalues in k-space is shown in Fig. 1.12, where each intersection in the lattice represents an eigenvalue indicated by the symbol •. The length of the vector from the origin to an eigenvalue equals $k_{p,q,r}$. Eigenvalues that lie along each of the three axes represent axial modes; those that lie on the coordinate planes $k_x k_y, k_x k_z$, and $k_y k_z$ (excluding the eigenvalues on the axes) represent tangential modes; all other eigenvalues (i.e. all eigenvalues excluding those on the axes and the coordinate planes) represent oblique modes. From Eq. 1.52 it is evident that the distance between adjacent eigenvalues in the k_x, k_y, and k_z directions are $\pi/L_x, \pi/L_y$, and π/L_z respectively. Hence the volume associated with each eigenvalue is a cube with a volume of $\pi^3/L_x L_y L_z$, which equals π^3/V.

The number of modes below a specified wavenumber, k, is equal to the number of eigenvalues that are contained within one-eighth of a spherical volume with radius, k, as indicated in Fig. 1.13. If there were only oblique modes this would simply be carried out by dividing $(4\pi k^3/3)/8$ by π^3/V; however, the existence of axial and tangential modes means that this

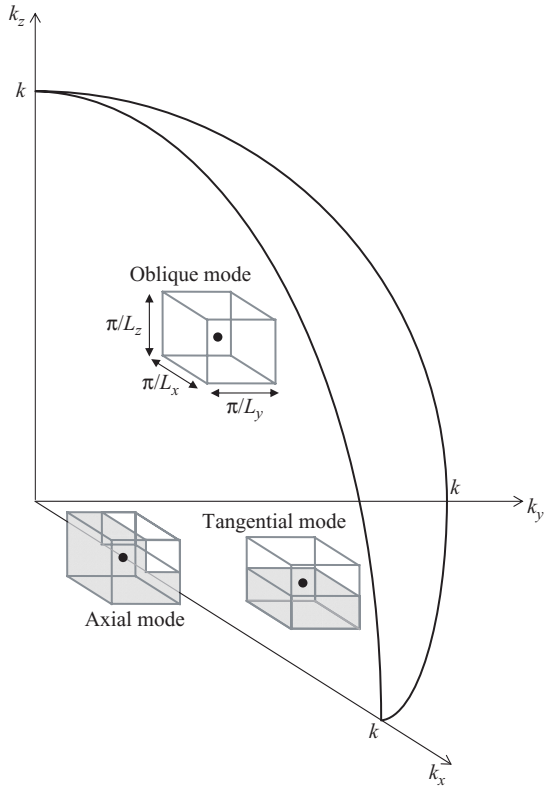

Figure 1.13

Sketch indicating how the volumes associated with the eigenvalues for axial, tangential, and oblique modes fall inside or outside the permissible volume in k-space. The shaded volumes indicate those fractions of the volumes associated with the axial and tangential modes that fall outside the permissible volume in k-space. The octant volume with radius, k, encloses eigenvalues below wavenumber, k.

would be incorrect. This is because part of the cube volume that is associated with these mode types falls outside of the permissible volume in k-space that can only have zero or positive values of k_x, k_y, and k_z. From Fig. 1.13 we also see that for tangential modes on the coordinate planes, one-half of the cube volume falls outside this permissible volume and for axial modes, three-quarters of the cube volume falls outside. Therefore calculating the number of modes is a three-step process. The first step is to divide $(4\pi k^3/3)/8$ by π^3/V to give an estimate for the number of oblique modes that also includes one-quarter of the axial modes and one-half of the tangential modes. The second step is to account for the other halves of the tangential modes that lie in the area on the three coordinate planes; this fraction of the total number of modes is calculated by taking one-half of $(\pi k^2/4)/(\pi^2/(L_xL_y + L_xL_z + L_yL_z))$. The latter step included the axial modes on each of the three coordinate axes as halves. Hence there only remains one-quarter of the axial modes that have not yet been accounted for. The third step determines this remaining fraction of the total number of modes by taking one-quarter of $k/(\pi/(L_x + L_y + L_z))$. The sum of these three components gives the number of modes, $N(k)$, below the wavenumber, k,

$$N(k) = \frac{k^3 V}{6\pi^2} + \frac{k^2 S_T}{16\pi} + \frac{kL_T}{16\pi} \tag{1.55}$$

where the total area of the room surfaces, S_T is $2(L_xL_y + L_xL_z + L_yL_z)$ and the total length of all the room edges, L_T, is $4(L_x + L_y + L_z)$.

As we are working in k-space we calculate the modal density, $n(\omega)$, in modes per radian, and then convert to the modal density, $n(f)$, in modes per Hertz, which is more convenient for practical calculations. The general equation for the modal density, $n(\omega)$, in terms of ω is

$$n(\omega) = \frac{dN(k)}{d\omega} = \frac{dN(k)}{dk}\frac{dk}{d\omega} \tag{1.56}$$

To calculate $n(\omega)$ we now need to find $dk/d\omega$ which is equal to the reciprocal of the group velocity, c_g. The group velocity is the velocity at which wave energy propagates across the space. For sound waves in air, the group velocity is the same as the phase velocity, c_0. Hence the general equation to convert $n(\omega)$ to $n(f)$ is

$$n(f) = 2\pi n(\omega) = \frac{2\pi}{c_g}\frac{dN(k)}{dk} \tag{1.57}$$

which gives the modal density for a box-shaped room as

$$n(f) = \frac{4\pi f^2 V}{c_0^3} + \frac{\pi f S_T}{2c_0^2} + \frac{L_T}{8c_0} \tag{1.58}$$

where the modal density for each frequency band is calculated using the band centre frequency.

For rooms that are not box-shaped, and for typical rooms in the high-frequency range, a reasonable estimate of the modal density can be found by using only the first term in Eq. 1.58, to give

$$n(f) = \frac{4\pi f^2 V}{c_0^3} \tag{1.59}$$

Estimates for the statistical modal density of axial, tangential, and oblique modes can be estimated from (Morse and Ingard, 1968)

$$n_{axial}(f) = \frac{6V^{1/3}}{c_0} \tag{1.60}$$

$$n_{tangential}(f) = \frac{6\pi f V^{2/3}}{c_0^2} - \frac{6V^{1/3}}{c_0} \tag{1.61}$$

$$n_{oblique}(f) = \frac{4\pi f^2 V}{c_0^3} - \frac{3\pi f V^{2/3}}{c_0^2} + \frac{3V^{1/3}}{2c_0} \tag{1.62}$$

for which it is assumed that $L_T \approx 12V^{1/3}$ and $S_T \approx 6V^{2/3}$ (Jacobsen, 1982). This simplifies the calculation for rooms that are almost (but not exactly) box-shaped.

1.2.5.2 Mode count

The mode count, N, in a frequency band with a bandwidth, B, can be determined in two ways. Either by using Eq. 1.54 to calculate the individual mode frequencies and then by counting the number of modes that fall within the band or by using the statistical modal density to determine a statistical mode count, N_s, in that band, where

$$N_s = n(f)B \tag{1.63}$$

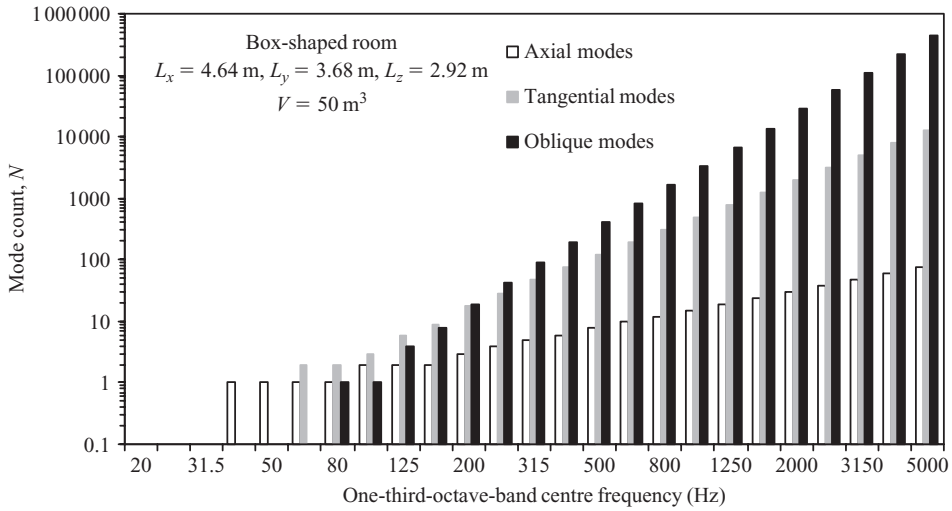

Figure 1.14

Mode count for axial, tangential, and oblique modes in a 50 m^3 box-shaped room.

In a box-shaped room, the mode with the lowest frequency will always be an axial mode. As the band centre frequency increases, the number of oblique modes in each band increases at a faster rate than the number of axial modes or the number of tangential modes. As an example we can look at the trends in the mode count for a 50 m^3 room. The room dimensions are determined using the ratio $4^{1/3}$:$2^{1/3}$:1 for x:y:z. This ratio is sometimes used in the design of reverberation rooms to avoid dimensions that are integer multiples of each other; this avoids different modes having the same frequency. As we usually work in one-third-octave-bands it is of interest to know the number of modes that fall within each band. The mode counts for the axial, tangential, and oblique modes are shown in Fig. 1.14. For typical rooms we can describe the mode count using three different ranges: A, B, and C. In range A, the frequency bands either contain no modes or a few axial and/or a few tangential modes. In range B, the blend of the three different mode types varies between adjacent frequency bands depending on the room dimensions. In range C, the mode count is always highest for oblique modes and always lowest for axial modes. For this particular example, range A corresponds to one-third-octave-bands below 80 Hz, range B lies between the 80 and 200 Hz bands, and range C corresponds to bands above 200 Hz.

1.2.5.3 Mode spacing

The average frequency spacing between adjacent modes, δf, is calculated from the modal density using

$$\delta f = \frac{1}{n(f)} \tag{1.64}$$

As sound insulation calculations are almost always carried out in one-third-octave or octave-bands it tends to be more informative to calculate the mode counts in these frequency bands rather than use the mode spacing.

1.2.5.4 Equivalent angles

Part of the definition of a diffuse field is that there is equal probability of a sound wave arriving from any direction, i.e. from any angle. Hence it is instructive to look at the range of angles associated with the plane waves that form local modes. We have previously described a local mode in a qualitative manner by following the journey of a plane wave around a room. To quantitatively describe the plane wave field we need to account for the different propagation directions after reflection from each surface. The general equation for a plane wave (Eq. 1.13) describes propagation in a single direction; hence each mode is comprised of more than one plane wave. For each mode we can define equivalent angles, θ_x, θ_y, and θ_z; these angles are defined from lines that are normal to the x, y, and z-axis respectively. They are defined in k-space for any eigenvalue in the lattice (see Fig. 1.15). For each mode, one plane wave points in the direction of this vector in k-space. The direction of the other plane waves can be found by reflecting the vector into the other octants of k-space. Axial, tangential, and oblique modes are therefore described by two, four, and eight plane waves respectively. For each mode, the equivalent angles are related to the mode wavenumber, $k_{p,q,r}$, and the constants, k_x, k_y, and k_z by

$$k_x = k_{p,q,r} \sin\theta_x \qquad k_y = k_{p,q,r} \sin\theta_y \qquad k_z = k_{p,q,r} \sin\theta_z \tag{1.65}$$

hence, from the constant definitions in Eq. 1.52, the equivalent angles for each mode are

$$\theta_x = \operatorname{asin}\left(\frac{pc_0}{2L_x f_{p,q,r}}\right) \qquad \theta_y = \operatorname{asin}\left(\frac{qc_0}{2L_y f_{p,q,r}}\right) \qquad \theta_z = \operatorname{asin}\left(\frac{rc_0}{2L_z f_{p,q,r}}\right) \tag{1.66}$$

Later on we will need to consider the angles of incidence for the waves that impinge upon a room surface in the calculation of sound transmission. Here we are only assessing the range of equivalent angles for plane waves that propagate across the space to form room modes. Figure 1.16 shows the equivalent angles for the same 50 m^3 room that was used for the mode count, where each point corresponds to a single room mode. Note that we are ignoring the fact that specular reflection would not occur in real rooms at high frequencies. In the low-frequency range, where there are relatively few modes, there is a limited range of angles. As the frequency increases, the number of modes increases (the majority tending to be oblique modes), and the range expands to cover the full range of angles between 0° and 90°. For axial modes, one angle is 90° and the other two angles are 0° (e.g. $f_{1,0,0}$ has $\theta_x = 90°$, $\theta_y = 0°$, and $\theta_z = 0°$). For tangential modes, one angle is 0°, and the other two angles are oblique. For oblique modes, all three angles are oblique.

Equivalent angles do not in themselves identify a frequency above which the modal sound field approximates to a diffuse field; we have already noted other important features that define a diffuse field. However, they do illustrate how one aspect of a diffuse field concerning sound arriving from all directions can potentially be satisfied in a modal sound field. In the study of sound transmission it is useful to be able to switch between thinking in terms of modes, and in terms of waves travelling at specific angles.

1.2.5.5 Irregularly shaped rooms and scattering objects

The description of local modes was based on an empty box-shaped room. Rooms in real buildings are not all box-shaped and they usually contain scattering objects such as furniture.

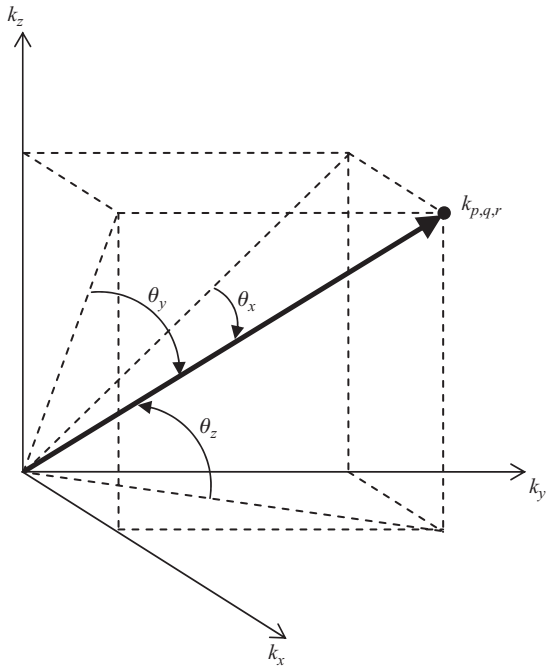

Figure 1.15

Equivalent angles in *k*-space.

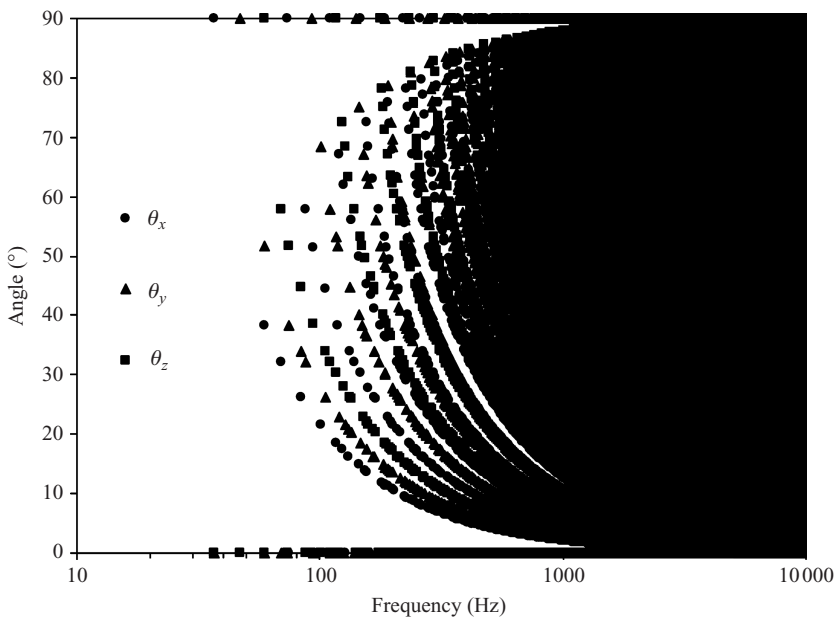

Figure 1.16

Equivalent angles for the modes of a 50 m^3 box-shaped room.

In the laboratory, it is common to use non-parallel walls and diffusers to try and create a diffuse field in the central zone of the room. This does not mean that the local mode approach is instantly irrelevant; far from it. Scattering objects can be seen as coupling together the local modes of the empty room, giving rise to hybrid versions of the original mode shapes (Morse and Ingard, 1968). These hybrid versions no longer have the symmetrical sound pressure fields associated with individual local modes in an empty box-shaped room. In the limit, as the room shape becomes increasingly irregular (or sufficient scattering objects are placed inside a box-shaped room) and the room surfaces have a random distribution of acoustic surface impedance, we can effectively consider all the room modes to be some form of oblique mode. As we approach this limit we can leave the local mode model behind us and assume there is a close approximation to a diffuse field in the central zone of the room.

1.2.6 Damping

In our discussion on room modes we assumed that there was a perfect reflection each time the plane wave was reflected from a room boundary. In reality there will always be damping mechanisms that reduce the sound pressure level. When discussing room acoustics we usually refer to absorption and reverberation times, rather than damping. From a room acoustics perspective, the sound source and the listener are located within one space, so from the point-of-view of a listener in the source room, any sound that doesn't return to them has been absorbed. However, with sound insulation our concern is usually for the person that hears the sound in the receiving room, and from their point-of-view the sound has been transmitted. As we are particularly interested in the exchange of sound energy between spaces and structures, it is useful to start treating them in a similar manner by using the same terminology to describe absorption and transmission. Hence it is convenient to relate different damping mechanisms to the loss factors used in Statistical Energy Analysis; these are the internal loss factor, the coupling loss factor, and the total loss factor (Lyon and DeJong, 1995).

With internal losses the sound energy is converted into heat. Hence high internal loss factors are beneficial for the noise control engineer who is trying to reduce sound levels. Internal losses occur when the sound wave hits absorptive surfaces or objects (e.g. sound absorbent ceiling tiles, carpet, porous materials) and as the wave travels through the air due to air absorption. The former is usually more important than the latter because air absorption only becomes significant at high frequencies and in large rooms. Information on sound absorption mechanisms and sound absorbers can be found in a number of textbooks (e.g. Mechel, 1989/1995/1998; Mechel and Vér, 1992; Kuttruff, 1979).

With coupling losses, the sound energy is transmitted to some other part of the building that faces into the room. This could be an open door or window where the sound exits, never to return. It could also be a wall or a floor in the room which is caused to vibrate by the impinging sound waves.

The sum of the internal and coupling loss factors equals the total loss factor, and this is related to the reverberation time of the room. We therefore start this section on damping by deriving reflection and absorption coefficients for room surfaces that will lead to a discussion of reverberation times and loss factors for rooms.

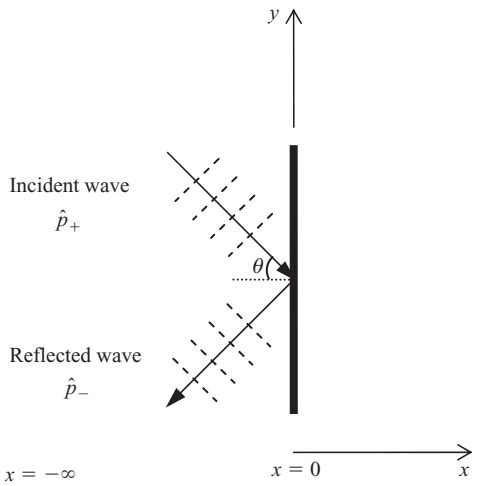

Figure 1.17

Plane wave incident at an angle, θ, upon a surface, and the specularly reflected wave.

1.2.6.1 Reflection and absorption coefficients

A plane wave incident upon a room surface at $x = 0$ can be described using the term, $\hat{p}_+ \exp(-ikx)$ where $\hat{p}_+$ is an arbitrary constant. The term for the reflected wave is $R\hat{p}_+ \exp(ikx)$ where R is defined as the reflection coefficient,

$$R = |R| \exp(i\gamma) \tag{1.67}$$

As seen from Eq. 1.67, the reflection coefficient is complex. It describes the magnitude and phase change that occurs upon reflection. In diffuse fields the waves that are incident upon a surface have random phase, so the information on the phase change is usually ignored.

We now consider a plane wave that is incident upon a surface at an angle, θ; defined such that $\theta = 0°$ when the wave propagates normal to the surface. The aim here is to relate the reflection coefficient to the specific acoustic impedance or admittance. It is assumed that the surface is locally reacting so that the normal component of the particle velocity only depends on the region at the surface where the sound pressure is incident.

The incident wave propagates in the xy plane towards a surface at $x = 0$ as shown in Fig. 1.17. The incident wave is described by

$$p_+(x, y, t) = [\hat{p}_+ \exp(-ik(x \cos\theta + y \sin\theta))] \exp(i\omega t) \tag{1.68}$$

The incident wave is specularly reflected from the surface and the reflection coefficient is used to describe the amplitude of the reflected wave, $\hat{p}_- = R\hat{p}_+$. Hence the reflected wave is

$$p_-(x, y, t) = [R\hat{p}_+ \exp(-ik(-x \cos\theta + y \sin\theta))] \exp(i\omega t) \tag{1.69}$$

The particle velocity in the x-direction (i.e. normal to the surface) is found using Eq. 1.16, which gives

$$u_x = -\frac{1}{i\omega} \frac{1}{\rho_0} \frac{\partial p}{\partial x} \tag{1.70}$$

Therefore the particle velocities for the incident and reflected waves are

$$u_{x+}(x,y,t) = \frac{\cos\theta}{\rho_0 c_0}[\hat{p}_+ \exp(-ik(x\cos\theta + y\sin\theta))]\exp(i\omega t) \tag{1.71}$$

$$u_{x-}(x,y,t) = -\frac{\cos\theta}{\rho_0 c_0}[R\hat{p}_+ \exp(-ik(-x\cos\theta + y\sin\theta))]\exp(i\omega t) \tag{1.72}$$

At the surface (i.e. at $x = 0$), the resultant pressure is $p_+ + p_-$, and the resultant particle velocity normal to the surface is $u_{x+} + u_{x-}$. The ratio of the resultant pressure to this resultant particle velocity equals the normal acoustic surface impedance (Eq. 1.29). Hence the specific acoustic impedance of a surface is related to the reflection coefficient by

$$Z_{a,s} = \frac{1}{\cos\theta}\frac{1+R}{1-R} \tag{1.73}$$

which is re-arranged to give the reflection coefficient in terms of either the specific acoustic impedance or admittance

$$R = \frac{Z_{a,s}\cos\theta - 1}{Z_{a,s}\cos\theta + 1} = \frac{\cos\theta - \beta_{a,s}}{\cos\theta + \beta_{a,s}} \tag{1.74}$$

In practice it is usually more convenient to work in terms of absorption rather than reflection. The sound absorption coefficient, α, is defined as the ratio of the intensity absorbed by a surface to the intensity incident upon that surface; hence it takes values between 0 and 1. The intensity in a plane wave is proportional to the mean-square pressure (Eq. 1.19), so the absorption coefficient is related to the reflection coefficient by

$$\alpha = 1 - |R|^2 \tag{1.75}$$

The absorption coefficient can be calculated using Eqs 1.74 and 1.75 in terms of either the specific acoustic impedance or admittance. For a plane wave that is incident upon a locally reacting surface at an angle, θ, the angle-dependent absorption coefficient, α_θ, is

$$\alpha_\theta = \frac{4Z_{Re}\cos\theta}{(Z_{Re}^2 + Z_{Im}^2)\cos^2\theta + 2Z_{Re}\cos\theta + 1} = \frac{4\beta_{Re}\cos\theta}{(\beta_{Re} + \cos\theta)^2 + \beta_{Im}^2} \tag{1.76}$$

where the real and imaginary parts of the specific acoustic impedance are

$$Z_{a,s} = Z_{Re} + iZ_{Im} \tag{1.77}$$

and the real and imaginary parts of the specific acoustic admittance are

$$\beta_{a,s} = \frac{1}{Z_{a,s}} = \beta_{Re} - i\beta_{Im} \tag{1.78}$$

At normal incidence, $\theta = 0°$, hence the normal incidence absorption coefficient, α_0, is

$$\alpha_0 = \frac{4\beta_{Re}}{(\beta_{Re} + 1)^2 + \beta_{Im}^2} \tag{1.79}$$

There can be significant variation in the absorption coefficient with angle. However, when there is a diffuse sound field incident upon a surface we assume that there is equal probability of sound waves impinging upon the surface from all directions. For diffuse fields we therefore use the statistical sound absorption coefficient, α_{st}, given by

$$\alpha_{st} = \int_0^{\pi/2} \alpha_\theta \sin(2\theta)\mathrm{d}\theta \tag{1.80}$$

The statistical absorption coefficient is calculated from the specific acoustic admittance using (Morse and Ingard, 1968)

$$\alpha_{st} = 8\beta_{Re}\left(1 + \frac{\beta_{Re}^2 - \beta_{Im}^2}{\beta_{Im}}\operatorname{atan}\left(\frac{\beta_{Im}}{\beta_{Re}^2 + \beta_{Im}^2 + \beta_{Re}}\right) - \beta_{Re}\ln\left(\frac{(\beta_{Re}+1)^2 + \beta_{Im}^2}{\beta_{Re}^2 + \beta_{Im}^2}\right)\right) \quad (1.81)$$

1.2.6.2 Absorption area

Rooms not only have absorbent surfaces, but they also contain absorbent objects (e.g. furniture, people) and there will be air absorption. For practical purposes, the absorption area, A, in m^2 is useful in describing the absorption provided by surfaces, objects, and air. The absorption area is defined as the ratio of the sound power absorbed by a surface or object, to the sound intensity incident upon the surface or object. For a surface the absorption area is the product of the absorption coefficient and the surface area. The absorption area essentially describes all the absorption in the room using a single area; hence an absorption area of 10 m^2 corresponds to an area of 10 m^2 that is totally absorbing.

For a room with I surfaces, J objects, and air absorption, the total absorption area, A_T is

$$A_T = \sum_{i=1}^{I} S_i\alpha_i + \sum_{j=1}^{J} A_{obj,j} + A_{air} \quad (1.82)$$

Air absorption depends upon frequency, temperature, relative humidity, and static pressure. The absorption area for air is calculated from the attenuation coefficient in air, m, in Neper/m and the volume of air in the space, V, using

$$A_{air} = 4mV \quad (1.83)$$

The attenuation coefficient in dB/m can be calculated according to ISO 9613-1 and converted to Neper/m by dividing by $10\lg(e)$.

Calculated values for A_{air} at 20°C, 70% RH and $P_0 = 1.013 \times 10^5$ Pa are shown in Fig. 1.18. For rooms with an absorption area of at least 10 m^2 due to surfaces and objects, A_{air} will only usually form a significant fraction of A in the high-frequency range. For furnished, habitable rooms (such as those in dwellings, commercial buildings, and schools), air absorption in the building acoustics frequency range can often be ignored in volumes $<150\,m^3$.

1.2.6.3 Reverberation time

When a sound source in a room is stopped abruptly, the sound energy decays away due to the damping mechanisms that are present in the room. This feature is called reverberation and is assessed by plotting a decay curve. This is a plot of the decaying sound pressure level against time, starting from the time at which the sound source is stopped, usually denoted as the time, $t = 0$.

For sound insulation, the reverberation time is needed to relate the sound power radiated into a space to the average sound pressure level in that space and to quantify either the absorption

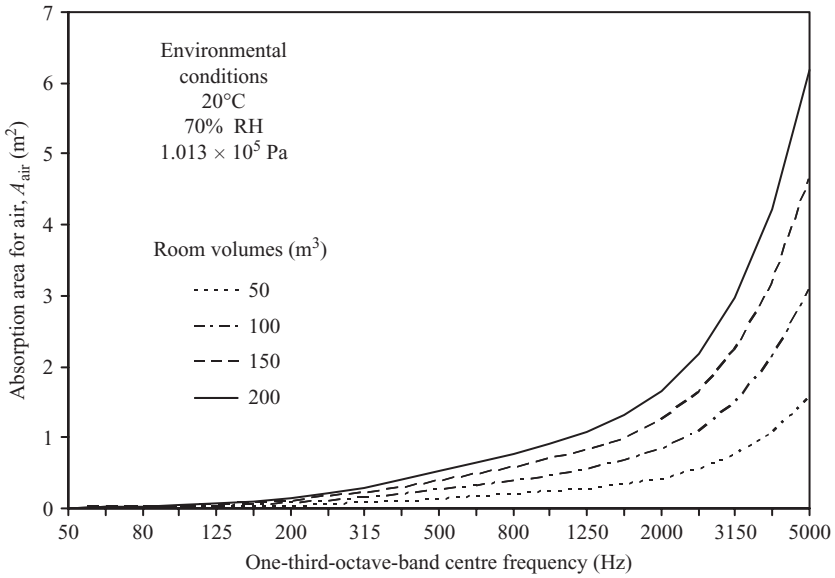

Figure 1.18

Absorption area for air in different room volumes.

in a space or the total loss factor of a space. In room acoustics, several other parameters are used to describe different aspects of the sound field relating to reverberation and the subjective evaluation of sound in spaces (ISO 3382).

The reverberation time, T, is the time in seconds that is taken for the sound pressure level to decay by 60 dB, or in terms of energy, for the sound energy to decay to one-millionth of its initial value. This definition is well-suited to the decay curve that occurs in a diffuse field; a straight line decay as shown in Fig. 1.19. Some decay curves can be approximated by a single straight line over the full 60 dB decay, but there are many that do not follow this simple form. In addition, it is not always possible to measure a 60 dB decay due to the presence of background noise. Therefore we need a definition that can be used when decay curves have more than one slope over the 60 dB decay range. This definition also needs to quantify the time taken for the level to decay by 60 dB by using linear regression over a specified decay range (e.g. 30 dB) so that it is not imperative to use the full 60 dB decay. Hence, the reverberation time is more usefully defined as the time in seconds that would be required for the sound pressure level to decay by 60 dB when using linear regression over a specified part of the decay curve. As we can now use any range for the linear regression, such as 10, 15, 20, or 30 dB, it is necessary to use the notation, T_X, where X identifies the evaluation range used in the linear regression, i.e. T_{10}, T_{15}, T_{20}, T_{30}. With measured decay curves, the starting point for the linear regression is usually 5 dB below the initial level, to the end point at $X + 5$ dB (ISO 354 and ISO 3382). In Section 3.8.3 we will see that 5 dB is used as the starting point primarily because the signal processing distorts the initial part of the decay curve.

We can now look at reverberation times with a diffuse field and a non-diffuse field in a box-shaped room.

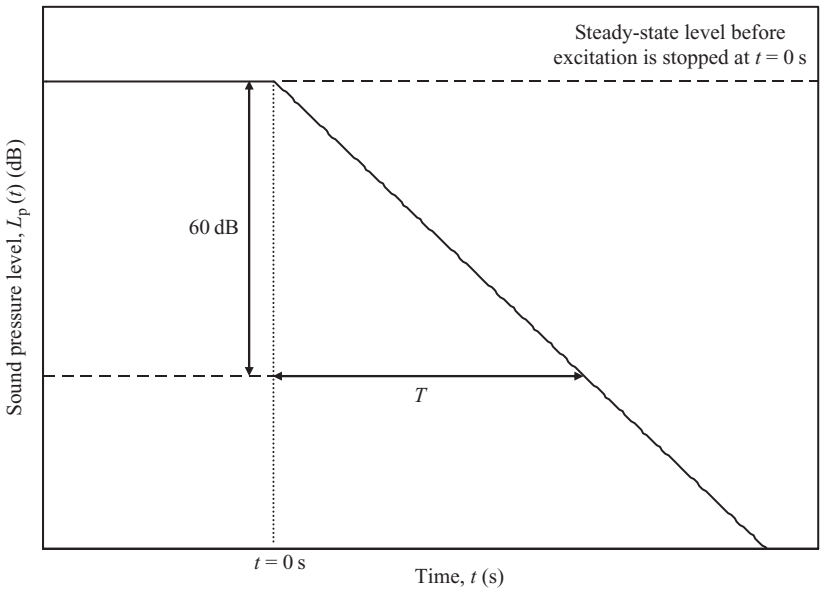

Figure 1.19

Ideal straight line decay curve showing the decrease in the sound pressure level with time after the excitation has stopped.

1.2.6.3.1 *Diffuse field*

In a diffuse sound field, the mean free path, d_{mfp}, can be used to calculate the average time, Δt, between two successive diffuse reflections from the room boundaries,

$$\Delta t = \frac{d_{mfp}}{c_0} \tag{1.84}$$

we can then use Δt to calculate the number of diffuse reflections, N, in time, t, using

$$N = \frac{t}{\Delta t} = \frac{c_0 t}{d_{mfp}} \tag{1.85}$$

The decay process can now be assessed by looking at the probability of waves impinging upon surface areas in the room with different absorption coefficients. This uses the approach taken by Kuttruff (1979). We take a room containing a sound source fed by a stationary signal such as white noise and assume that the resulting sound field is diffuse. When the sound source is stopped at time, $t = 0$, the waves continue to travel across the room volume, and each time they impinge upon a room boundary, a fraction of the energy is reflected, with the remaining fraction being absorbed. The binomial probability distribution is used to assess two possible outcomes when a sound wave impinges upon a room boundary: either the wave is reflected from (and absorbed by) surface area, S_1, or it is reflected from (and absorbed by) the remaining surface area in the room, $S_2 = S_T - S_1$. These outcomes must be statistically independent; hence the probability that a wave is reflected from (and absorbed by) surface area, S_1, is the same every time that the wave impinges upon a room boundary. This is conceivable in a room where each surface area with a different absorption coefficient is uniformly distributed over the total surface area of the room, and there are diffuse reflections from all the room surfaces.

The binomial probability distribution, $P(N_1 \backslash N)$ gives the number of times, N_1, that a wave is reflected from surface area, S_1, out of a total number of reflections, N. The probability of a reflection from surface area, S_1, is S_1/S_T, hence the probability of a reflection from the remaining surface area in the room, S_2, is S_2/S_T or $1-(S_1/S_T)$. The binomial probability distribution is

$$P(N_1 \backslash N) = \binom{N}{N_1} \left(\frac{S_1}{S_T}\right)^{N_1} \left(1 - \frac{S_1}{S_T}\right)^{N-N_1} \tag{1.86}$$

where the binomial coefficient is calculated using

$$\binom{N}{N_1} = \frac{N!}{N_1!(N-N_1)!} \tag{1.87}$$

Each time a wave impinges upon surface area, S_1, the mean-square pressure is reduced by the factor $(1-\alpha_1)$ where α_1 is the diffuse field sound absorption coefficient for surface area, S_1. The same process occurs with surface area, S_2, with the coefficient, α_2. So, after N reflections, of which N_1 reflections are from surface area, S_1, and $N-N_1$ reflections are from the remaining surface area, S_2, the mean-square pressure as a function of N_1, $p^2(N_1)$, is

$$p^2(N_1) = p^2(0)(1-\alpha_1)^{N_1}(1-\alpha_2)^{N-N_1} \tag{1.88}$$

where $p^2(0)$ is the mean-square pressure at time, $t=0$.

Taking into account all possible values of N_1 from zero to N, we can calculate the expected value, $E(N_1)$ of random variable, N_1, which has the probability distribution, $P(N_1 \backslash N)$. As we are particularly interested in the decay of the sound pressure we note that $E(N_1)$ equals the population mean (i.e. the average value) of the mean-square pressure,

$$E(N_1) = \sum_{N_1=0}^{N} p^2(N_1)P(N_1 \backslash N) = p^2(0)\left[\left(\frac{S_1}{S_T}\right)(1-\alpha_1) + \left(1-\frac{S_1}{S_T}\right)(1-\alpha_2)\right]^N \tag{1.89}$$

The term within the square bracket is equal to $(1-\overline{\alpha})$ where $\overline{\alpha}$ is the average diffuse field sound absorption coefficient

$$\overline{\alpha} = \frac{S_1\alpha_1 + \left(1-\frac{S_1}{S_T}\right)\alpha_2}{S_T} \tag{1.90}$$

Hence for rooms with I surface areas that each have a different absorption coefficient (instead of $I=2$ as has just been assumed), the expression can be generalized to

$$\overline{\alpha} = \frac{\sum_{i=1}^{I} S_i\alpha_i}{\sum_{i=1}^{I} S_i} = \frac{1}{S_T}\sum_{i=1}^{I} S_i\alpha_i \tag{1.91}$$

The average diffuse field sound absorption coefficient, $\overline{\alpha}$, is a weighted arithmetic average of the absorption coefficients, where each coefficient has been weighted according to its surface area. From Eq. 1.89 the mean-square pressure $p^2(t)$ at time, t, is therefore described by

$$p^2(t) = p^2(0)(1-\overline{\alpha})^N = p^2(0)\exp(N\ln(1-\overline{\alpha})) \tag{1.92}$$

It is important to note from Eq. 1.92 that the mean-square pressure in a diffuse field has an exponential decay. Therefore when plotting the sound pressure level in decibels against time, the decay curve is a straight line. We will soon look at decay curves in non-diffuse fields, where

the mean-square pressure does not have an exponential decay, and the decay curve is not a single straight line across the 60 dB decay range.

At time $t = T$, the definition of the reverberation time is such that $p^2(T)$ is one-millionth of $p^2(0)$, hence combining Eqs 1.85 and 1.92 gives

$$\frac{p^2(T)}{p^2(0)} = 10^{-6} = \exp\left(\frac{c_0 T}{d_{\text{mfp}}} \ln(1-\bar{\alpha})\right) \tag{1.93}$$

This gives the reverberation time formula that is commonly referred to as Eyring's equation (Eyring, 1930),

$$T = \frac{-d_{\text{mfp}} 6 \ln 10}{c_0 \ln(1-\bar{\alpha})} = \frac{-24V \ln 10}{c_0 S_{\text{T}} \ln(1-\bar{\alpha})} \tag{1.94}$$

and by taking air absorption into account, this becomes

$$T = \frac{-24V \ln 10}{c_0(S_{\text{T}} \ln(1-\bar{\alpha}) - 4mV)} \tag{1.95}$$

When considering the effect of the room volume, V, and the total surface area, S_{T}, on the diffuse field reverberation time, it is useful to think in terms of the mean free path. The reverberation time is proportional to the mean free path for a diffuse field (Eq. 1.47), hence the longer the mean free path, the longer the time between successive reflections from the room surfaces. So if we choose a point in this room to measure the reverberation time, it will have taken longer for the waves to travel around the room before returning to our chosen point. Each time the wave hits a surface, a fraction of the wave energy will be absorbed. Assuming a fixed value for the absorption coefficient of room surfaces, the reverberation time will therefore increase with increasing room volume.

For a diffuse field where the average diffuse field absorption coefficient, $\bar{\alpha}$, is much smaller than unity, we can assume that $\bar{\alpha} \approx -\ln(1-\bar{\alpha})$. Using this approximation in Eq. 1.94 leads to Sabine's equation (Sabine, 1932),

$$T = \frac{d_{\text{mfp}} 6 \ln 10}{c_0 \bar{\alpha}} = \frac{24V \ln 10}{c_0 S_{\text{T}} \bar{\alpha}} \tag{1.96}$$

To take account of absorption from objects and the air, as well as from the room surfaces, Eq. 1.96 is more conveniently written in terms of the total absorption area, A_{T} (Eq. 1.82) as

$$T = \frac{24V \ln 10}{c_0 A_{\text{T}}} \tag{1.97}$$

Assuming that the steady-state sound pressure level in the diffuse field is 60 dB at time $t = 0$, the time-varying sound pressure level in decibels that defines the idealized decay curve is

$$L_{\text{p}}(t) = 10 \lg\left(\frac{p^2(t)}{p^2(0)}\right) = 60 - \frac{60t}{T} \tag{1.98}$$

The Sabine equation is based on the assumption that $\bar{\alpha}$ is sufficiently small that $\bar{\alpha} \approx -\ln(1-\bar{\alpha})$, whereas the Eyring equation is applicable to any value of $\bar{\alpha}$. In general, Eyring's equation gives reasonable estimates in rooms where there is uniform surface absorption and diffuse surface reflections, however, it is also appropriate in box-shaped rooms with uniform surface absorption and specular surface reflections (Hodgson, 1993, 1996).

1.2.6.3.2 Non-diffuse field: normal mode theory

In non-diffuse fields the decay curves cannot usually be approximated by a straight line across the entire 60 dB decay range. To understand some of the reasons for this, we return to consider local room modes in a box-shaped room. In each frequency band, the decay curve will be determined by the individual room modes that are decaying within that band, and the interaction between these modes.

We will focus on decay curves in the low-frequency range. When we consider the mode count in one-third-octave-bands for typical rooms, bands in the low-frequency range have relatively few modes compared to those in the mid- and high-frequency ranges (refer back to the 50 m^3 room in Fig. 1.14). In reality, we cannot strictly compartmentalize the decaying modes into individual frequency bands. This is due to the damping associated with each mode; a decaying mode may influence the decay in the two bands that are adjacent to the band in which the mode is strictly assumed to fall. However, compartmentalization is used here to provide some insight into the way that axial, tangential, and oblique modes determine the decay curve for a band. The normal mode theory used to calculate the decay curves is taken from Kuttruff (1979) and Bodlund (1980); the latter reference also provides corrections to earlier investigations by Larsen (1978).

Assume that we have a box-shaped room with locally reacting surfaces. This room contains a sound source that is fed by a sinusoidal signal with the same frequency as the mode of interest. In reality, most rooms have modes that are relatively closely spaced. This means that a sinusoidal signal will also excite other room modes unless all the surfaces have very low absorption coefficients and the modes are all well-separated in terms of frequency. However, here we will assume that we are able to excite only a single mode. When the sound source is stopped at time, $t = 0$, the waves continue to travel along the path that is defined for this particular room mode. Upon each reflection from a room surface, a fraction of the energy is reflected, and the remaining fraction is absorbed.

When looking at the reverberant decay of an individual mode, m, the mean-square pressure decays away exponentially according to

$$p^2(t) = p^2(0)\exp(-2\delta_m c_0 t) \tag{1.99}$$

where $\delta_m = \beta_{a,s}\,(\varepsilon_{p,m}/L_x + \varepsilon_{q,m}/L_y + \varepsilon_{r,m}/L_z)$ in which $\beta_{a,s}$ is the specific acoustic admittance, and $\varepsilon_{p,m}$, $\varepsilon_{q,m}$ and $\varepsilon_{r,m}$ correspond to mode, $f_{p,q,r}$ (if $p = 0$, then $\varepsilon_{p,m} = 1$ else $\varepsilon_{p,m} = 2$; if $q = 0$, then $\varepsilon_{q,m} = 1$ else $\varepsilon_{q,m} = 2$; if $r = 0$ then $\varepsilon_{r,m} = 1$ else $\varepsilon_{r,m} = 2$).

The reverberation time, T_m, for an individual mode can be calculated from Eq. 1.99 at time $t = T_m$ using

$$\frac{p_m^2(T_m)}{p_m^2(0)} = 10^{-6} = \exp\left(-2c_0 T_m \beta_{a,s}\left(\frac{\varepsilon_{p,m}}{L_x} + \frac{\varepsilon_{q,m}}{L_y} + \frac{\varepsilon_{r,m}}{L_z}\right)\right) \tag{1.100}$$

which gives,

$$T_m = \frac{3\ln 10}{c_0 \beta_{a,s}\left(\frac{\varepsilon_{p,m}}{L_x} + \frac{\varepsilon_{q,m}}{L_y} + \frac{\varepsilon_{r,m}}{L_z}\right)} \tag{1.101}$$

The denominator in Eq. 1.101 is referred to as the damping constant of the mode. From Eq. 1.101 it is possible to identify three trends for the different mode types when the specific acoustic admittance is independent of frequency: (1) the axial modes associated with each room dimension have different reverberation times to each other when $L_x \neq L_y \neq L_z$;

(2) when the tangential modes are considered in three groups defined by $p = 0$, $q = 0$, and $r = 0$, each group will have the same reverberation time; and (3) all oblique modes have the same reverberation time.

For engineering calculations it is convenient to relate the reverberation time directly to the absorption coefficient. Normal mode theory uses the specific acoustic admittance, which is the reciprocal of the specific acoustic impedance; hence it is linked to the absorption coefficient. From Eq. 1.76 we see that the absorption coefficient is dependent upon the angle of incidence and the specific acoustic impedance. Depending on the mode, the waves will be incident upon the room surfaces at different angles. For axial modes the waves always impinge upon two opposite surfaces at an angle of incidence that is normal to these surfaces. For oblique and tangential modes, the angle of incidence varies depending upon the mode and the room boundary upon which the waves are impinging. For simplicity, the angle dependence is ignored in the following examples and a single value for the specific acoustic admittance is used for all of the room surfaces. This still allows us to see the general effect of the modes on the decay curves; we simply acknowledge that the situation is more complex in reality.

Equation 1.101 can now be used to calculate the decay curve for each of the M individual modes within a frequency band. This can be compared with the decay curve for the frequency band itself. It is assumed that the sound source is fed with a white noise signal with an rms volume velocity spectral density, Q_{sd}. It is convenient to set the sound pressure level at $t = 0$ to a level of 60 dB for the frequency band, hence we need to establish the level at $t = 0$ for each of the M modes in that band. For the mth mode, the spatial average mean-square sound pressure at time $t = 0$ is (Bodlund, 1980)

$$\langle p_m^2 \rangle_s = \frac{\rho_0^2 c_0^4 Q_{\mathrm{sd}}^2 \pi}{12 V^2 \ln 10} T_m \tag{1.102}$$

for which it is assumed that the specific acoustic admittance for the room surfaces is a real value, much less than unity, and uniform over all the surfaces.

Using Eq. 1.102 to set the level for each mode at $t = 0$, the sound pressure level, $L_{\mathrm{p},m}(t)$, in decibels, for the mth decaying mode in a frequency band is

$$L_{\mathrm{p},m}(t) = 10 \lg \left(\frac{p_m(t)}{p_m(0)} \right)^2 = 60 - \frac{60t}{T_m} + 10 \lg \left(\frac{\langle p_m^2 \rangle_s}{\sum_{m=1}^{M} \langle p_m^2 \rangle_s} \right) = 60 - \frac{60t}{T_m} + 10 \lg \left(\frac{T_m}{\sum_{m=1}^{M} T_m} \right) \tag{1.103}$$

The sound pressure level, $L_{\mathrm{p}}(t)$, in decibels for the frequency band can then be calculated from the energetic sum of the decay curves for the individual modes in the band,

$$L_{\mathrm{p}}(t) = 10 \lg \left(\sum_{m=1}^{M} 10^{L_{\mathrm{p},m}(t)/10} \right) \tag{1.104}$$

We can now look at decays in rooms with the same volume (50 m^3) but different L_x, L_y, and L_z dimensions. The specific acoustic admittance for all room surfaces is assumed to be real, independent of frequency, and independent of the angle of incidence. Although it does not correspond to any particular material commonly used for walls and floors, a value of $\beta_{\mathrm{a,s}} = 0.01$ is used to give reverberation times less than 2 s. Note that smooth, heavy concrete walls and floors would usually have much smaller values, which would lead to longer reverberation times. In contrast to measured decay curves, the decay curves from this model can be evaluated from

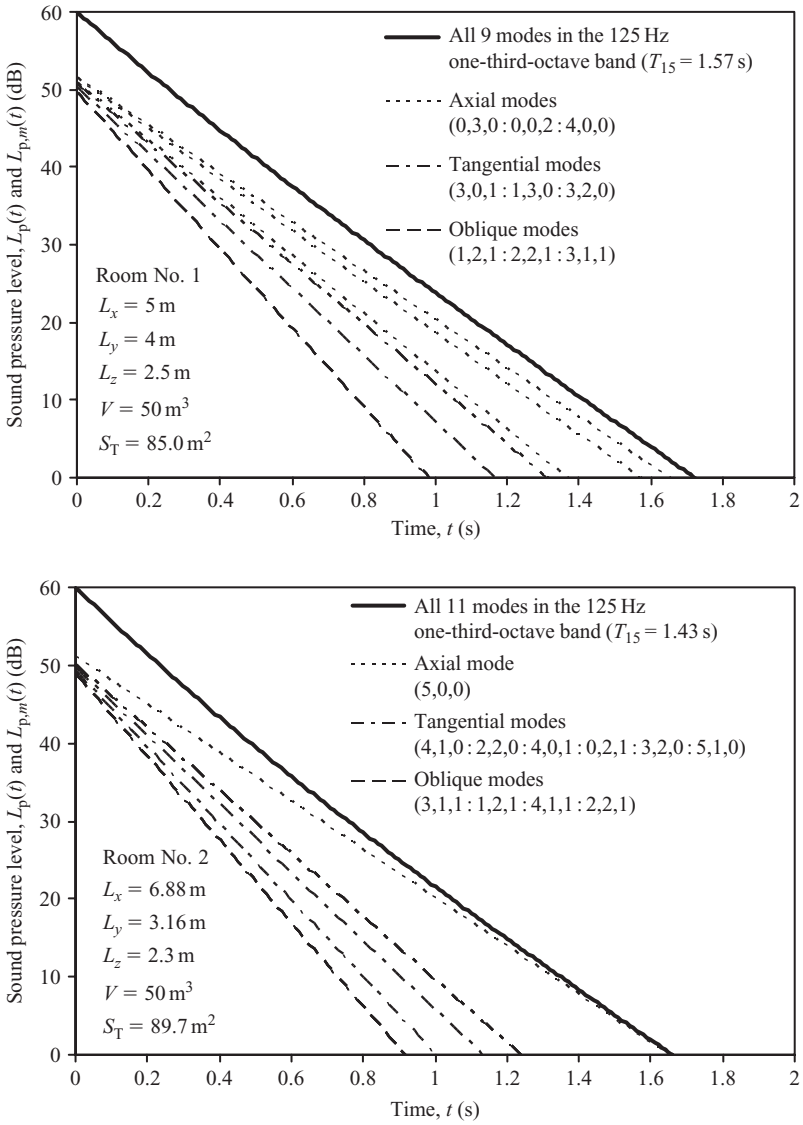

Figure 1.20

Decay curves for box-shaped rooms No. 1 and No. 2. Each room has a volume of 50 m^3 but with different L_x, L_y, and L_z dimensions. The curves are shown for individual modes in the 125 Hz one-third-octave-band along with the resulting curve for that band.

$t = 0$ to calculate the reverberation time. This is because the model does not include the effect of direct sound from the sound source, and, unlike a measurement, there is no distortion of the initial part of the decay curve from the signal processing.

As sound fields in practice can rarely be considered as diffuse in the low-frequency range we will initially look at the 125 Hz one-third-octave-band. The decay curves from two different 50 m^3 rooms (No. 1 and No. 2) are shown in Fig. 1.20 for the frequency band and the individual

modes in this band. For each individual mode the decay curves are straight lines. In contrast, the resulting decay curve for the frequency band is a curve; this is easier to see if a straight edge is placed against it. The decay curves for these two rooms are different. However, in this particular example the initial part of the decay curve has a similar slope in both rooms, hence the reverberation time, T_{15}, is similar too.

The axial modes tend to have longer reverberation times than the tangential modes, which, in turn, tend to be higher than for the oblique modes. For this reason the energy of individual axial modes at $t = 0$ is slightly higher than individual tangential or oblique modes. We recall that the decay curve for the frequency band is calculated from the energetic sum of the decays for the individual modes (Eq. 1.104). Therefore, it is only in the early part of the decay, say within the initial 20 or 30 dB, that the majority of the different room modes play a role in determining the decay curve of the frequency band. In the later part of the decay, the decay curve for the frequency band is primarily determined by the modes with the longest reverberation times. These are always axial modes. This is clearly seen with room No. 2 where there is only a single axial mode, $f_{5,0,0}$ in the frequency band. In the late part of the decay curve, the slope is primarily determined by this one axial mode. Hence for typical rooms in the low-frequency range, the axial modes play an important role in determining the decay curve of the frequency band. This will be more apparent when one room dimension is significantly longer than the other two dimensions. In this situation, the decay curve of the frequency band is predominantly determined by the axial mode(s) with wave propagation along the longest dimension. This allows some insight into which surfaces require low-frequency absorbers to reduce the reverberation time of the frequency band by reducing the reverberation time of specific modes.

In practice, the measured decay curve for the frequency band will fluctuate about the predicted straight line decay due to interaction between the modes causing beating. Also, in using a single value for the specific acoustic admittance we have effectively assumed a single absorption coefficient for all angles of incidence which is not appropriate for many common walls and floors. In the low-frequency range the absorption coefficient can be lower at normal incidence than at oblique incidence. This would make the curvature more distinct due to even longer reverberation times for the axial modes.

The model also allows us to compare the decay curve for a diffuse field with the decay curves for individual frequency bands as the band centre frequency increases. To do this we will choose the 100, 1000, and 5000 Hz one-third-octave-bands for a different 50 m^3 room (room No. 3). It is important to note that the assumption of purely specular reflection for the 1000 and 5000 Hz bands is unrealistic in practice as walls and floors are often slightly irregular with scattering objects near the room surfaces. However, it gives us a useful insight into the effects of different mode counts and the different blends of mode types in each frequency band. Figure 1.21a shows the decay curves for the three frequency bands. The curvature of the decay in the 100 Hz band is in marked contrast to the approximately straight decay of the 5000 Hz band. The reasons for this difference can be seen by grouping together the decay curves for each mode type (axial, tangential, or oblique) as shown in Fig. 1.21b. In the 100 Hz band the initial 20 dB decay is determined by all three mode types. However, the later part of the decay curve is predominantly determined by the axial modes with minimal influence from the tangential and oblique modes. This is in contrast to the 1000 and 5000 Hz bands where the number of axial modes is small compared to the number of tangential or oblique modes; hence, there is only a minor influence from the axial modes on the decay curve for the frequency band. As the frequency increases, there are many more oblique modes than axial or tangential

modes. As all oblique modes have the same reverberation time, and the decay curve for each individual mode is a straight line, it follows that the decay curve at high frequencies tends towards a straight line determined by the oblique modes. This is seen in Fig. 1.21b where the decay curve for the 5000 Hz band is very similar to the grouped decay curve for the oblique modes.

For a room with uniform locally reacting surfaces, normal mode theory gives a useful insight into the reasons for curvature of the decay curves. However, it does not fully describe the degree of curvature that occurs in practice. This is partly due to the fact that walls and floors are not purely locally reacting; they can act as surfaces of extended reaction.

Locally reacting surfaces and surfaces of extended reaction: It is very convenient to be able to consider the reverberation time as independent of any interaction between the room modes and the structural modes of the walls and floors. So far it has been assumed that although the sound waves impinging upon a surface are absorbed, this absorption is a 'local matter' between the sound wave and the point on the surface from which it is reflected. From the point-of-view of an impinging sound wave there are two types of room surface that are responsible for absorption: locally reacting surfaces and surfaces of extended reaction (Morse and Ingard, 1968). These two types can be defined by referring to the normal acoustic surface impedance; this is the ratio of the complex sound pressure at the surface to the component of the complex sound particle velocity that is normal to the surface. If a wave impinges upon a point on the surface, a locally reacting surface is one where the particle velocity normal to the surface is only affected by the sound pressure at that point, and is unaffected by the pressure at adjacent points on the surface. In contrast, a surface of extended reaction is one where the particle velocity normal to the surface is affected by the pressure at adjacent points on the surface. Surfaces of extended reaction therefore include plates undergoing bending wave motion, and porous surfaces where the sound propagates inside the porous material in a direction parallel to the surface.

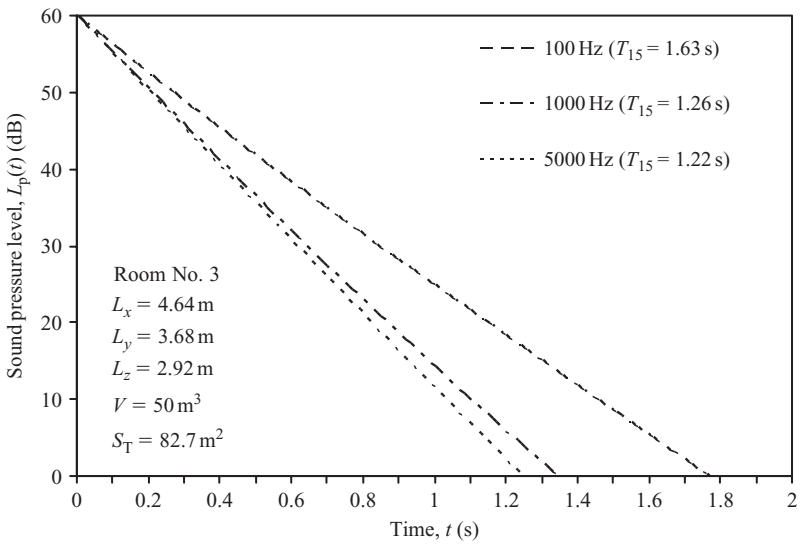

Figure 1.21(a)

Decay curves for box-shaped room No. 3 (100, 1000, and 5000 Hz one-third-octave-bands).

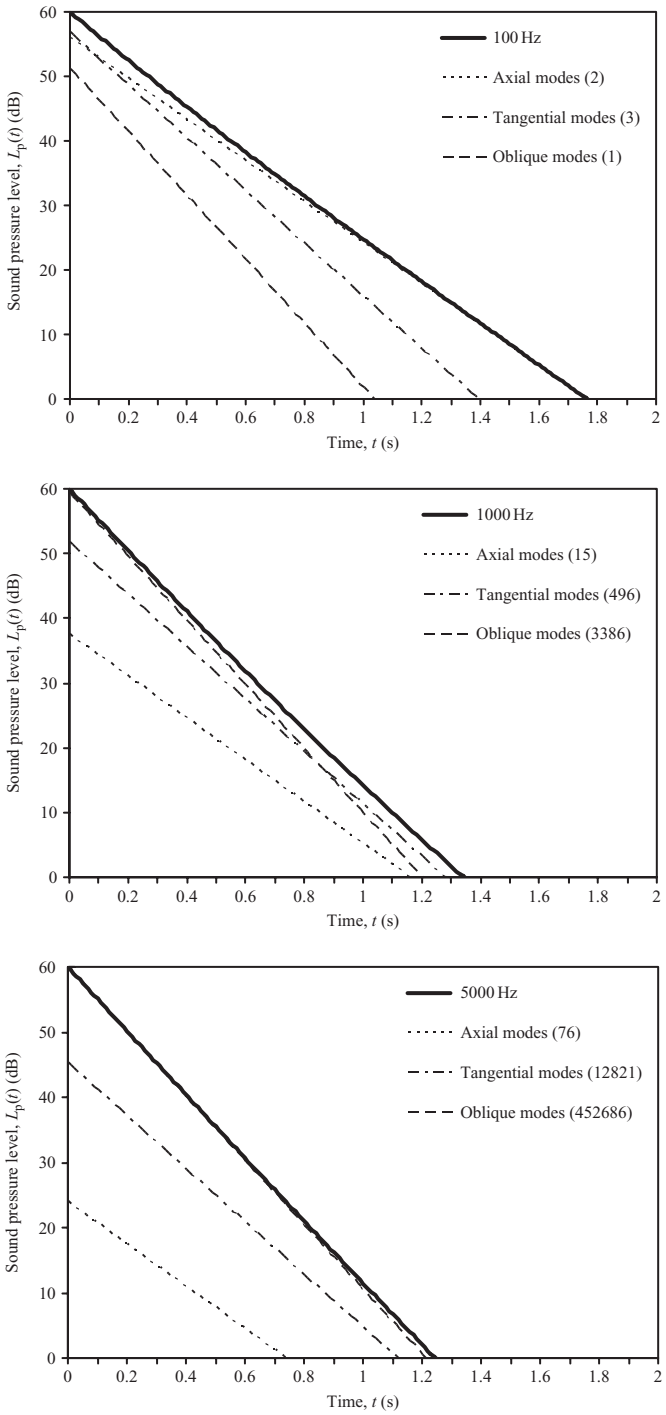

Figure 1.21(b)

Decay curves for the 100, 1000, and 5000 Hz one-third-octave-bands along with the grouped decay curve for each mode type. The number of modes corresponding to each mode type in the one-third-octave-band are shown in brackets.

For practical purposes, the assumption of locally reacting room surfaces is very useful in simplifying the calculation of reverberation time. In many rooms, small areas of rigid frame, porous, absorbent material are fixed to the room surfaces to reduce the reverberation time. Many of these absorbers can be considered as locally reacting. The assumption of locally reacting surfaces is often reasonable due to other factors that introduce uncertainty into the calculation; these are non-uniform distribution of absorption, application of laboratory measurements of absorption coefficients to rooms with non-diffuse fields, specific room geometry, and scattering from objects and surfaces in the room. Bare walls and floors undergoing bending wave motion are surfaces of extended reaction, responsible for transmitting sound to other parts of the building. In this situation the reverberation time is not only determined by the room modes, it is determined by the interaction between the room modes and the structural modes of the walls and floors (Pan and Bies, 1988). This blurs the boundary between the study of room acoustics and structure-borne sound.

For a room with locally reacting surfaces that have a frequency-independent value for the specific acoustic admittance, the normal mode model indicates that the group of oblique modes will have the same reverberation time, and each group of tangential modes with $p = 0$ or $q = 0$ or $r = 0$ have the same reverberation time. However, experimental evidence from a reverberation chamber with 280 mm thick concrete walls and floors indicates that there can be significant variation between the reverberation times of individual modes within these groups (Munro, 1982). This is primarily because the walls and floors are not locally reacting (Pan and Bies, 1988). It has been shown both theoretically and experimentally that the reverberation time in a room can be altered by changing the total loss factor and/or the modal density of its walls and floors (Pan and Bies, 1990). Experiments in the same reverberation chamber demonstrate that by increasing the total loss factor of a bending wave mode on one concrete wall (by wedging wooden blocks between this wall and another wall to increase the structural coupling losses), it is possible to change the reverberation time of an individual room mode (Pan and Bies, 1988). However, this needs to be kept in perspective when predicting reverberation times in rooms. There are other reasons why it is difficult to accurately predict reverberation times; mainly the existence of non-diffuse sound fields and the application of laboratory measurements of absorption or scattering coefficients to a specific situation in the field. The fact that walls and floors are not locally reacting is simply one more reason.

In practice, walls and floors are usually partly or completely covered with a locally reacting absorber, such as carpet on a heavy concrete floor. Therefore it is not always necessary for calculations to consider the effect of modal interaction; reasonable estimates can often be obtained by assigning an absorption coefficient to the areas of wall and floor that are not covered by the locally reacting absorber. This absorption coefficient may be based on measurements or empiricism. In many cases the wall or floor will act as both a surface of extended reaction and a locally reacting surface, although one of these may be more important than the other. For example, some masonry/concrete walls have highly porous surfaces. A reasonable estimate of the reverberation time can often be found by using a measured absorption coefficient and simply treating the wall as a locally reacting surface; it may be unnecessary to consider the fact that it also acts as a surface of extended reaction due to bending wave vibration. This allows calculation of the room reverberation time using absorption coefficients in equations such as Eq. 1.94 or 1.96.

Despite the fact that real walls and floors are not purely locally reacting, normal mode theory shows that the curved decay for a frequency band is due to the different reverberation

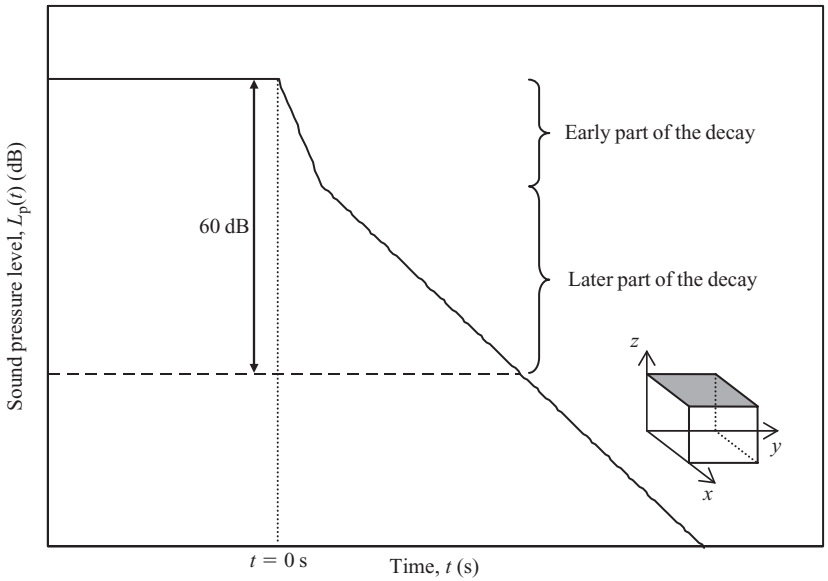

Figure 1.22

Example of a decay curve with a double slope; this can occur in rooms with a highly absorptive ceiling, but where the walls and the floor have relatively low absorption.

times for the modes within that band. Interaction between room modes and structural modes therefore results in a range of reverberation times for individual modes; hence there will still be curved decays in some frequency bands. In fact, measured data suggest that the range of reverberation times for individual modes is much larger than calculated from normal mode theory, resulting in decay curves with a greater degree of curvature (Bodlund, 1980).

1.2.6.3.3 *Non-diffuse field: non-uniform distribution of absorption*

Non-diffuse fields also occur due to non-uniform distribution of absorption over the room surfaces; one common example occurs when there is a highly absorptive ceiling but the walls and the floor have relatively low absorption. In these situations the decay curve can also show curvature or a distinct double slope as illustrated in Fig. 1.22. Considering the different modes, it is possible to make a basic qualitative assessment of the reasons for this double slope. When the early part of the decay is predominantly determined by the oblique modes (as in the previous example for the 5000 Hz band) we can expect large numbers of these modes to be rapidly attenuated as they impinge upon the highly absorbent ceiling. This gives rise to the fast decay rate in the early part of the decay curve. However, some of the axial and tangential modes will only be reflected from the side walls which have low absorption. Hence we can expect these modes to have relatively long reverberation times and contribute to the late part of the decay, which compared to the early part, will have a much slower rate of decay. The main features of the decay curve can be predicted by dividing the modes into two groups (Nilsson, 2004). The first group contains modes where the waves propagate almost parallel to the ceiling (grazing waves). In the second group the modes propagate at angles that are oblique to the ceiling (non-grazing waves). Using this grouping, the non-grazing waves determine the early part of the decay curve and the grazing waves determine the late part of the curve. Other prediction

formulae for rooms with non-uniform distribution of absorption can be found in work by Fitzroy (1959), Arau-Puchades (1988), and Neubauer (2001).

1.2.6.4 Internal loss factor

In later chapters we will look at predicting sound transmission between two rooms using Statistical Energy Analysis (SEA). It will then become useful to denote the different rooms using a subscript. The internal loss factor is usually denoted as η_{int} but here we will start using the notation, η_{ii}, for the internal loss factor of a room subsystem, i, in an SEA model.

Internal losses describe the conversion of sound energy into heat by absorption; if this is the only process that is described by the total absorption area, the internal loss factor is given by

$$\eta_{\text{int}} = \eta_{ii} = \frac{c_0 A_{\text{T}}}{8\pi f V} \tag{1.105}$$

1.2.6.5 Coupling loss factor

The coupling loss factor, η_{ij}, describes resonant transmission between a room (subsystem i) and a plate (subsystem j) that faces into the room. This is described in Section 4.3.1.1.

1.2.6.6 Total loss factor

The total loss factor, η_i, of a subsystem, i, is the sum of its internal loss factor and all the coupling loss factors from that subsystem,

$$\eta_i = \eta_{ii} + \sum_{j=1}^{J} \eta_{ij} \quad (i \neq j) \tag{1.106}$$

and is related to the reverberation time by

$$\eta_i = \frac{6 \ln 10}{2\pi f T} = \frac{2.2}{fT} \tag{1.107}$$

For most rooms, the sum of the coupling loss factors is much smaller than the internal loss factor, and the latter provides a reasonable estimate of the total loss factor. For a room where the total absorption area, A_{T}, is calculated from the measured reverberation time (and hence includes both internal and coupling losses), the total loss factor can be written as

$$\eta_i = \frac{c_0 A_{\text{T}}}{8\pi f V_i} \tag{1.108}$$

1.2.6.7 Modal overlap factor

The modal overlap factor, M, describes the degree of overlap in the modal response. It is defined as the ratio of the 3 dB modal bandwidth, $\Delta f_{3\,\text{dB}}$, to the average frequency spacing between mode frequencies, Δf, and is calculated from

$$M = \frac{\Delta f_{3\,\text{dB}}}{\Delta f} = f \eta n \tag{1.109}$$

where $\Delta f_{3\,\text{dB}}$ (which is also referred to as the half-power bandwidth) is equal to the frequency spacing between the two points on the modal response where the level is 3 dB lower than the peak level, and η is the loss factor.

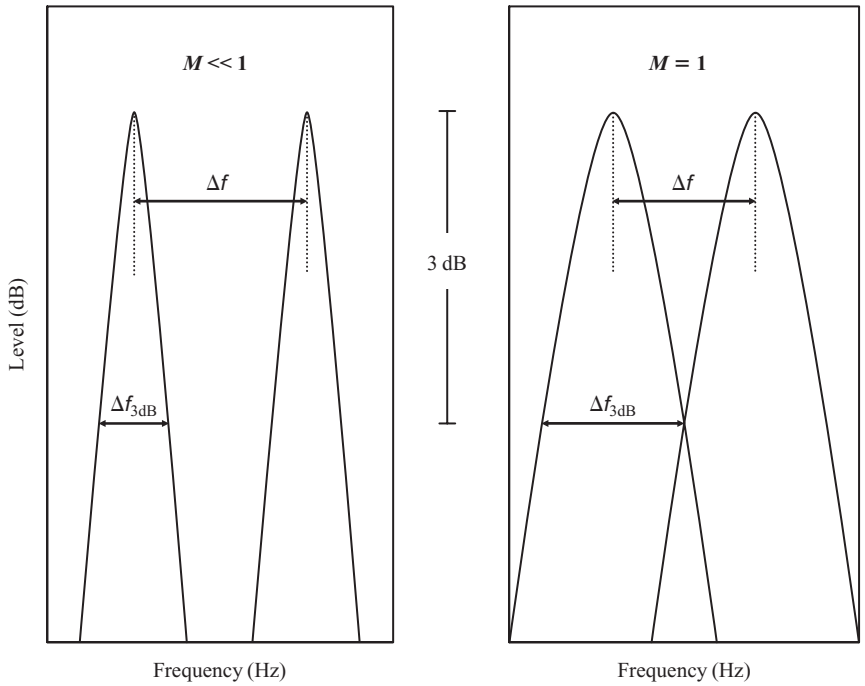

Figure 1.23

Modal response for two adjacent modes with modal overlap factors, $M \ll 1$ and $M = 1$.

An example of the response due to two adjacent modes with a frequency spacing, Δf is shown in Fig. 1.23. This idealized response could represent either the sound pressure level in a room or the velocity level on a wall. When $M \ll 1$ there is no overlap of the 3 dB bandwidths and there can be deep troughs between the two modes. When $M = 1$, the modal responses overlap at the point where the levels are 3 dB below the peak level. As $M \gg 1$ the response becomes increasingly uniform due to the absence of deep troughs.

Figure 1.24 shows the modal overlap factor for different room volumes and reverberation times. The modal overlap factor is often less than unity in the low-frequency range.

A cut-off frequency, f_M, that identifies the lowest frequency associated with a minimum value of the modal overlap factor can be found by substituting Eqs 1.59 and 1.107 in Eq. 1.109 to give

$$f_M = \sqrt{\frac{MTc_0^3}{8.8\pi V}} \tag{1.110}$$

With a modal overlap factor of three, this cut-off frequency is often referred to as the Schroeder cut-off frequency, f_S, and quoted as (Schroeder, 1962)

$$f_S = 2000\sqrt{\frac{T}{V}} \tag{1.111}$$

For a room of fixed volume, long reverberation times mean that the damping loss factor is low; hence the modal overlap is also low which results in higher cut-off frequencies. Usually we want to calculate the cut-off frequency from measured reverberation times. When these are approximately constant over the building acoustics frequency range, the average reverberation

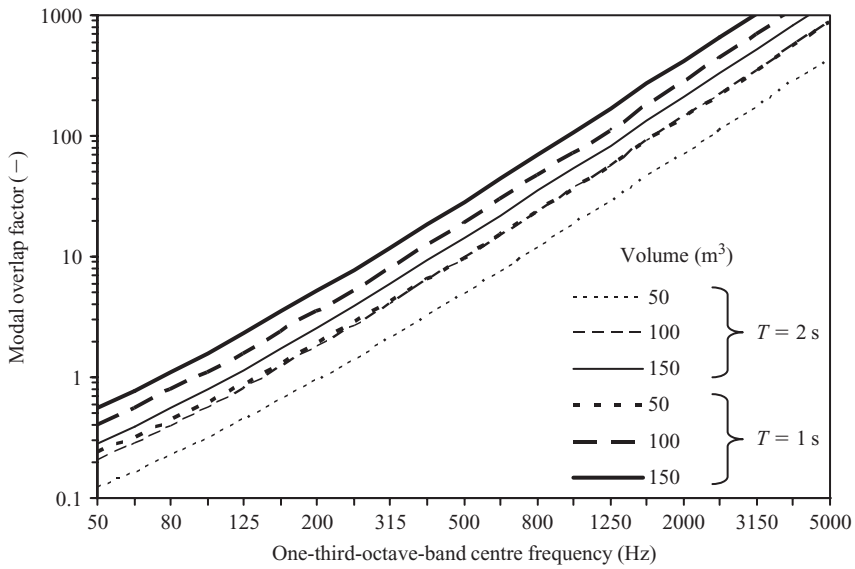

Figure 1.24

Modal overlap factors for different room volumes and reverberation times.

time can be used. Otherwise, an initial estimate for the cut-off frequency can be found from the arithmetic average of the reverberation time over a large part of the frequency range. This will then identify a more relevant part of the frequency range over which the reverberation times can be averaged to refine the estimate.

Figure 1.25 shows the Schroeder cut-off frequency for a range of room volumes and reverberation times. For room volumes less than 60 m^3 with reverberation times between 0.5 and 1 s, the lowest cut-off frequency will be in the 200 Hz one-third-octave-band, and often in higher frequency bands.

1.2.7 Spatial variation in sound pressure levels

In the measurement and prediction of sound insulation it is almost always the temporal and spatial average sound pressure level in each room that is of interest rather than the level at a particular point in space at a particular point in time. For this reason, measurement procedures require time-averaged sound pressure levels to be measured at a number of different points in a room and averaged. However, an average value is only useful in the analysis of sound insulation measurements and predictions if we know what it represents. It is therefore necessary to look at the spatial variation of time-averaged sound pressure levels both in theory and in practice.

We start with the theory for the sound field near room boundaries, and then move on to discuss the sound pressure level distribution in a room due to individual modes and in the idealized diffuse sound field. We then consider practical situations where there is a direct sound field near the loudspeaker, and spaces in which the sound pressure level decreases with distance. This allows us to interpret some example measurements of sound fields in frequency bands, and to see the benefit in using statistical descriptions for the spatial variation in the sound pressure level.

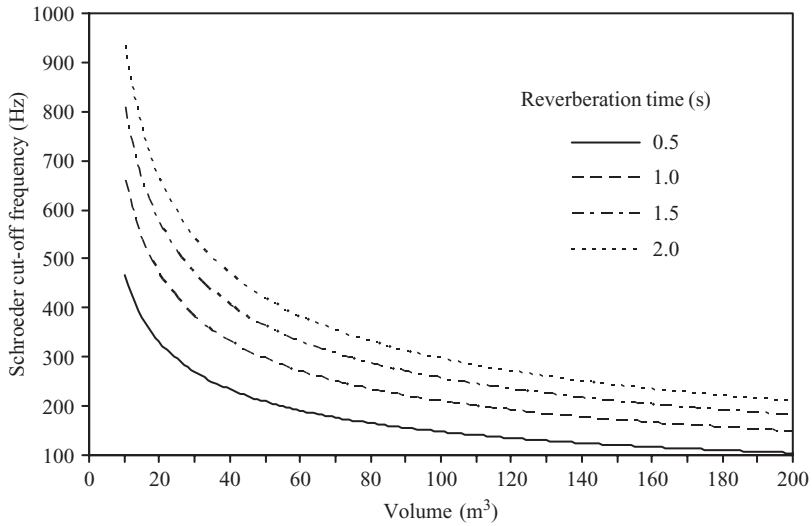

Figure 1.25

Schroeder cut-off frequency for different room volumes and reverberation times.

1.2.7.1 Sound fields near room boundaries

In a diffuse field the phase relationship between all waves passing through a single point in space is random. However, near a room boundary there will be a non-random phase relationship between the incident wave and the reflected wave. When a sound wave is incident upon a room boundary the reflected wave combines with the incident wave to give an interference pattern in the vicinity of this boundary (Waterhouse, 1955).

Initially it is assumed that all the room boundaries are perfectly reflecting and rigid. Under this assumption the sound field close to any surface, edge, or corner in a room can be compared to the sound field far from the surface. This approach is often used to quantify the total sound energy stored in a room where it can be assumed that there is a diffuse field in the central zone of the room. In practice there are a wide range of acoustic surface impedances for walls and floors in buildings and it is necessary to be aware of their effect on the sound field.

1.2.7.1.1 Perfectly reflecting rigid boundaries

To gain an insight into the sound field near a wall or floor in a room, we start with the situation where a harmonic plane wave is incident upon a surface, such as a wall or floor, at an angle that is perpendicular to the surface, i.e. at normal incidence. The surface is positioned at $x = 0$ in the yz plane (see Fig. 1.26). It is assumed that the surface is large compared to the wavelength and that there are no other surfaces that affect the sound field. The incident wave, $\hat{p}_+ \exp(-ikx)$ travels from $-\infty$ towards $x = 0$ where it is reflected from the surface to give the reflected wave, $\hat{p}_- \exp(ikx)$. This conveniently means that the exponential terms equal unity at the surface where $x = 0$. The resulting sound pressure due to the incident and reflected waves is

$$p(x,t) = [\hat{p}_+ \exp(-ikx) + \hat{p}_- \exp(ikx)] \exp(i\omega t) \tag{1.112}$$

where $\hat{p}_+$ is an arbitrary constant for the incident wave. The constant for the reflected wave, $\hat{p}_-$, is related to $\hat{p}_+$ by the reflection coefficient of the surface, R (Eq. 1.67), where $\hat{p}_- = R\hat{p}_+$.

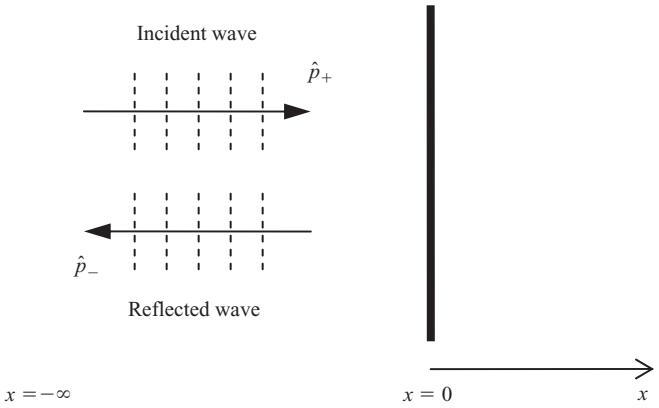

Figure 1.26

Plane waves incident upon, and reflected from a room boundary.

By squaring the real part of Eq. 1.112 and taking the time-average, the mean-square sound pressure at a distance, x, from the surface in the negative x-direction is

$$\langle p^2 \rangle_t = \hat{p}_+^2 (0.5 + 0.5|R|^2 + |R| \cos(2kx + \gamma)) \tag{1.113}$$

For perfect reflection from a rigid surface there is no phase shift (i.e. $\gamma = 0$), so $R = |R| = 1$ and Eq. 1.113 becomes

$$\langle p^2 \rangle_t = \hat{p}_+^2 (1 + \cos(2kx)) \tag{1.114}$$

At $x = 0$, the sound pressure for the incident and reflected waves is in phase, so $\langle p^2 \rangle_t = 2\hat{p}_+^2$. At $x = \lambda/4$ the incident and reflected waves are out of phase with each other and the mean-square pressure is zero.

The particle velocities for the incident and reflected waves are found from the sound pressure terms using Eq. 1.18. This gives $\frac{\hat{p}_+}{\rho_0 c_0} \exp(-ikx)$ for the incident wave and $-\frac{\hat{p}_-}{\rho_0 c_0} \exp(ikx)$ for the reflected wave that travels in the opposite direction. The resulting particle velocity is,

$$u(x,t) = \frac{1}{\rho_0 c_0} [\hat{p}_+ \exp(-ikx) - \hat{p}_- \exp(ikx)] \exp(i\omega t) \tag{1.115}$$

At $x = 0$, the particle velocity is zero when the surface is perfectly reflecting and rigid (i.e. $\hat{p}_- = \hat{p}_+$).

In practice, sound waves in a room are incident from many different directions upon a reflecting surface, so the next step is to consider a single wave that is incident at an angle, θ, to the x-axis. For the reflected wave we will assume specular reflection from the surface. For an oblique angle of incidence, the Cartesian coordinate system is rotated by θ so that x in Eq. 1.112 is replaced by x', where $x' = x \cos\theta + y \sin\theta$. This gives

$$p(x,y,t) = [\hat{p}_+ \exp(-ik(x\cos\theta + y\sin\theta)) + \hat{p}_- \exp(-ik(-x\cos\theta + y\sin\theta))] \exp(i\omega t) \tag{1.116}$$

Hence for oblique incidence, the time-averaged mean-square pressure at a distance, x, from a perfectly reflecting, rigid surface is

$$\langle p^2 \rangle_t = \hat{p}_+^2 (1 + \cos(2kx\cos\theta)) \tag{1.117}$$

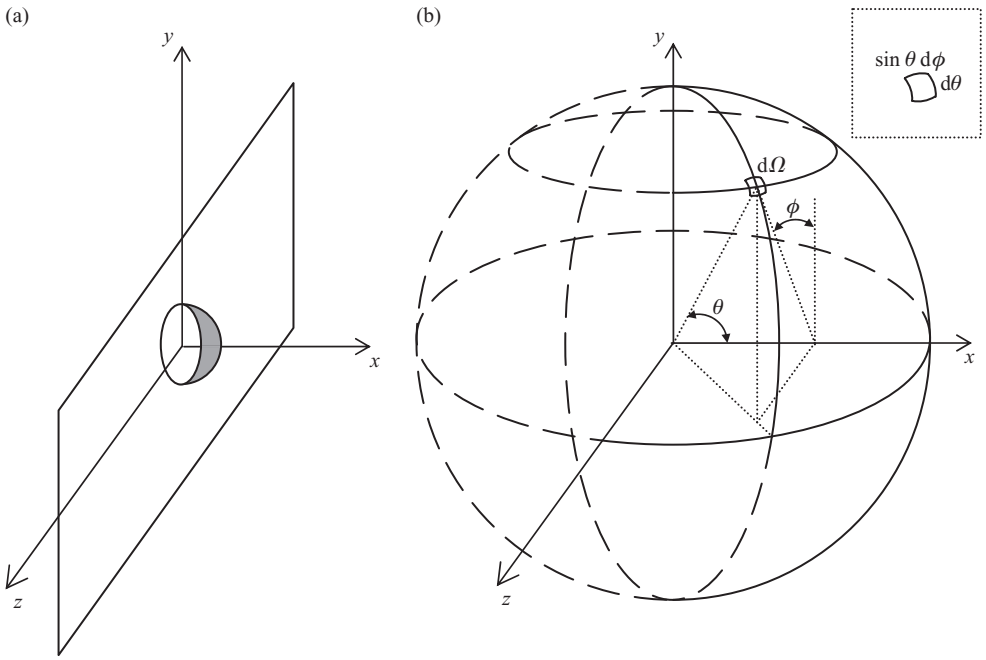

Figure 1.27

(a) Sound waves incident from all possible angles upon a perfectly reflecting surface form a hemisphere around a small area on the surface. (b) Spherical coordinate system with the element of the solid angle used to average the mean-square pressure over the hemisphere.

We can now consider waves that are incident upon the surface from all possible angles. This forms a hemisphere that encloses a small area on the surface as shown in Fig. 1.27. The incident waves are assumed to be incoherent, i.e. to have random phase, therefore the mean-square pressure in Eq. 1.117 can be averaged over all possible angles of incidence using

$$\langle p^2 \rangle_t = \frac{1}{2\pi} \int_0^{2\pi} \int_0^{\pi/2} [\hat{p}_+^2 (1 + \cos(2kx \cos\theta))] \sin\theta \, \mathrm{d}\theta \mathrm{d}\phi = \hat{p}_+^2 \left(1 + \frac{\sin(2kx)}{2kx}\right) \tag{1.118}$$

where the spherical coordinate system is shown in Fig. 1.27 and the element of the solid angle, $\mathrm{d}\Omega$, is $\sin\theta \, \mathrm{d}\theta \mathrm{d}\phi$.

From Eq. 1.118 the asymptotic value for the mean-square pressure at a distance far from the surface, $\langle p_\infty^2 \rangle_t$, is equal to $\hat{p}_+^2$. At this point it is convenient to change over from using negative x values for the distance and use positive values for the distance, d, along the x-axis. Hence the ratio of the mean-square pressure at a distance, d, from this surface, to the mean-square pressure at a point far away from the surface is (Waterhouse, 1955)

$$\frac{\langle p^2 \rangle_t}{\langle p_\infty^2 \rangle_t} = 1 + \frac{\sin(2kd)}{2kd} \tag{1.119}$$

This is plotted in Fig. 1.28 as the sound pressure level difference in decibels against $2kd$. The smallest distance at which there is no difference between the level near the surface and the level far away from the surface occurs at $2kd = \pi$, where $d = \lambda/4$. The largest level differences

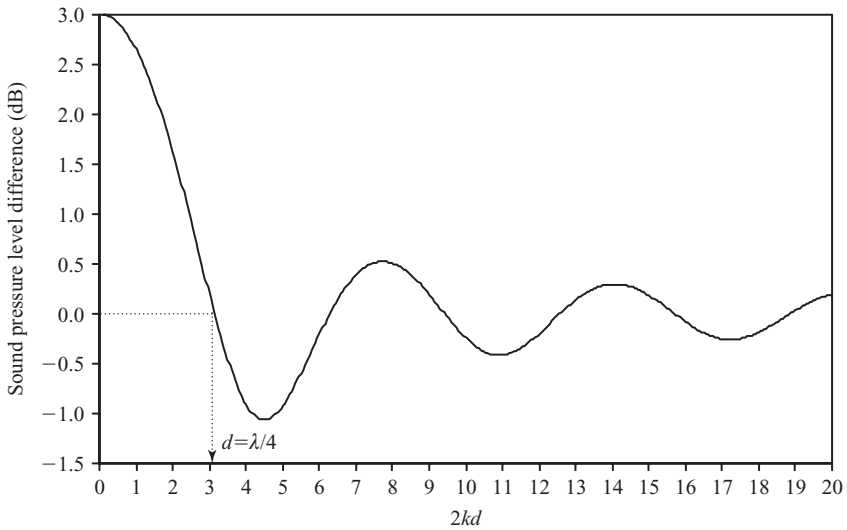

Figure 1.28

Sound pressure level difference between a point at a distance, d, from a perfectly reflecting surface and a point far away from the surface.

(magnitude) occur at distances less than $\lambda/4$ from the surface. At high frequencies and/or large distances from the surface the sound pressure level difference tends towards 0 dB. If we start at a distance $d = \lambda/4$ from the surface and move towards the surface the level difference tends towards 3 dB. Equation 1.119 applies to single frequencies rather than frequency bands, although it also gives reasonable estimates for one-third-octave-bands and octave-bands of white noise at distances up to $\lambda/4$ from the surface (Waterhouse, 1955). To illustrate its practical application, the level difference against frequency at different distances from the reflecting surface is shown in Fig. 1.29.

When measuring the reverberant sound pressure level in a room it is necessary to avoid measuring near the room boundaries in these interference patterns. The requirements for the minimum distance between a microphone and the room boundaries depend on the level of accuracy required, and the practical aspect of finding sufficient measurement positions in small rooms. Measurements are usually carried out simultaneously in all the frequency bands over the building acoustics frequency range. For this reason it is common to quote the minimum distance as a fixed value based upon the lowest frequency of interest; rather than quoting a fraction of a wavelength. In the Standards for field and laboratory sound insulation measurements the minimum measurement distances from the room boundaries are quoted as 0.5, 0.7, and 1.2 m (ISO 140 Parts 3, 4, 5, 6, & 7). Equation 1.119 can be used to estimate the level difference at these distances from walls or floors. At 50 Hz the level difference is 1.4 dB for a distance of 1.2 m. At 100 Hz a level difference of 1.8 dB occurs for a distance of 0.5 m, and 0.8 dB for 0.7 m.

The interference patterns at the edges and the corners also need consideration. The ratio for the mean-square sound pressure at a distance, d, from an edge or a corner due to both the incident and reflected waves, relative to the mean-square sound pressure at a point far away from the edge or corner is given by Waterhouse (1955).

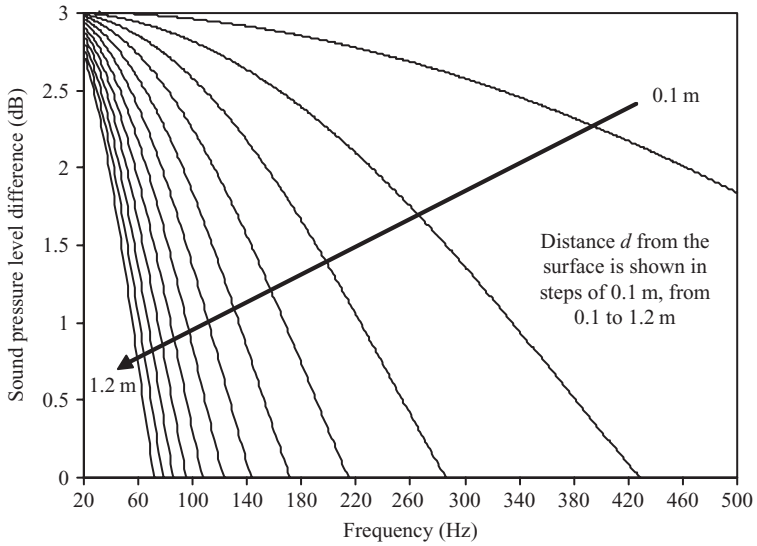

Figure 1.29

Sound pressure level difference between a point at a distance, d, from a perfectly reflecting surface and a point far away. Note that the curves have been truncated at the frequency where $d = \lambda/4$. These single frequency values are also applicable to white noise in one-third-octave or octave-bands.

For an edge that lies along the x-axis, the mean-square sound pressure ratio at a point (y, z) is

$$\frac{\langle p^2 \rangle_t}{\langle p_\infty^2 \rangle_t} = 1 + j_0(2ky) + j_0(2kz) + j_0(2kd_x) \tag{1.120}$$

where $j_0(a) = \sin(a)/a$ and $d_x^2 = y^2 + z^2$.

For a corner positioned at the origin of the Cartesian coordinates the mean-square sound pressure ratio at a point (x, y, z) is

$$\frac{\langle p^2 \rangle_t}{\langle p_\infty^2 \rangle_t} = 1 + j_0(2kx) + j_0(2ky) + j_0(2kz) + j_0(2kd_x) + j_0(2kd_y) + j_0(2kd_z) + j_0(2kd) \tag{1.121}$$

where $d_y^2 = x^2 + z^2$, $d_z^2 = x^2 + y^2$ and $d^2 = x^2 + y^2 + z^2$.

Figure 1.30 allows comparison of the sound pressure level difference for a surface, edge, and a corner. To create this particular example, d is used to represent different distances from the surface, edge, or corner: namely, the distance perpendicular to the surface along the x-axis, the distance from the edge along the line $y = z$, and the distance from the corner along the line $x = y = z$. At the boundary position where $d = 0$, the level differences are 3, 6, and 9 dB for the surface, edge, and corner respectively. Image sources can be used to visualize this finding. Figure 1.31 shows the actual source for a plane wave front near these boundaries along with the image sources. For the surface, edge, and corner there are 1, 3, and 7 reflected waves respectively; this gives the total number of sources as 2, 4, and 8 respectively. The image sources have the same amplitude and phase as the actual source, therefore the sound pressure from the actual source and the image sources is in phase at the boundary position ($d = 0$). Hence the level differences correspond to 10 times the logarithm (base 10) of the total number of sources.

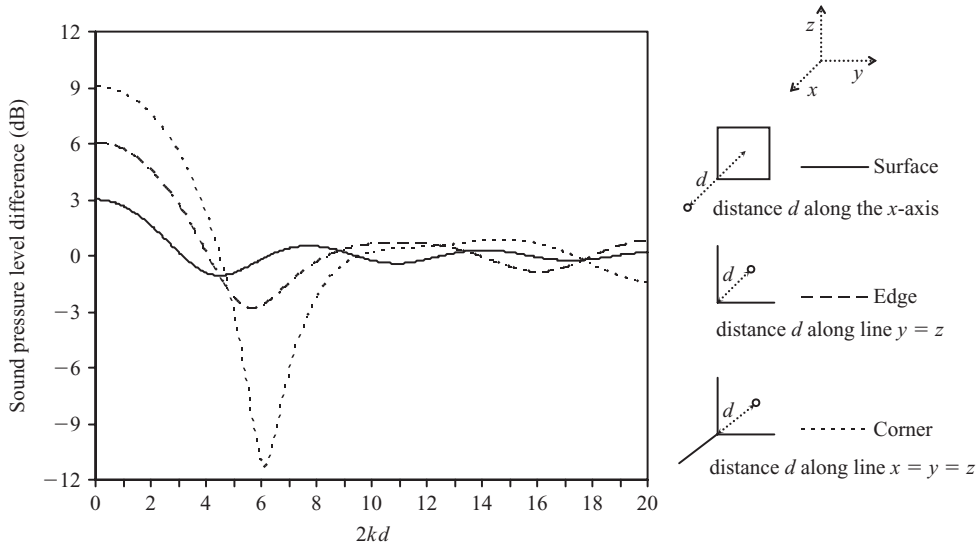

Figure 1.30

Sound pressure level difference between a point at a distance, *d*, from a surface, edge, and corner relative to a point far away.

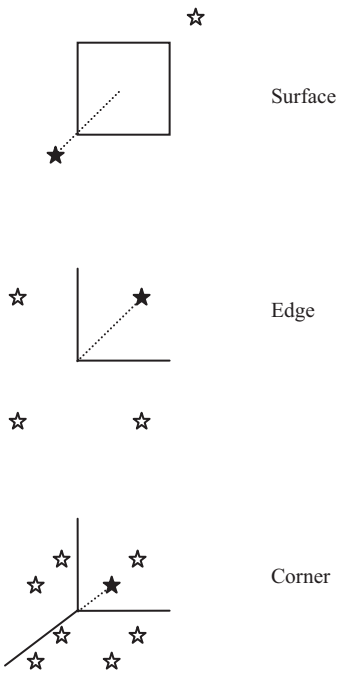

Figure 1.31

Source (★) and image sources (☆) for a plane wave front incident upon a surface, edge, and corner.

The level differences due to interference patterns near edges and corners tend to be larger in magnitude than with a surface and extend to greater distances. However, we will soon look at calculating the total energy stored in a room where it is necessary to account for the energy stored in the interference patterns of surfaces, edges, and corners. When the sound field in the central zone of the room is reasonably diffuse it is found that the energy stored in edge and corner zones is relatively small compared to the energy stored near room surfaces. This is because the surfaces account for large areas in most rooms (Waterhouse, 1955).

1.2.7.1.2 Other boundary conditions

Up till now we have assumed that the room boundaries are perfectly reflecting and rigid, i.e. the normal acoustic surface impedance is infinite. Therefore at the surface, the particle velocity normal to these boundaries is zero. Many walls and floors in buildings have low-absorption coefficients in the low-frequency range where interference patterns in rooms are important; so the assumption that they are perfectly reflecting is reasonable. However, habitable rooms almost always have fairly absorptive surfaces to provide suitable acoustics for the occupants of the building so we need to consider the effect of absorption. In addition we know that real room surfaces are not rigid because they are set into vibration by impinging sound waves. In reality the sound waves that impinge upon the walls and floors cause them to vibrate; hence the particle velocity at, and normal to the room surfaces must be the same as the surface vibration of the wall or floor, and not zero. When we focus on sound transmission, the vibration of these room surfaces becomes particularly important. Room surfaces range from a single sheet of 12.5 mm plasterboard on a timber frame, to a few hundred millimetres of solid concrete; all of these surfaces have finite values for the acoustic surface impedance.

If we restrict our attention to sound waves impinging upon a surface at normal incidence, then the effect of absorptive non-rigid surfaces can be assessed by using Eq. 1.113 to calculate the mean-square pressure. This requires knowledge of the reflection coefficient which can be calculated from the specific acoustic impedance using Eq. 1.74, and can be related to the absorption coefficient using Eq. 1.75.

In order to assess the sound field near a surface it is useful to reference the mean-square pressure from Eq. 1.113 to the mean-square pressure of the free-field incident wave, $\langle p_+^2 \rangle_t$, where

$$\langle p_+^2 \rangle_t = \frac{\hat{p}_+^2}{2} \tag{1.122}$$

The sound field can then be shown using the sound pressure level difference, $10 \lg (\langle p^2 \rangle_t / \langle p_+^2 \rangle_t)$, where 0 dB corresponds to the level of the free-field incident wave.

Figure 1.32 shows examples of the sound pressure level difference for normal incidence as a function of $2kx$ in front of a surface at $x = 0$. Note that the distance, x, is in the negative x-direction. These examples use a range of values for the specific acoustic impedance to represent different surfaces. For a rigid surface the specific acoustic impedance is infinite. Real values for the specific acoustic impedance are chosen to show a range of absorption coefficients up to unity. The complex value, $1 + 8i$, is used to represent a single sheet of 12.5 mm plasterboard (10.8 kg/m^2) at 50 Hz; this plate has a low surface density and is used to provide contrast to the assumption of a rigid surface. The complex value, $1 - 2i$, can occur at a single frequency when a porous material is placed in front of a thick heavy wall to provide absorption in the room.

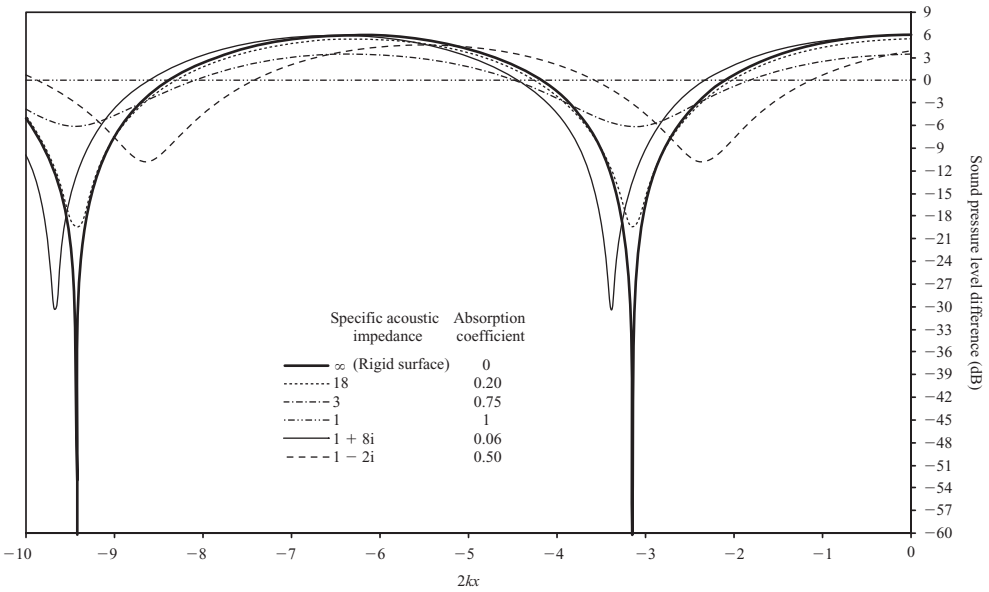

Figure 1.32

Sound field in front of a surface formed by the incident and reflected waves for normal incidence. Surfaces with different specific acoustic impedances are positioned at $x = 0$.

When the specific acoustic impedance is unity then the absorption coefficient is also unity and the incident wave is completely absorbed at the surface. Therefore the sound field in front of the surface only comprises the incident wave, and the sound pressure level difference is 0 dB for all values of $2kx$. In contrast, at the rigid surface there is a perfect reflection so that there is pressure doubling, a level difference of 6 dB. As we move away from the surface, there are sharp interference minima (troughs) where the incident and reflected waves are exactly out of phase with each other. There are also interference maxima with peak values of 6 dB where the waves are in phase with each other. The minima occur when $2kx = -(2n-1)\pi$ where $n = 1, 2, 3$, etc.

When the specific acoustic impedance has real or complex values, resulting in absorption coefficients between 0 and 1, the depths of the minima and the height of the maxima are significantly reduced in comparison to the rigid surface. Also, in comparison to surfaces with real or infinite impedance, complex impedances can significantly change the value of $2kx$ at which the minima and maxima occur. In the next section we will look at the modal sound field by assuming perfectly reflecting and rigid boundaries; hence the features we have seen here for real boundaries will be of relevance again.

1.2.7.2 *Sound field associated with a single mode*

Before we look at sound fields where there are many modes, it is instructive to look at the sound field associated with an individual mode. We will use the box-shaped room with perfectly reflecting and rigid boundaries and send a sinusoidal signal to a loudspeaker positioned in one of the corners.

For a sound source positioned at x_s, y_s, z_s, the mean-square sound pressure level at a receiver point x, y, z that is associated with mode, $f_{p,q,r}$, is calculated using normal mode theory (Morse and Ingard, 1968)

$$\langle p^2_{p,q,r}(x,y,z,x_s,y_s,z_s)\rangle_t = \left| \frac{\omega\rho_0 c_0^2 Q_{\text{rms}}\psi_{p,q,r}(x,y,z)\psi_{p,q,r}(x_s,y_s,z_s)}{V\Lambda_{p,q,r}\sqrt{4\omega^2_{p,q,r}\zeta^2_{p,q,r}+(\omega^2-\omega^2_{p,q,r})^2}} \right|^2 \tag{1.123}$$

where ω is the frequency of the sinusoidal signal, Q_{rms} is the rms volume velocity of the source, $\zeta_{p,q,r}$ is the damping constant, and $\Lambda_{p,q,r} = 1/(\varepsilon_p\varepsilon_q\varepsilon_r)$ for which ε_p, ε_q, and ε_r have already been defined next to Eq. 1.99.

The damping constant, $\zeta_{p,q,r}$, can be linked back to δ_m that was previously used to describe the reverberant decay of an individual mode in Eq. 1.99. In terms of the damping constant, the decay of the mean-square sound pressure for mode, $f_{p,q,r}$, is

$$p^2(t) = p^2(0)\exp(-2\zeta_{p,q,r}t) \tag{1.124}$$

We can now describe the damping constant in terms of the reverberation time or loss factor. From Eq. 1.101 the damping constant is related to the reverberation time, $T_{p,q,r}$, for an individual mode by

$$\zeta_{p,q,r} = \frac{3\ln 10}{T_{p,q,r}} \tag{1.125}$$

which is related to the loss factor for an individual mode, $\eta_{p,q,r}$, using

$$\eta_{p,q,r} = \frac{6\ln 10}{2\pi f T_{p,q,r}} = \frac{\zeta_{p,q,r}}{\pi f} \tag{1.126}$$

From Eqs 1.51 and 1.52 the local mode shape (also called an eigenfunction), $\psi_{p,q,r}$, that describes the sound pressure distribution in space for the receiver position is

$$\psi_{p,q,r}(x,y,z) = \cos\left(\frac{p\pi x}{L_x}\right)\cos\left(\frac{q\pi y}{L_y}\right)\cos\left(\frac{r\pi z}{L_z}\right) \tag{1.127}$$

and for the source position is

$$\psi_{p,q,r}(x_s,y_s,z_s) = \cos\left(\frac{p\pi x_s}{L_x}\right)\cos\left(\frac{q\pi y_s}{L_y}\right)\cos\left(\frac{r\pi z_s}{L_z}\right) \tag{1.128}$$

We will soon look at how different source positions affect the excitation of individual modes. For the moment it is only necessary to ensure that we can excite any mode; hence the source needs to be positioned at any one of the corners, for example at 0,0,0. When the source is at a corner, $|\psi_{p,q,r}(x_s,y_s,z_s)| = 1$ for any mode. This allows us to focus on the way that $\psi_{p,q,r}(x,y,z)$ affects the spatial distribution of the mean-square sound pressure.

The maximum value that $|\psi_{p,q,r}(x,y,z)|$ can take is 1; hence for an individual mode, the maximum mean-square sound pressure occurs at receiver positions where $|\psi_{p,q,r}(x,y,z)| = 1$. These maximum values occur at positions referred to as anti-nodes and their position in the room depends upon the individual mode, $f_{p,q,r}$. However, when the receiver is positioned at any of the eight corners of the box-shaped room, then $|\psi_{p,q,r}(x,y,z)| = 1$ for all modes. Hence, the corner of a room is an ideal point to detect which modes have been excited.

For any individual mode in a box-shaped room, the sound field on any of the three orthogonal planes forming the room is symmetrical about the lines perpendicular to the axes.

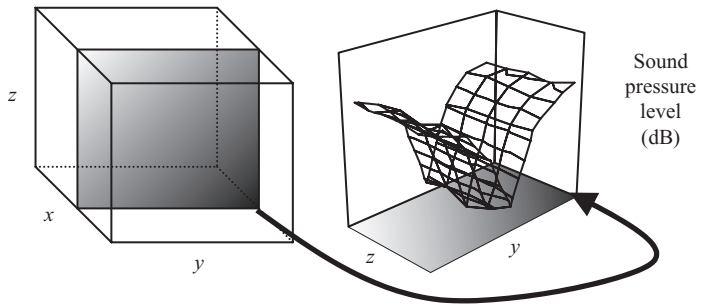

Figure 1.33

Illustration showing how the sound pressure levels from each plane in the box-shaped room is displayed on each three-dimensional surface plot. In this example it is the *yz* plane midway along the *x* dimension, L_x. Each plane is shown with a graduated shaded area so that corners with the darkest and the lightest shading can be used as reference points to identify sound pressure levels at different positions on the plane. If more than one plane is shown, then all these planes have the same sound pressure level distribution.

When at least one of the cosine terms in $\psi_{p,q,r}(x, y, z)$ is 0, the sound pressure is also 0, so there will be planes of zero pressure perpendicular to the *x*, *y*, or *z*-axes. In a box-shaped room these are referred to as nodal planes; these exist where $x = nL_x/2p$, $y = nL_y/2q$ and $z = nL_z/2r$ for $n = 1, 3, 5$, etc. For any mode, $f_{p,q,r}$, there will be *p* nodal planes perpendicular to the *x*-axis, *q* nodal planes perpendicular to the *y*-axis, and *r* nodal planes perpendicular to the *z*-axis.

For rooms with volumes less than 30 m^3, there will only be one mode or a few modes in individual one-third-octave-bands between 50 and 100 Hz. These modes are usually the axial modes $f_{1,0,0}$, $f_{0,1,0}$, $f_{0,0,1}$, $f_{2,0,0}$, $f_{0,2,0}$, the tangential modes $f_{1,1,0}$, $f_{0,1,1}$, $f_{1,0,1}$ and the oblique mode $f_{1,1,1}$.

The graphs in this section can be interpreted with reference to Fig. 1.33. Examples of the sound pressure level distribution are shown for axial modes $f_{1,0,0}$ and $f_{0,0,1}$ (Fig. 1.34), the tangential mode, $f_{1,1,0}$ (Fig. 1.35), and the oblique mode $f_{1,1,1}$ (Fig. 1.36). To allow a practical interpretation of the sound field, the decibel scale has been used. However the use of decibels is not ideal because the mean-square pressure is zero on the nodal planes. In reality there will not be zero mean-square sound pressure for two reasons. Firstly, there will always be some background noise in the measurement, and secondly, not all real surfaces are perfectly reflecting and rigid. For the latter reason the surfaces will absorb some of the incident sound and there will not be perfect cancellation along nodal planes, i.e. there will not be pure standing waves. This was previously seen in Section 1.2.7.1.2 when we looked at the sound field near room boundaries where the specific acoustic impedance of the surfaces had complex or finite real values. The maximum level for each mode has therefore been normalized to 0 dB, and we will assume that the background noise level is 60 dB below this maximum level; so levels of −60 dB on these graphs represent the nodal planes with zero mean-square pressure.

The main features of the modal sound field are the large spatial variations in the sound pressure level. The highest levels occur at the room boundaries, with the nodal planes sited away from these boundaries.

This model of the sound field gives us a basic insight into the sound field in a room. However by assuming that the room boundaries are perfectly rigid we have not considered the interaction between the sound in the room and the vibration of the walls and floors. In addition we have not yet considered the situation where frequency bands ‘contain’ zero, one, or more modes.

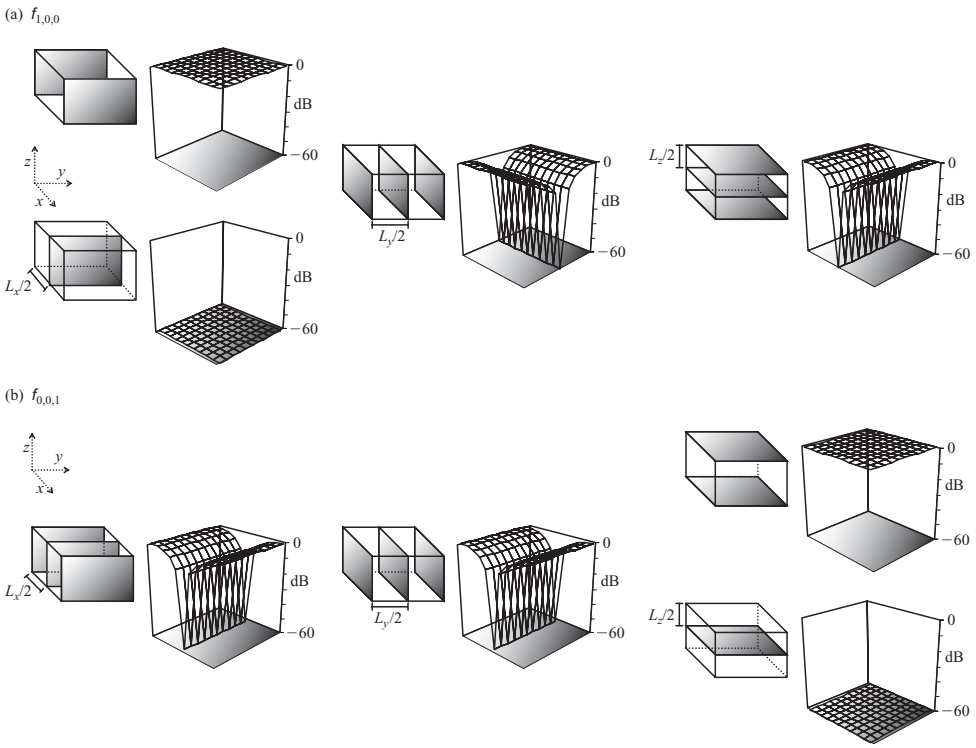

Figure 1.34

Sound pressure level distribution for axial modes: (a) $f_{1,0,0}$ and (b) $f_{0,0,1}$.

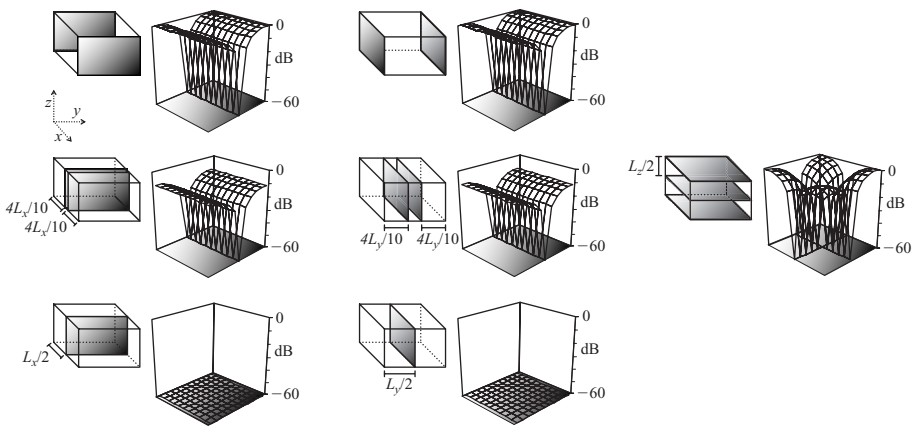

Figure 1.35

Sound pressure level distribution for the tangential mode, $f_{1,1,0}$.

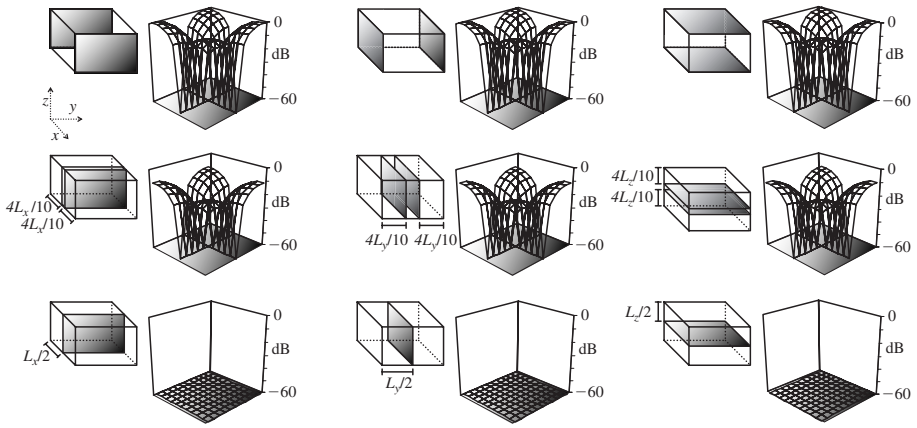

Figure 1.36

Sound pressure level distribution for the oblique mode $f_{1,1,1}$.

1.2.7.3 Excitation of room modes

We need to consider the excitation of room modes in two different situations: one in a source room where the airborne sound insulation is being measured by using a loudspeaker to generate the sound field, and the other in a receiving room where the room surfaces radiate sound into the receiving room, which excites the receiving room modes. The latter situation primarily concerns the coupling between energy stored in walls, floors, or other spaces, and the energy stored in the receiving room modes and is discussed in Chapter 4. At this point, we just consider the effect of using a single loudspeaker at different positions in the source room, and how those different positions affect the excitation of room modes in the low-frequency range. For individual frequencies the mean-square sound pressure due to each room mode can be calculated using Eq. 1.123 and summed to give the overall mean-square sound pressure. This is similar to carrying out a swept-sine measurement with a constant amplitude signal from the loudspeaker. In practice the airborne sound insulation is usually measured using broad-band noise, but single frequencies gives a clearer understanding of the effect of different source positions.

Three different source positions are assessed: one near a corner, another at the mid-point along one wall, and another that is exactly in the centre of the room. In practice it is rarely possible to put the loudspeaker exactly at the corner, although we can place it near the corner; so we will assume that the acoustic centre of the loudspeaker is at 0.5,0.5,0.25 m which is nearest to the corner at 0,0,0.

The receiver position is at L_x,L_y,L_z, which is in the corner opposite the loudspeaker. A microphone would not be placed in a corner for standard sound insulation measurements; it would be positioned away from the room boundaries. However, we only want to assess which modes have been excited so we do not need to know the absolute sound pressure levels. For this reason the receiver position is at a point in the room where all modes have an anti-node (i.e. in a corner).

The damping constants for the individual modes are calculated from Eqs 1.125 and 1.101 using a frequency-independent value for the specific acoustic admittance ($\beta_{a,s} = 0.01$).

Predicted curves for the sound pressure level are shown in Fig. 1.37 for the same 50 m^3 box-shaped room that was used to look at the mode count in one-third-octave-bands. The peaks in

the sound pressure level are due to the room modes that have been excited. On each curve, the axial, tangential, and oblique modes have been plotted at their respective eigenfrequencies. When there are relatively few modes and the modes are all well-separated we see that if a mode frequency coincides with a peak in the sound pressure level curve, this indicates that this particular mode has been excited; if it coincides with a trough in the curve, then it has not been excited. If a mode frequency occurs on the curve between a trough and a peak, then either the mode has not been excited, or it has been excited but it has such a low sound pressure level that there is no discernible peak. This numerical experiment indicates the difficulty in using physical experiments to find the mode count where a microphone and a sound source are placed in a single position. The problem is that counting the peaks in the response is unlikely to identify all of the modes; this equally applies to vibration measurements used to identify structural modes of vibration.

When the source is near a corner there are many more peaks in the sound pressure level curve than when the source is at the centre of the room; hence many more modes are excited by a corner position than the central point. When the source is near a corner, all the modes below 100 Hz have been excited and are clustered at or near the peaks in the sound pressure level curve. In contrast, when the source is at the centre of the room, the first five modes have not been excited at all, and there are clusters of modes that have not been excited near the troughs of the sound pressure level curve. The modes that have not been excited have one or more nodal planes that cut through the source position at the centre of the room (e.g. see $f_{1,1,1}$ in Fig. 1.37). Similarly, when the source is mid-way along one wall, the modes that have not been excited also have one or more nodal planes that cut through the source position (e.g. see $f_{1,0,0}$ and $f_{1,1,1}$ in Fig. 1.37).

For field airborne sound insulation measurements in non-diffuse sound fields it is necessary to excite the majority of the modes in the source room. For this reason, loudspeaker positions near the corners are used in box-shaped rooms as well as in other shapes of room. In addition it is necessary to take average measurements from more than one source position. However, it must also be ensured that the direct sound from the loudspeaker does not cause significant excitation of the walls or floors compared to excitation by the reverberant sound field.

1.2.7.4 *Diffuse and reverberant fields*

The Schroeder cut-off frequency is sometimes used to estimate the lowest frequency above which the sound field can be considered to be diffuse. This is the frequency at which the modal overlap factor equals three; hence it identifies the lowest frequency above which the sound energy is relatively uniform in the central zone of a room.

In practice, a diffuse field cannot be realized throughout the entire room volume due to the fact that rooms are defined by the walls and floors that form the room boundaries. These boundaries give rise to interference patterns close to the surfaces, edges, and corners; hence the energy density is not uniform throughout the space. In addition these boundaries absorb sound (to varying degrees) so that there must be a net power flow from the sound source to the boundaries, whereas in a diffuse field the net power flow is zero. Under laboratory conditions it is possible to achieve a suitable degree of diffusivity through careful room design, by using diffusing elements in the room, and by defining measurement positions away from the room boundaries. Hence close approximations to diffuse fields in the building acoustics frequency range only tend to exist in the central zones of large reverberant chambers. Such chambers are carefully designed and validated for the laboratory measurement of absorption or sound

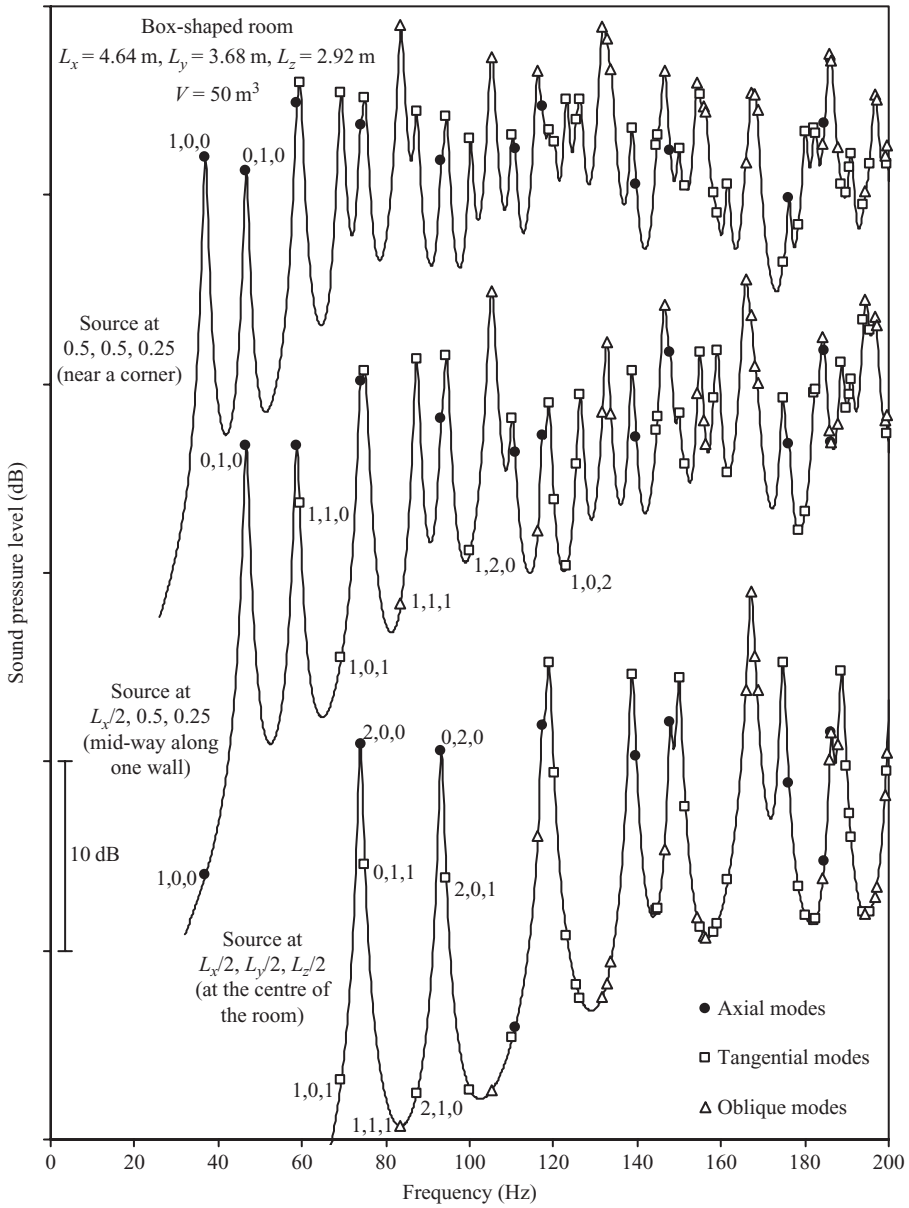

Figure 1.37

Excitation of room modes with three different source positions. Curves for the sound pressure level in the corner position (L_x, L_y, L_z) are shown along with the axial, tangential and oblique mode frequencies to assess which modes are, and which modes are not excited by the source position. Note that the curves have been offset from each other; this allows the relative levels along each individual curve to be assessed, but not the relative levels between different curves.

power levels. In laboratory measurements of airborne and impact sound insulation we also come across close approximations to diffuse sound fields in the source and receiving rooms.

In general it is better to avoid referring to a diffuse sound field in a room because we must add several caveats to any such statement. At frequencies above the lowest room mode it is

simpler if we just refer to a reverberant field. This acknowledges the fact that the room response varies over the building acoustics frequency range due to the existence of one, a few, several, or many modes in the different frequency bands. It also serves as a reminder that interference patterns exist at the room boundaries, and that it is only in the central zone of reverberant rooms that sound fields resemble (to varying degrees) a diffuse field.

1.2.7.5 Energy density

The energy density, w, equals the energy per unit volume. For a sound field comprised of plane waves, Eq. 1.19 describes the sound intensity, i.e. the energy that flows through a unit surface area in unit time. Therefore, as a plane wave will travel a distance equal to c_0 in unit time, the energy density in any reverberant sound field comprised of plane waves (which includes diffuse or modal sound fields) is

$$w_r = \frac{I}{c_0} = \frac{\langle p^2 \rangle_{t,s}}{\rho_0 c_0^2} \tag{1.129}$$

Hence the energy density is directly proportional to the temporal and spatial average mean-square sound pressure, $\langle p^2 \rangle_{t,s}$.

1.2.7.5.1 Diffuse field

As any kind of signal can be described by using many impulses, the steady-state energy density in a diffuse field can be derived by considering the impulse response of a room (Barron, 1973; Kuttruff, 1979). We assume that a room contains a point source that generates an impulse at time, $t = 0$. This point source generates spherical waves for which the intensity is inversely proportional to the square of the distance travelled (Eq. 1.26). At an arbitrary receiver position in the room, the sound intensity is the sum of the intensity from the direct path and the many indirect paths involving at least one reflection from a room boundary. For direct propagation from the source to the receiver, we define the intensity at the receiver to be I_0, after it has travelled the source–receiver distance, r_0. For each propagation path that involves at least one reflection, we can consider an image source that generates an identical impulse to the actual source at $t = 0$. At time, t, impulses from the actual source or an image source will have travelled a distance, $c_0 t$. For the image sources, a fraction of the sound intensity is absorbed upon each reflection from the room boundaries; hence from Eq. 1.92 the intensity is attenuated by the factor

$$\exp\left(\frac{c_0 t}{d_{mfp}} \ln(1 - \bar{\alpha})\right) \tag{1.130}$$

At an arbitrary receiver point, the intensity from an image source at time, t, is therefore given by

$$\frac{I_0 r_0^2}{(c_0 t)^2} \exp\left(\frac{c_0 t}{d_{mfp}} \ln(1 - \bar{\alpha})\right) \tag{1.131}$$

At time, t, we now need to determine how many impulses from image sources will arrive at the receiver in a small time interval, δt. This is equivalent to finding the number of reflections arriving during this time interval, and can be calculated from the temporal density of reflections (Eq. 1.49), using

$$\frac{4\pi c_0^3 t^2}{V} \delta t \tag{1.132}$$

Therefore the total intensity arriving at the receiver after a specific time, t_1, can be found by integrating the intensity from all reflections according to

$$I = \int_{t_1}^{\infty} \frac{I_0 r_0^2}{(c_0 t)^2} \exp\left(\frac{c_0 t}{d_{\text{mfp}}} \ln(1-\bar{\alpha})\right) \frac{4\pi c_0^3 t^2}{V} \mathrm{d}t \tag{1.133}$$

and the energy density can be found using

$$w_{\text{r}} = \frac{I}{c_0} = \int_{t_1}^{\infty} \frac{W}{V} \exp\left(\frac{c_0 t}{d_{\text{mfp}}} \ln(1-\bar{\alpha})\right) \mathrm{d}t \tag{1.134}$$

where the sound power, W, for the spherical wave source is

$$W = 4\pi r_0^2 I_0 \tag{1.135}$$

The choice of time, t_1, for the lower limit of the integral needs to consider the fact that the direct sound does not arrive at the receiver until $t = r_0/c_0$, and that the exponential decay in a diffuse field can only start after the first reflections arrive at the receiver (i.e. when $t > r_0/c_0$). Therefore if the lower limit of the integral is taken to be $t_1 = 0$, the energy density will include the time interval before the direct sound has arrived and the exponential decay has begun. Using $t_1 = 0$ to estimate the energy density in a diffuse field, w_{r}, gives the classical equation

$$w_{\text{r}} = \frac{4W}{c_0 A} \tag{1.136}$$

where $A = -S_{\text{T}} \ln(1-\bar{\alpha})$.

The time interval during which the direct sound travels to the receiver can be excluded by using $t_1 = r_0/c_0$ to give an estimate of the energy density that is dependent upon r_0 (Barron, 1973). In large spaces such as concert halls, this dependence on source–receiver distance is often important. However, for sound insulation in typical rooms it is not necessary (or practical) to relate the energy density to specific source–receiver distances. On the basis that the exponential decay in a diffuse field can only start after the first reflections arrive at the receiver position; it is necessary to find a lower limit for the integration that represents the average time taken to travel from the source to the receiver when there is one reflection. This can be determined by using the mean free path (Kuttruff, 1979; Vorländer, 1995). Although the mean free path is the average distance travelled after leaving one boundary and striking the next boundary, it is reasonable to assume that the average distance from either the source or the receiver to any room boundary is approximately equal to half the mean free path. Therefore the mean free path represents the average path length between the source and receiver when there is one reflection. Taking the lower limit of the integral to be $t_1 = d_{\text{mfp}}/c_0$ gives the energy density of the diffuse sound field, w_{r}, as

$$w_{\text{r}} = \frac{4W}{c_0 A}(1-\bar{\alpha}) \tag{1.137}$$

where $A = -S_{\text{T}} \ln(1-\bar{\alpha})$

If there is significant air absorption then for each image source, the intensity is attenuated by the factor

$$\exp\left(\frac{c_0 t}{d_{\text{mfp}}} \ln(1-\bar{\alpha})\right) \exp(-m c_0 t) \tag{1.138}$$

and the resulting energy density is (Vorländer, 1995)

$$w_r = \frac{4W}{c_0 A} \exp\left(-\frac{A}{S_T}\right) \tag{1.139}$$

where $A = -S_T \ln(1-\overline{\alpha}) + 4mV$.

Equating Eq. 1.129 to any of the above equations for the diffuse field energy density (Eqs 1.136, 1.137, or 1.139) gives the basic relationship between reverberant sound pressure and absorption area for a fixed sound power input into a room; namely, that the sound pressure in a room is reduced by increasing the absorption area, and vice versa. In diffuse fields with an exponential decay, the decay curve is a straight line over the full 60 dB range; hence there is a simple and unambiguous relationship between the reverberation time and the absorption area.

Having seen that there is more than one equation for the energy density in a diffuse field, we need to discuss the equations that are used in practice. Although Eq. 1.139 is the more accurate equation, it is not always necessary to consider air absorption. In practice, Eq. 1.137 is usually adequate. In most rooms with volumes less than 200 m^3 and reverberation times less than 2 s at 20°C and 50% RH the error in neglecting air absorption in the calculation of the diffuse field energy density is only greater than 1 dB in one-third-octave-bands above 3150 Hz. In the measurement Standards for sound insulation, the classical equation (Eq. 1.136) is used to derive equations that link the sound power to the reverberant sound pressure level in a room (Section 3.5.1). This is reasonable in transmission suites (where reverberation times are at least 1 s) because negligible errors are incurred when using Eq. 1.136. However, for field sound insulation measurements (where reverberation times in furnished rooms are approximately 0.5 s), consideration could be given to use of Eq. 1.137 to determine the apparent sound reduction index (Vorländer, 1995).

1.2.7.5.2 *Reverberant sound fields with non-exponential decays*

In comparison with diffuse fields, it is more awkward to make a link between the sound power radiated into a room and the reverberant sound pressure level for a non-diffuse field. For modal sound fields, some insight can be gained by using normal mode theory and the specific acoustic admittance of the room boundaries; however, this does not give a completely general solution that corresponds to the practical situation (Jacobsen, 1982; Bodlund, 1980). For non-diffuse fields, it is the reverberation time that provides a practical link between the sound power and the reverberant sound pressure level. The difficulty lies in evaluating decay curves from non-diffuse fields because they are not straight lines across the entire 60 dB decay range. For this reason it is necessary to identify which part of the decay curve should be used to calculate the reverberation time.

From normal mode theory in Section 1.2.6.3.2 we have seen that it is only within the initial 20 or 30 dB of the decay curve that the majority of room modes play a role in determining the decay curve of the frequency band. The late part of the decay is determined by a relatively small number of modes with longer decay times. In the steady-state situation, energy is stored in all modes; hence, it is appropriate to determine the reverberation time using an evaluation range in which the majority of the room modes play a role in forming the decay curve. Furthermore, as any signal can be represented by a train of impulses, we can describe the steady-state sound pressure by the energetic sum of a train of impulse responses. For each impulse response, only the initial 20 dB drop of its decay curve will determine the steady-state sound pressure level to within 0.1 dB. Therefore T_{10}, T_{15}, or T_{20} should be used to determine the absorption area, rather

than T_{30} or T_{60}. The energy density in reverberant sound fields with non-exponential decays can then be estimated by using the equations for the diffuse field energy density (Eqs 1.136, 1.137, and 1.139).

1.2.7.6 Direct sound field

So far we have considered the sound field in the central zone of a room without considering the sound field close to the sound source, i.e. the direct field. Most sound insulation measurements use an omnidirectional loudspeaker and we need to consider the direct field near the sound source in order to assess how far the microphone should be from the loudspeaker when we want to measure the reverberant sound pressure level in the central zone of the room without any strong influence from the direct field.

For an omnidirectional source that emits a sound power, W, and is positioned away from the room boundaries, the energy density of the direct field, w_d, at a distance, d, from the source is

$$w_d = \frac{W}{4\pi c_0 d^2} \tag{1.140}$$

Figure 1.38 shows the energy density due to the direct and the reverberant fields in a 50 m^3 room at distances up to 1 m from the sound source. The energy density due to the direct field decreases by 6 dB every time the distance is doubled. The distance from the sound source at which the energy density in the direct field (Eq. 1.140) equals the energy density in the diffuse field (Eq. 1.137) is described as the reverberation distance, r_{rd}. When $\overline{\alpha} \approx -\ln(1-\overline{\alpha})$ the reverberation distance can be estimated using

$$r_{rd} \approx \sqrt{\frac{S_T \overline{\alpha}}{16\pi}} \tag{1.141}$$

In rooms with volumes less than 150 m^3 and reverberation times greater than 0.5 s, the reverberation distance is usually less than 1 m. To measure the reverberant sound pressure level the preferred option is to position the microphone at distances slightly greater than the reverberation distance. However in most rooms a practical choice for the minimum distance between the microphone and most loudspeakers is 1 m; this is commonly used for airborne sound insulation measurements (ISO 140 Parts 3 & 4).

1.2.7.7 Decrease in sound pressure level with distance

There are two main types of room in which there can be a significant decrease in the sound pressure level with distance from the source: (1) large rooms (often with volumes greater than 200 m^3) with absorbent surfaces and/or large scattering objects and (2) corridors or passageways, usually with highly absorbent ceilings. Computer models (usually based around a geometrical ray approach) can be used to calculate the sound pressure level distribution, but for corridors it is still possible to gain some insight using simpler models.

Long corridors, such as those in flats, offices, and schools, are usually broken up into smaller lengths of corridor by fire doors. This typically results in sections of corridor that are less than 30 m in length, and where the dimensions of the cross-section are between 1.5 and 5 m. Noise control measures in the corridor often require absorptive ceilings; hence these elongated spaces can show a significant decrease in the sound pressure level with distance. As the sound propagates down the corridor, there are two types of internal damping that reduce the sound

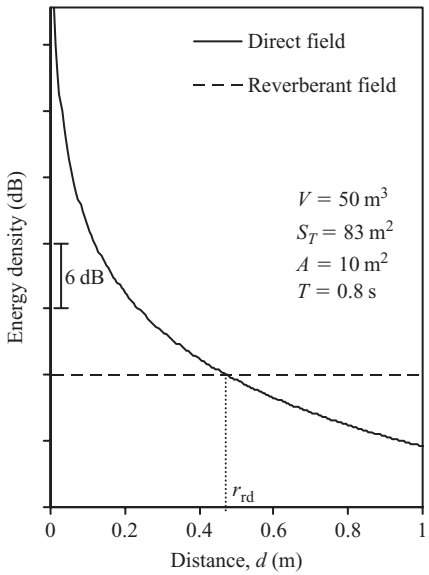

Figure 1.38

Energy density due to the direct and reverberant fields in a room at distances up to 1 m from the sound source.

pressure level: air absorption (which will be considered as negligible) and absorption by the corridor surfaces.

For a thorough overview of models for long enclosures the reader is referred to the book by Kang (2002). A simple model can be based on a corridor of infinite length that is divided into a number of very thin box-shaped sections of depth, dL (Redmore and Flockton, 1977). Effectively we are considering a large number of two-dimensional sound fields that are coupled together along the length of the corridor (see Fig. 1.39). The following derivation and the resulting equation (Eq. 1.145) are different from that in Redmore and Flockton (1977). However, it gives the same equation that was later determined empirically in scale model experiments of corridors by Redmore (1982).

It is assumed that the energy density in each section of volume, dV, is uniform and that the corridor surfaces have an average absorption coefficient, α. We arbitrarily choose a section at $x = 0$ in this infinite corridor, and follow sound propagating in the positive x-direction. In each two-dimensional sound field, sound energy impinges upon the corridor surfaces, c_0/d_{mfp} times every second; the mean free path for a two-dimensional field is given later in Eq. 1.185. The power absorbed by the corridor surfaces is

$$W_{\mathrm{abs}} = w\mathrm{d}V\frac{c_0}{d_{\mathrm{mfp}}}\frac{A}{U\mathrm{d}L} = \frac{Ec_0U\alpha}{\pi L_y L_z} \tag{1.142}$$

where $A = U\mathrm{d}L\alpha$, and the perimeter of the corridor section, $U = 2L_y + 2L_z$.

The absorbed power is related to the loss factor by

$$W_{\mathrm{abs}} = \omega\eta E \tag{1.143}$$

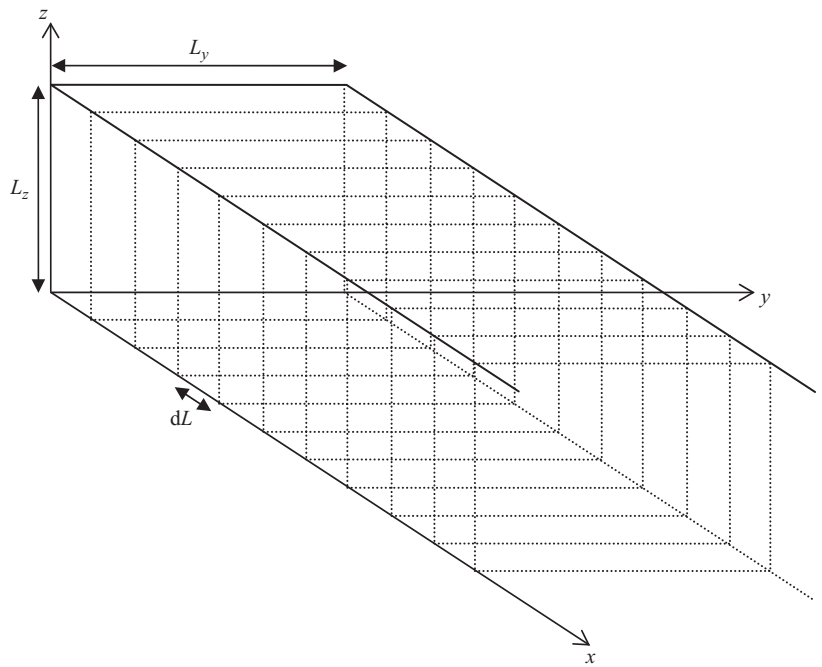

Figure 1.39

Corridor divided into sections.

hence equating Eqs 1.142 and 1.143 gives the loss factor as

$$\eta = \frac{c_0 U \alpha}{2\pi^2 f L_y L_z} \tag{1.144}$$

After travelling a distance, d, down the infinitely long corridor, the sound energy is reduced by the factor $\exp(-k\eta d)$, which gives the decrease in the sound pressure level in decibels as

$$\Delta L_{\text{inf}} = \frac{10}{\ln 10} \frac{1}{\pi} \frac{U \alpha d}{L_y L_z} \tag{1.145}$$

Equation 1.145 applies to an infinitely long corridor (i.e. without ends). In practice, sound will be partially reflected and partially absorbed from the end(s) of the corridor. We now consider a corridor that extends to infinity in the negative x-direction, but has a termination at $x = D$ (e.g. at the fire doors). It will be assumed that there are no interference effects between the incident and reflected sound at the receiver. In addition, we will not consider how the sound is injected into the corridor; this avoids consideration of the direct field from the sound source. To do this it is assumed that the thin corridor section at $x = 0$ starts with uniform energy density, and that sound propagates in the positive x-direction. The decrease in sound pressure level after the sound has travelled a distance, d, down the corridor is (Redmore and Flockton, 1977)

$$\Delta L = -10 \lg \left(10^{-\Delta L_{\text{inf}}/10} + R 10^{-\Delta L_{\text{inf}}((2D-d)/d)/10}\right) \tag{1.146}$$

where the surface at the end of the corridor has a reflection coefficient, R.

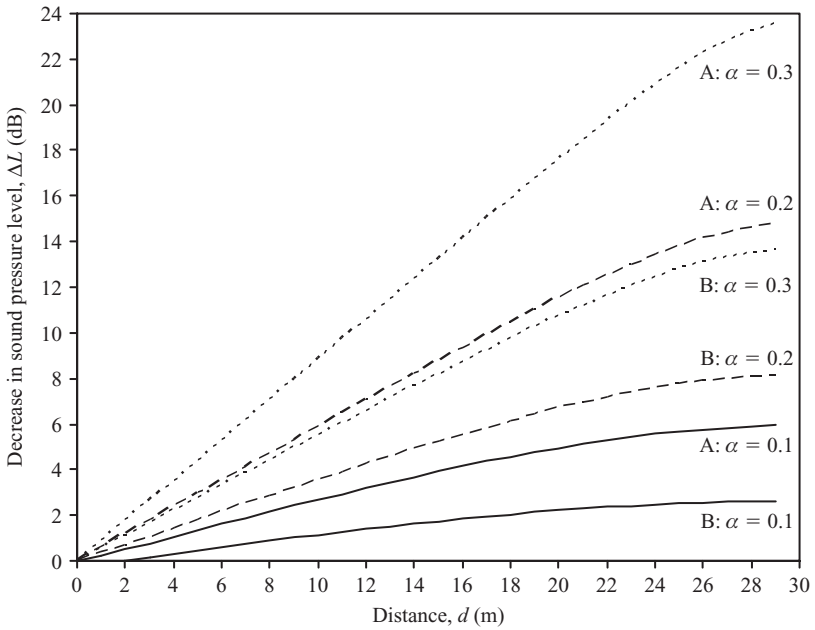

Figure 1.40

Decrease in sound pressure level along a corridor. Two different cross-sections ($L_y \times L_z$) are shown: A (1.5×2.5 m) and B (3×3 m). The corridor surfaces have average absorption coefficients of 0.1, 0.2, or 0.3. The surface that forms the end of the corridor has a reflection coefficient, $R = 0.95$.

Figure 1.40 shows the calculated decrease in level along two different corridors with different average absorption coefficients. The partial reflection at the end of the corridor causes the initial decrease in sound pressure level per unit distance to be larger than it is towards the end of the corridor.

1.2.7.8 *Sound fields in frequency bands*

So far we have focused on the sound field at single frequencies in box-shaped rooms that have perfectly reflecting rigid boundaries. We usually measure sound insulation in one-third-octave or octave-bands in rooms with a wide variety of boundaries. These bands contain many modes with different decay times and, when considering interaction with the room boundaries, it becomes more complex to predict this sound field. To look at the superposition of modes that occurs in real rooms we now look at some example measurements of sound pressure levels in one-third-octave-bands.

1.2.7.8.1 *Below the lowest mode frequency*

Below the lowest mode frequency we expect the sound field to be homogeneous and uniform throughout the space. This assumption is reasonable when there is no significant overlap from the response of the lowest mode into frequency bands below the lowest mode frequency.

To gain an impression of the sound field we can look at sound pressure level measurements in a 29 m^3 source room, and an 18 m^3 receiving room, both with timber-frame walls and floors

(Hopkins and Turner, 2005). The lowest mode frequency is calculated to be 39 Hz for the source room and 59 Hz for the receiving room. Therefore we will look at the 20 Hz one-third-octave-band because this is well-below the lowest mode in both rooms. A broad-band noise source was used with measurement positions in a three-dimensional grid (including positions at the room boundaries). To gain a visual impression of the sound field, sound pressure levels from three different measurement planes are shown in Figs 1.41a and 1.41b for the source and receiving rooms respectively. In the source room there is a peak in the sound pressure level immediately next to the loudspeaker. Further away from the loudspeaker in the source room, and throughout the receiving room, the spatial variation within a single measurement plane can be as low as 2 dB or as high as 12 dB. Although the sound field is relatively uniform in some measurement planes it will not always be homogeneous throughout the room volume. The non-uniform sound field in the receiving room may be attributed to structural modes and resonances of the walls and floors that occur below the lowest room mode. The mass–spring–mass resonance frequency of the timber-frame separating wall is estimated to fall in the 31.5 Hz one-third-octave-band.

For field measurements it is worth noting that both source and receiving rooms can have quite large spatial variations in the sound pressure level below the lowest calculated mode frequency.

1.2.7.8.2 *Reverberant field: below the Schroeder cut-off frequency*

In rooms with volumes less than 30 m^3 the sound field in one-third-octave-bands below 100 Hz is sometimes dominated by the response of a single mode. However, in the low-frequency range the situation is usually more complex due to the influence of one, two, or three modes that fall within a frequency band.

In most dwellings the height (L_z) of a room is less than the width (L_x) and the depth (L_y). Therefore the lowest mode frequency will be $f_{1,0,0}$ or $f_{0,1,0}$, and when $L_x \neq L_y$, one of these modes will usually be the only mode that falls exactly within the lower and upper limits of the associated one-third-octave-band. Depending on the amount of damping and the bandwidth, the response from one or more modes in adjacent bands can overlap into this band. As an example we can look at the measured sound pressure level distribution in a 34 m^3 receiving room with masonry/concrete walls and floors for the 50 Hz one-third-octave-band; this has a measured reverberation time of 1.2 s. For this room the Schroeder cut-off frequency is in the 500 Hz band. Broad-band excitation was applied in the source room, so it is representative of the situation that is encountered in field sound insulation tests. The sound field is shown in Fig. 1.41c and can generally be described as symmetrical in each plane. The first three modes are $f_{1,0,0}$, $f_{0,1,0}$, and $f_{1,1,0}$ for which the calculated mode frequencies (assuming rigid walls) are 43, 47, and 64 Hz respectively. Although $f_{0,1,0}$ is calculated to be the only mode that falls exactly within the limits of the 50 Hz band, there is evidence of overlapping response from one or both of the $f_{1,0,0}$ and $f_{1,1,0}$ modes. This is evident from the nodal planes along both the x and y-axes where the sound pressure levels are lowest in the middle of both these axes, rather than just the y-axis as would occur if the response was only due to $f_{0,1,0}$. We previously noted that real walls and floors are not rigid and will dissipate energy; hence the sound pressure in nodal planes will not be zero as implied by normal mode theory for sinusoidal excitation of a single mode in a room with rigid boundaries. However, these nodal planes still cause a high degree of spatial variation in the sound field. For the 50 Hz band in this example, there is a difference of 28 dB between the lowest level in the central zone of the room and the highest

(a) Source room (29 m^3), 20 Hz one-third-octave-band. The loudspeaker position is indicated by ✯

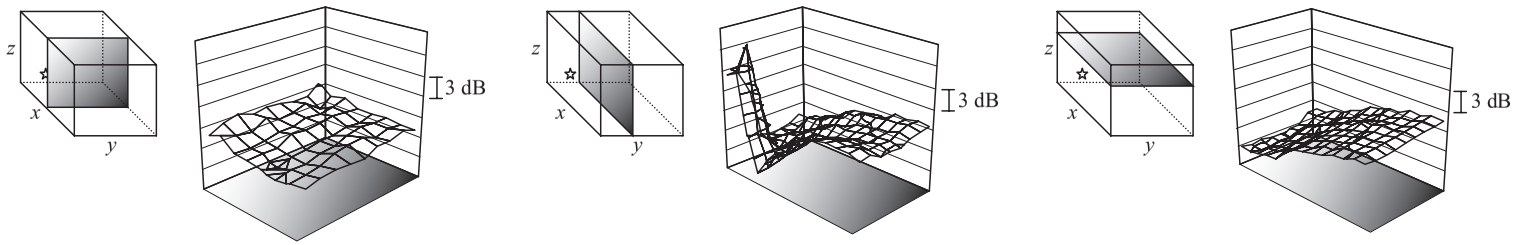

(b) Receiving room (18 m^3), 20 Hz one-third-octave-band

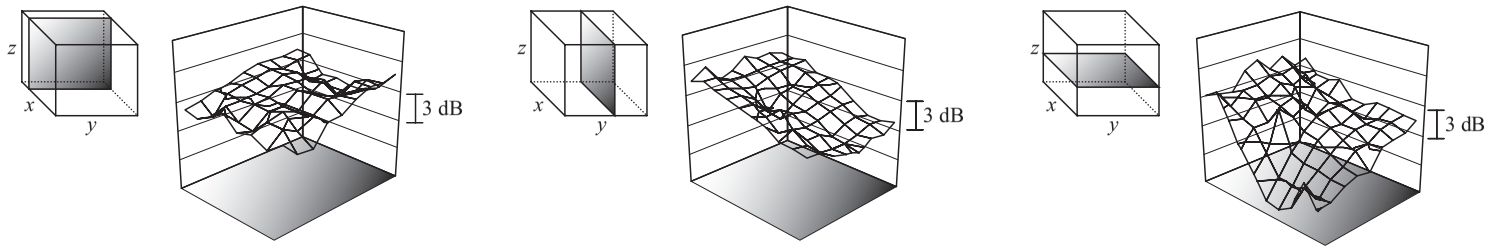

Figure 1.41

Measured sound pressure level distribution in rooms. For each figure, the same scale is used in each of the three plots to allow an assessment of the differences between the sound pressure levels in the different planes; however, different scales are used for different rooms and different frequency bands.

(c) Receiving room (34 m^3), 50 Hz one-third-octave-band

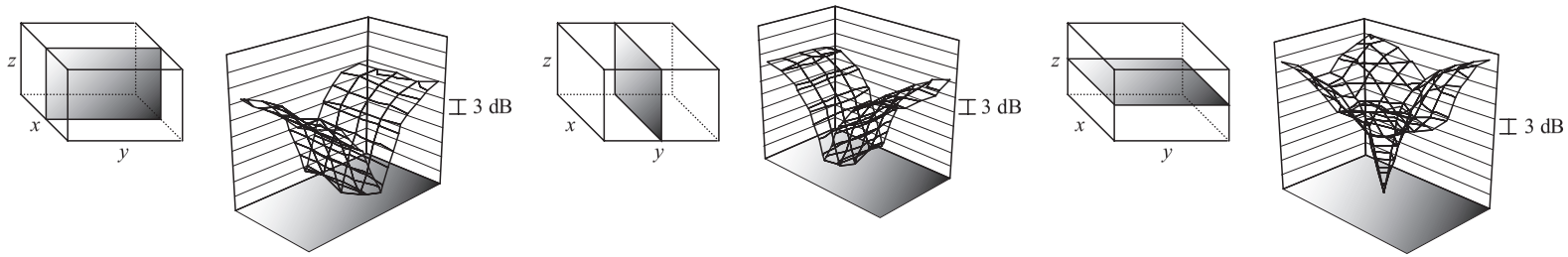

(d) Receiving room (18 m^3), 80 Hz one-third-octave-band

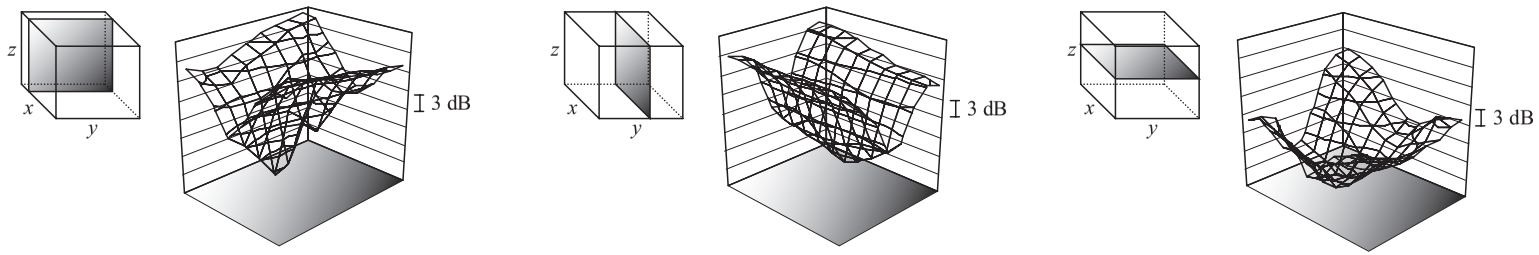

Figure 1.41

(*Continued*)

(e) Receiving room (18 m^3), 160 Hz one-third-octave-band

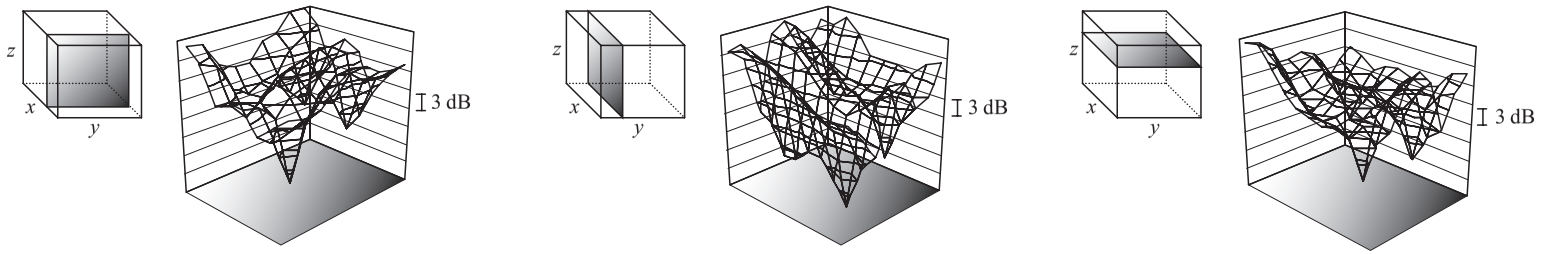

(f) Receiving room (34 m^3), 500 Hz one-third-octave-band

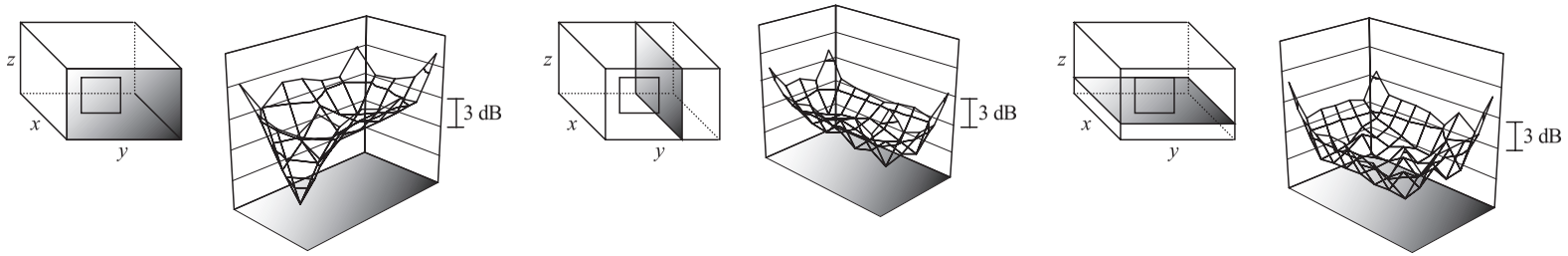

Figure 1.41

(*Continued*)

level that is ≈0.5 m from the room boundaries. For sound insulation measurements with broad-band noise sources, measured data suggests that this difference will usually be between 17 and 28 dB for typical rooms in the low-frequency range (Hopkins and Turner, 2005; Simmons, 1996); background noise will always limit the lowest level that is measurable in the nodal planes.

The highest sound pressure levels exist in corners and near wall/floor surfaces, with low levels near the centre of the room. This highlights an important issue for spatial average sound pressure level measurements in small rooms. Field sound insulation measurement procedures usually require that the microphone is positioned at a minimum distance of 0.5 m from the boundaries with guidance that this minimum distance should be increased to 1.2 m below 100 Hz (ISO 140 Part 4). In small rooms this means that the microphone is positioned in the central zone of the room where the sound pressure level is lowest. Therefore the spatial average levels are not representative of either the room average sound pressure level or the level perceived by room occupants who often sit and sleep near the room boundaries.

For a room height, L_z, which is between 2.1 and 2.4 m, the $f_{0,0,1}$ mode will fall within the 63 Hz or 80 Hz one-third-octave-band. This mode gives rise to low sound pressure levels on the $z = L_z/2$ measurement plane (the plane that lies in the middle of the z-axis) compared to the levels on the $z = 0$ and the $z = L_z$ measurement planes. Figure 1.41d shows the data for the 80 Hz one-third-octave-band in an 18 m^3 receiving room with timber frame walls and floors with a measured reverberation time of 0.5 s. For this room the Schroeder cut-off frequency is in the 315 Hz band. We might expect the time-averaged sound pressure level in each measurement plane for a box-shaped room to be symmetrical in frequency bands containing the first few modes. However, the spatial variation is asymmetric; this usually occurs when one or more of the room dimensions are equal to at least one wavelength. In most rooms there are recessed windows or lobby areas associated with the door, i.e. smaller volumes connected to the main rectangular space. As the room shape and the surface impedance of the room surfaces become increasingly irregular with scattering objects in the room, the local mode shapes effectively become hybrid mode shapes which do not have symmetrical sound pressure fields. Above the first few modes there is usually a marked degree of asymmetry and complexity in the sound field. An example is shown in Fig. 1.41e for the 160 Hz one-third-octave-band in the 18 m^3 receiving room of timber-frame construction. Asymmetry not only occurs in the receiving room, but also in the source room, although this is partly due to higher levels in the direct field of the loudspeaker.

1.2.7.8.3 Reverberant field: at and above the Schroeder cut-off frequency

At and above the Schroeder cut-off frequency the sound field becomes increasingly uniform in the centre of the room. However, at positions that are very close to the room boundaries there are still higher sound pressure levels due to the interference patterns.

An example is shown in Fig. 1.41f for the 500 Hz one-third-octave-band in a 34 m^3 receiving room with masonry/concrete walls and floors. This frequency band contains the Schroeder cut-off frequency. Compared to the average level in the centre of the room, the average measured levels at the wall surfaces are ≈3 dB higher, the edges are ≈6 dB higher, and the corners are ≈8 dB higher; these correspond to the predicted values 3, 6, and 9 dB that were discussed earlier in Section 1.2.7.1.1. Higher sound pressure levels did not occur at a few grid points near the room surface with a recessed window in the external wall because the microphone was then ≈200 mm further away from the room boundary. This feature can be seen in Fig. 1.41f where the window position is indicated on the diagram.

Above the Schroeder cut-off frequency the spatial variation usually decreases significantly so it is more useful to look at the standard deviation rather than plots of the spatial distribution of the sound pressure level.

1.2.7.9 Statistical description of the spatial variation

When measuring and predicting the sound pressure level in rooms, it is almost always the spatial average value that is required. Hence we need to be able to quantify the spatial variation of the sound pressure level in terms of the normalized variance of the mean-square sound pressure, and the standard deviation of the sound pressure level in decibels. The normalized standard deviation, ε, is the ratio of the standard deviation to the mean, which is squared to give the normalized variance, ε^2.

To determine the standard deviation and confidence intervals, it is necessary to know the probability distribution (probability density function) for the mean-square pressure, or identify one that gives a reasonable representation of the actual distribution. The standard deviation depends upon the type of excitation. For sound insulation we almost always use broad-band noise and measure in frequency bands; although sound insulation against pure tones is occasionally of interest with environmental noise sources. For frequency band measurements in rooms containing a single omnidirectional sound source emitting broad-band noise, estimates of the standard deviation can be found in the same way as for sound power measurements in a reverberant chamber (Schroeder, 1969; Lubman, 1974). For airborne sound insulation measurements we carry out spatial sampling of the sound pressure in the room that contains the loudspeaker, the source room. We will assume that the sound pressure is sampled at stationary microphone positions located at random points in the room; these positions are away from the room boundaries and at positions where the direct field from the source is insignificant. In this situation, the spatial variation of the mean-square pressure is represented by a gamma probability distribution for either modal or diffuse sound fields (Bodlund, 1976; Lubman, 1968; Schroeder, 1969; Waterhouse, 1968). This gamma distribution is asymmetric, right-skewed and is bounded at the lower end of the distribution by the minimum possible value for the mean-square pressure.

In practice it is necessary to consider temporal as well as spatial averaging. Here it is assumed that the uncertainty due to time-averaging of the random noise signal at each position is negligible; for further discussion of temporal averaging in measurements see Section 3.3.3.

The valid frequency ranges for the variance and standard deviation formulae in this section are defined in terms of the Schroeder cut-off frequency. At frequencies between $0.2f_S$ and $0.5f_S$ the normalized variance of the mean-square sound pressure can be estimated from (Lubman, 1974)

$$\varepsilon^2(p^2) = \left(1 + \frac{N}{\pi}\right)^{-1} \tag{1.147}$$

where N is the mode count in the frequency band (Section 1.2.5.2).

The corresponding standard deviation of the sound pressure level in decibels, σ_{dB}, can be estimated from Eq. 1.147 by taking account of the gamma distribution using (Craik, 1990)

$$\sigma_{\mathrm{dB}} \approx \frac{4.34}{-0.22 + \sqrt{1 + \frac{N}{\pi}}} \tag{1.148}$$

Using the statistical modal density to calculate the mode count for use in Eqs 1.147 and 1.148 gives a non-integer mode count compared to the integer value determined from the individual

mode frequencies by counting the number of modes that fall within each frequency band. The difference between the two methods is rarely large but the statistical approach is more robust. It accounts for the fact that most rooms are not perfect box-shaped rooms with rigid boundaries; in practice, a modal response will often occur in a frequency band that is adjacent to the band in which it was predicted to lie. It also avoids arbitrary decisions when an individual mode is calculated to lie very close to the boundary between two adjacent frequency bands. By using a statistical approach at frequencies with such low modal overlap we must expect the actual standard deviation in decibels to fluctuate about the smooth curve predicted by Eq. 1.148.

If the lower limit of $0.2f_S$ does not include the lowest frequency band of interest, then a reasonable estimate can still be calculated with Eq. 1.148 when the limit is lowered to that of the frequency band containing the lowest mode frequency (Hopkins and Turner, 2005). As noted by Lubman, this equation takes no account of other important factors: modal damping (reverberation time); combinations of small numbers of different room modes (axial, tangential, or oblique); and the degree to which the modes are excited. Despite these omissions, it generally gives estimates within ± 1 dB of measured values.

In a diffuse field at frequencies above f_S, the normalized variance can be calculated from the bandwidth, B, and the room reverberation time, T, according to (Schroeder, 1969)

$$\varepsilon^2(p^2) = \frac{1}{1 + 0.145BT} \tag{1.149}$$

for which the corresponding standard deviation in decibels is (Schroeder, 1969)

$$\sigma_{\text{dB}} = \frac{5.57}{\sqrt{1 + 0.238BT}} \tag{1.150}$$

In most rooms, Eqs 1.149 and 1.150 will give reasonable estimates at and above $0.5f_S$ (rather than above f_S); this allows continuity from Eqs 1.147 and 1.148 across the entire building acoustics frequency range. Whilst these equations are normally sufficient, it is sometimes necessary to take account of the direct sound field from the omnidirectional sound source. In this situation, the normalized variance above $0.5f_S$ can be calculated from (Michelsen, 1982)

$$\varepsilon^2(p^2) = \frac{1}{1 + 0.145BT} + \left[\frac{\sqrt{\frac{A}{16\pi}}}{160^2 d_{\text{min}}} \left(\frac{S_T \sqrt{A}}{V} \right)^3 \right] \tag{1.151}$$

where d_{min} is the minimum distance between the microphone and the sound source.

For airborne sound insulation measurements in both the laboratory and the field, $d_{\text{min}} = 1$ m (ISO 140 Parts 3 & 4), and the difference between Eqs 1.149 and 1.151 can become significant in the high-frequency range for low reverberation times and/or large rooms.

For Eq. 1.151, the corresponding standard deviation in decibels is (Michelsen, 1982)

$$\sigma_{\text{dB}} \approx 4.34 \sqrt{\varepsilon^2(p^2)} \tag{1.152}$$

Calculated standard deviations over the building acoustics frequency range (using Eqs 1.148, 1.151, and 1.152) are shown in Fig. 1.42 for a 50 m^3 room with different reverberation times and $d_{\text{min}} = 1$ m. Above 100 Hz the standard deviation increases as the reverberation time decreases. Note that these standard deviations are for one-third-octave-bands and that octave-bands will have lower values; hence octave-bands are sometimes used to reduce the required number of microphone positions in a room. As an aside it is worth noting that the standard

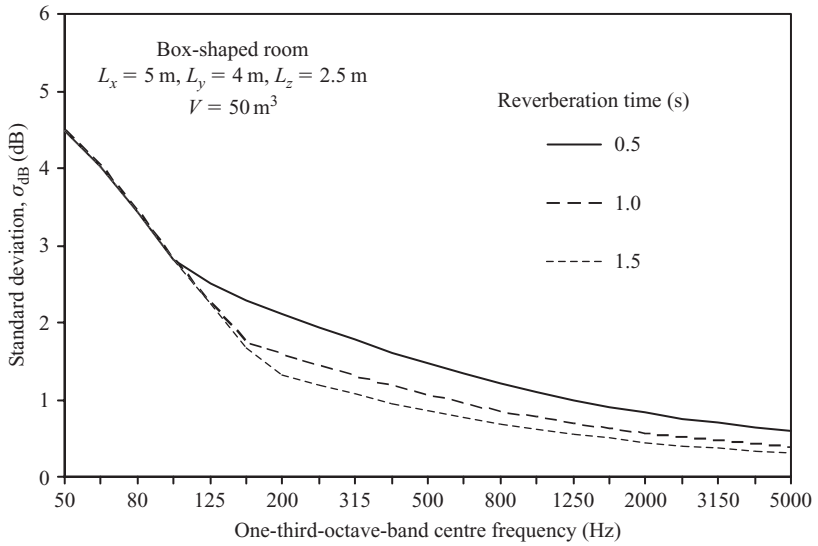

Figure 1.42

Predicted standard deviation for the spatial variation of the sound pressure level for a 50 m^3 source room with different reverberation times.

deviation for a pure tone in a diffuse sound field is 5.6 dB (Schroeder, 1969); this is much higher than the standard deviations that typically occur with broad-band noise measured in one-third-octave or octave-bands over the building acoustics frequency range.

Describing the spatial variation in the receiving room is of equal importance to the source room. However, the situation is more complex for three main reasons.

Firstly, the sound transmitted into the receiving room is not always broad-band in nature. It may contain peaks in the sound pressure level at single frequencies, for example at the critical frequencies of walls/floors/windows, or the mass–spring resonances of wall linings. In reality this may only occur with a few types of homogeneous isotropic building elements because the majority of building elements are constructed from small components (e.g. bricks forming a brick wall) such that there will be spatial variation in the dynamic properties of the element due to both workmanship and the material properties. This makes it less likely that there will be a well-defined pure tone for a critical frequency or mass–spring resonance.

Secondly, we are no longer dealing with a single point source; one or more room surfaces are acting as the sound sources. In the laboratory we assume that all the sound is radiated into the receiving room by the test element, whereas in the field, it is radiated by both separating and flanking elements. Michelsen (1982) and Olesen (1992) have investigated the standard deviation of sound pressure levels in the source and receiving rooms for sound insulation measurements in both the laboratory and the field. Radiating surfaces in the receiving room can be represented as an equivalent number of uncorrelated point sources, hence the larger the surface, the larger the number of point sources. The implication for the standard deviation in a receiving room is that it should be lower than the source room because of the increased number of uncorrelated point sources. Measured data does not confirm that lower values always occur in practice (Michelsen, 1982; Olesen, 1992; Hopkins and Turner, 2005).

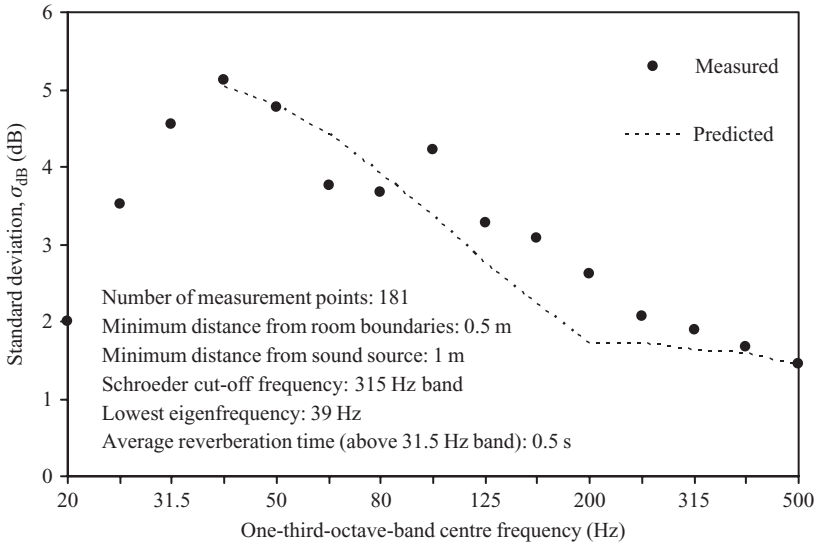

Figure 1.43

Comparison of measured and predicted standard deviations for the spatial variation of the sound pressure level in a 29 m^3 source room. Measured data are reproduced with permission from Hopkins and Turner (2005).

Thirdly, the gamma probability distribution may not be a reasonable representation of the actual distribution for mean-square sound pressure in a receiving room. If we consider the interaction between all the radiating surfaces and the space it is clear that the mean-square sound pressure at any point in the room is determined by a large number of variables. By assuming that these are independent random variables, the sound pressure level will be the sum of a large number of random quantities. The central limit theorem can therefore be used to infer that the spatial variation of the mean-square sound pressure will have a log-normal probability distribution, and the sound pressure level in decibels will have a normal (Gaussian) probability distribution (Lyon and DeJong, 1995).

Despite these three complexities, empirical evidence suggests that reasonable estimates for receiving rooms can be found by using the same equations as for source rooms.

Figures 1.43 and 1.44 show measured and predicted standard deviations for a 29 m^3 source room and a 34 m^3 receiving room (Hopkins and Turner, 2005). The microphone positions are at least 0.5 m from the room boundaries and at least 1 m from the sound source. Generally, there is good agreement between the measurements and the calculated values. The largest discrepancies tend to occur below $0.5f_S$; in practice, measured standard deviations will rarely be greater than 6 dB for typical rooms within this frequency range. The equations discussed above are only valid for sound fields above the lowest mode frequency. However, the measurements in the source room allow us to see the trend for the standard deviation below the lowest mode frequency in the 20 to 31.5 Hz frequency bands. In this range we assume that the sound field is uniform. Below the lowest mode frequency the standard deviation rapidly decreases due to the fading influence of the modes on the sound field. In practice, it is unlikely that the sound field in both source and receiving rooms can be considered as homogeneous and uniform in the first few frequency bands below the band that contains the lowest mode frequency.

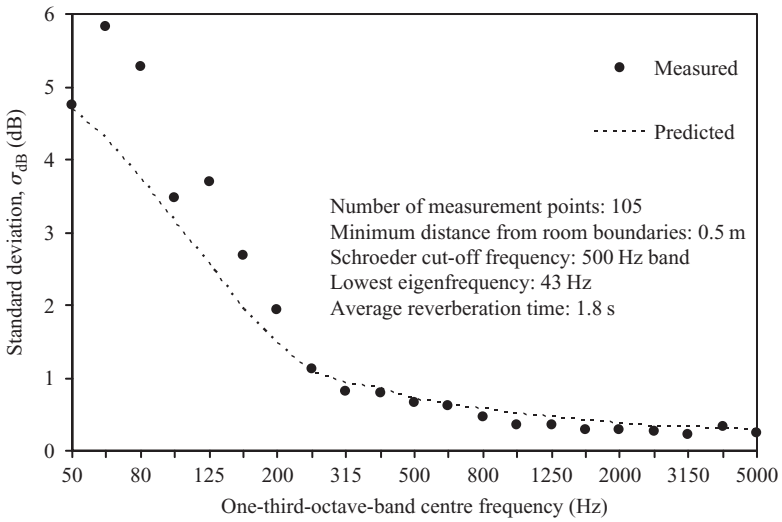

Figure 1.44

Comparison of measured and predicted standard deviations for the spatial variation of the sound pressure level in a 34 m^3 receiving room. Measured data are reproduced with permission from Hopkins and Turner (2005).

1.2.8 Energy

Although we are ultimately interested in the temporal and spatial average sound pressure level in rooms, sound transmission involves energy flow between spaces and structures. This makes it convenient to work with a single variable, energy; so we need to know the relationship between the temporal and spatial average values of sound pressure and energy in a room.

The energy in a room can be derived with two different approaches, one using sound pressure, and the other using sound particle velocity. The latter approach is used to describe the energy stored in structures such as plates and beams; hence it is included here to highlight the link between the way we deal with sound in spaces and the vibration of structures.

In both diffuse and non-diffuse fields, we can assume that the sound field is comprised of plane waves and calculate the sound energy using the plane wave intensity described by Eq. 1.19. The plane wave intensity quantifies the energy travelling through an imaginary surface of unit area in 1 s, where this surface lies perpendicular to the direction of wave propagation. The group velocity, c_g, is defined as the velocity at which wave energy propagates, which for longitudinal waves in air is the same as the phase velocity, c_0. Therefore the energy density in a reverberant field, w_r, that describes the energy in a unit volume is

$$w_r = \frac{I}{c_0} \tag{1.153}$$

Hence the energy stored in volume, V, is

$$E = w_r V = \frac{\langle p^2 \rangle_{t,s} V}{\rho_0 c_0^2} \tag{1.154}$$

where $\langle p^2 \rangle_{t,s}$ is the temporal and spatial average mean-square sound pressure.

An alternative way of deriving the room energy is from the product of the mass of air within the room and the temporal and spatial average mean-square sound particle velocity, $\langle u^2 \rangle_{t,s}$, where the latter can be found from the characteristic impedance of air (Eq. 1.18). This gives

$$E = m\langle u^2 \rangle_{t,s} = \rho_0 V \frac{\langle p^2 \rangle_{t,s}}{\rho_0^2 c_0^2} = \frac{\langle p^2 \rangle_{t,s} V}{\rho_0 c_0^2} \tag{1.155}$$

1.2.8.1 *Energy density near room boundaries: Waterhouse correction*

When calculating the sound energy stored in a reverberant room we need to consider the fact that energy density is not uniformly distributed throughout the space. Near the room boundaries the phase relationships between sound waves impinging upon a point are no longer random. This causes interference patterns and an increase in energy density close to the boundaries (Section 1.2.7.1).

To determine the total sound energy stored in a reverberant room from the energy calculated with Eq. 1.154 (using the spatial average sound pressure measured in the central zone of the room) the energy is multiplied by the following frequency-dependent correction term (Waterhouse, 1955)

$$1 + \frac{S_T \lambda}{8V} \tag{1.156}$$

where S_T is the total surface area of the room.

This term is widely referred to as the Waterhouse correction which is usually more convenient to use in decibels,

$$C_W = 10 \lg \left(1 + \frac{S_T \lambda}{8V} \right) \tag{1.157}$$

In the derivation of the correction term it is assumed that the room surfaces are perfectly reflecting, which is often a reasonable assumption in the low-frequency range where the term is most important. It is also assumed that sound waves are incident from all directions upon a reflecting surface which has dimensions that are large compared to the wavelength. This will not be a valid assumption where the sound field in the central zone of the room cannot be classified as reasonably diffuse, and the room dimensions are small. Another important assumption is that the energy stored in edge and corner zones is relatively small compared to the energy stored near room surfaces. This is a reasonable assumption in many shapes and sizes of room when the walls and floors have large surface areas. However, it is not necessarily appropriate for modal sound fields in the low-frequency range where there are relatively few oblique modes compared to axial and tangential modes. In this situation, numerical calculations indicate that the Waterhouse correction sometimes appears to give accurate results because it overestimates the energy stored near room surfaces (Agerkvist and Jacobsen, 1993). This compensates for the fact that the energy stored in edge and corner zones is not included in the correction term.

Example values for the Waterhouse correction are shown in Fig. 1.45 for box-shaped rooms with volumes in the range 50 to 200 m^3. For these rooms the correction term is greater than 1 dB in the low-frequency range which is often below the Schroeder cut-off frequency. This means that significant values for the correction term tend to occur at frequencies where the sound field in the central zone of the room is not a close approximation to a diffuse field. However, as a rule-of-thumb for the building acoustics frequency range, the Waterhouse correction term tends

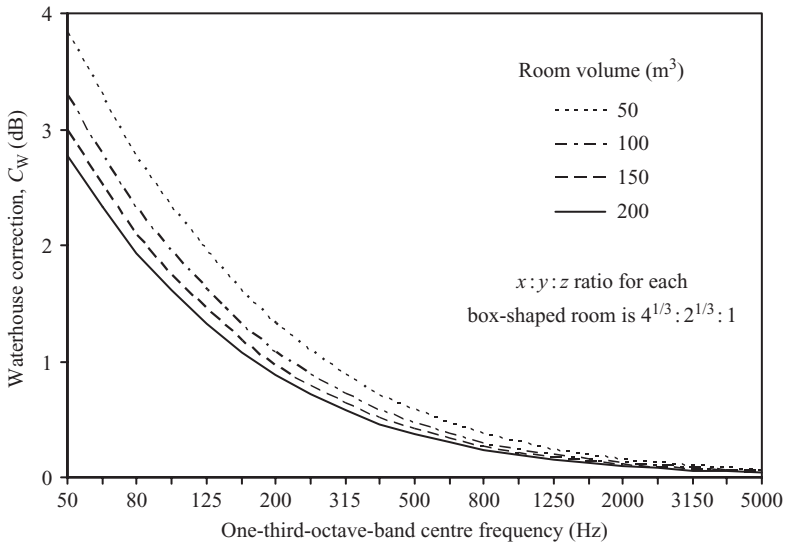

Figure 1.45

Waterhouse correction, C_W, for different room volumes.

to give a reasonable estimate for most empty box-shaped rooms with a minimum volume of 50 m^3. This assumes that the sound pressure level in the central zone is adequately sampled.

When calculating the sound power radiated into a room from sound pressure measurements made in the central zone of a reverberant room, the Waterhouse correction in decibels should be added to the sound pressure level in decibels. However, we do not need to account for interference patterns at the room boundaries when we calculate the diffuse field intensity that is incident upon a surface from the diffuse field sound pressure level. Hence there are some situations where we need to use the Waterhouse correction and some where we don't. Specific applications of the Waterhouse correction that apply to the measurement of sound insulation are noted in Chapter 3.

1.3 Cavities

Cavities exist in many different parts of a building, for example: ceiling voids, roof voids, between the joists in timber floors, in thermal glazing units, within cavity walls, and behind wall linings. They can play an important role in sound transmission because vibration is not only transmitted via structural connections between the plates that form a cavity, but also by the sound field in the cavity itself.

As with rooms we will retain use of the convenient box-shaped space but for cavities we will use L_z as the smallest dimension, the cavity depth (see Fig. 1.46).

1.3.1 Sound in gases

Almost all cavities in buildings are filled with air, so Eq. 1.1 for the speed of sound in rooms is also applicable to cavities. However, cavities such as those in insulating glass units are

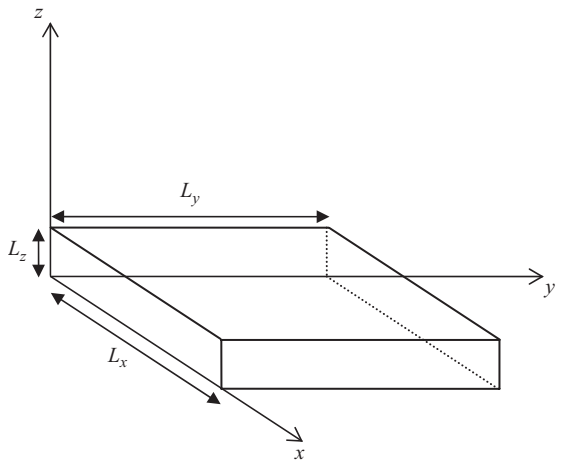

Figure 1.46

Box-shaped cavity.

sometimes filled with other gases. Therefore a more general approach to calculate the phase velocity, c, for any ideal gas is given by

$$c = \sqrt{\frac{1}{\kappa\rho}} = \sqrt{\frac{V}{\kappa nM}} = \sqrt{\frac{\gamma PV}{nM}} = \sqrt{\frac{\gamma R(T + 273.15)}{M}} \tag{1.158}$$

where κ is the gas compressibility (adiabatic), ρ is the gas density, V is the volume occupied by n moles of a gas, M is the molar mass of the gas (kg/mol), γ is the ratio of specific heats at constant pressure and constant volume which is 1.67 for monatomic gases such as helium, 1.41 for diatomic gases such as air, and 1.33 for polyatomic gases, P is the static pressure which is 1.013×10^5 Pa for air at atmospheric pressure, R is the universal gas constant which is 8.314 J/mol.K, and T is the temperature in °C.

Properties of gases that are components of air or gases that are sometimes used in insulating glass units are listed in the Appendix, Table A1.

1.3.2 Sound in porous materials

Cavities in walls and floors are sometimes partly filled or fully filled with porous materials to absorb sound energy and provide other benefits such as thermal insulation. Porous materials are also used around the perimeter of cavities to absorb sound and/or to control the spread of fire. Some examples are shown in Fig. 1.47.

Porous materials essentially consist of a skeletal frame (which could be formed from fibres, granules, or a polymer, etc.) that is surrounded by air. A wide range of porous materials are used in buildings, with a range of frames (e.g. mineral wool, polystyrene balls, open-cell foam, masonry blocks). Sound transmission through porous materials takes place due to airborne propagation through the pores and structure-borne propagation via the frame. However, there are varying degrees of coupling between these types of propagation, and they cannot simply be assumed to occur independently of each other. For this reason, sound propagation through

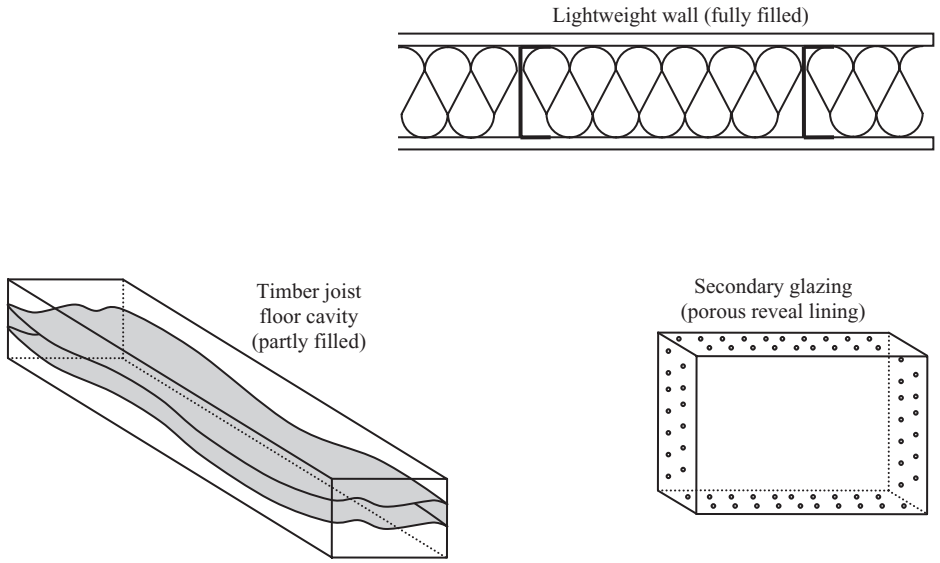

Figure 1.47

Examples of porous materials used in cavities.

porous materials is considerably more complex than in air; the subject is only touched upon here to introduce basic concepts and parameters that are needed in other chapters. For a thorough review of different models used to describe sound in porous materials, the reader is referred to Allard (1993).

1.3.2.1 Characterizing porous materials

Two simple parameters that can be used to describe the properties of porous materials are the porosity and the airflow resistance. For a more complete description of the material, other parameters such as the structure factor, shape factor, and tortuosity can be used to describe aspects relating to the propagation path through the pores. However, these parameters are rarely available, more awkward to measure, and are used in more complex models than will be looked at here.

1.3.2.1.1 Porosity

For porous materials, the porosity, ϕ, is defined as

$$\phi = \frac{V_{\text{air}}}{V_{\text{bulk}}} \tag{1.159}$$

where V_{air} is the volume of air within the material and V_{bulk} is the bulk volume (i.e. total volume) of the material.

For porous materials used in buildings, the porosity is usually in the range, $0.90 < \phi < 0.99$. For mineral wool it is typically $0.95 < \phi < 0.99$. Mineral wool (i.e. glass or rock fibre) is usually

made of solid fibres, hence if the material that binds these fibres together has negligible mass, the porosity can be estimated using

$$\phi = 1 - \frac{\rho_{\text{bulk}}}{\rho_{\text{fibre}}} \tag{1.160}$$

where ρ_{bulk} is the bulk density of the material and ρ_{fibre} is the density of the fibre.

1.3.2.1.2 *Airflow resistance*

Sound absorption by, and sound transmission through porous materials is partly described by their ability to resist airflow. This is quantified by the following parameters: airflow resistance, specific airflow resistance, and airflow resistivity.

The airflow resistance, R (Pa.s/m^3) is defined as

$$R = \frac{\Delta p}{q_{\text{v}}} \tag{1.161}$$

where Δp is the air pressure difference (referred to as differential pressure) across a layer of porous material with respect to the atmosphere (Pa), and q_{v} is the volumetric airflow rate passing through the layer (m^3/s). The volumetric airflow rate is

$$q_{\text{v}} = uS \tag{1.162}$$

where u is the linear airflow velocity (m/s) and S is the cross-sectional area of the porous material perpendicular to the direction of airflow (m^2).

The specific airflow resistance, R_{s} (Pa.s/m) applies to a specific thickness of a porous material; hence it is an appropriate specification parameter for both homogeneous and non-homogeneous materials as well as materials with a porous surface coating or perforated surface layer.

$$R_{\text{s}} = RS \tag{1.163}$$

The airflow resistivity, r (Pa.s/m^2) is the specific airflow resistance per unit thickness, and is only appropriate as a specification parameter for homogeneous materials.

$$r = \frac{S\Delta p}{dq_{\text{v}}} = \frac{RS}{d} = \frac{R_{\text{s}}}{d} \tag{1.164}$$

where d is the thickness of the layer of porous material in the direction of airflow (m).

NB: Specific airflow resistance and airflow resistivity are sometimes quoted in Rayls and Rayls/m respectively. The Rayl is used as a unit for the ratio of sound pressure to particle velocity and is equivalent to Pa.s/m.

For fibrous materials the airflow resistance depends upon the direction of airflow through the material. These materials are usually supplied and used in rectangular sheets, either cut from slabs or from a roll, hence the airflow can be measured in two directions as shown in Fig. 1.48: (1) in the plane of the sheet, the lateral airflow and (2) perpendicular to the plane of the sheet, the longitudinal airflow. In the literature it is usually measurements of the longitudinal airflow that are quoted (e.g. Bies and Hansen, 1980). In rooms or cavities where sheets of material are used to cover a surface it is the longitudinal direction that is needed to calculate the sound absorption coefficient for the surface. However, narrow cavities are sometimes separated by sheets of

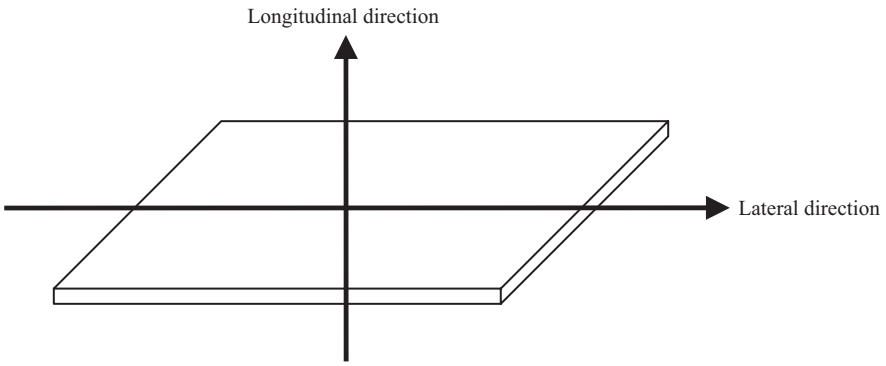

Figure 1.48

Airflow resistivity of a sheet of porous material – definition of lateral and longitudinal directions.

fibrous materials that form a junction between the different cavities. Depending on the orientation of these sheets it is either the lateral or longitudinal direction that is needed to calculate the absorption coefficient for the cavity boundary or sound transmission between cavities.

1.3.2.1.3 *Fibrous materials*

Fibrous materials are commonly used in cavities of walls and floors. The airflow resistance of fibrous materials is due to friction between the fibres and the air particles moving between the fibres, hence it can depend upon: size of fibres, shape/type of fibres (e.g. crimped, hollow), density of fibres, number of fibres per unit volume, and fibre orientation/distribution (e.g. random, stratified/layered, stratified with higher fibre density near the surface of the sheet).

Mineral wool is anisotropic as the fibres tend to lie in planes that are parallel to the plane of the sheet; the orientation of the fibres within each plane being random. Therefore the airflow resistivity in the lateral direction is significantly lower than in the longitudinal direction.

For mineral wool (i.e. glass or rock wool) empirical relationships can be found between airflow resistance and bulk density according to (Bies, 1988; Nichols, 1947)

$$r = \frac{k_1 \rho_{\text{bulk}}^{1+k_2}}{d_{\text{fibre}}^2} \tag{1.165}$$

where k_1 is a constant for a material that is manufactured in a particular way, k_2 is a constant that depends upon fibre orientation, and d_{fibre} is the fibre diameter (microns).

For one type of mineral wool with a known average fibre diameter, the constants k_1 and k_2 can be found from measured airflow resistivity data for a range of bulk densities. By plotting $\lg(r)$ against $\lg(\rho_{\text{bulk}})$, the data points should cluster along straight lines, and linear regression can be used to determine k_1 and k_2. An example is shown in Fig. 1.49 for the lateral and longitudinal airflow resistivity of rock wool (random fibre orientation, average $d_{\text{fibre}} = 4.75\,\mu\text{m}$, average $\rho_{\text{fibre}} = 2600\,\text{kg/m}^3$, porosity range was 0.94 (highest bulk density) $\leq \phi \leq 0.99$ (lowest bulk density), two different UK manufacturers). For the lateral airflow resistivity, $k_1 = 353$, $k_2 = 0.63$ over the bulk density range, $31 \leq \rho_{\text{bulk}} \leq 155\,\text{kg/m}^3$. For the longitudinal airflow resistivity, $k_1 = 780$, $k_2 = 0.59$ over the bulk density range, $38 \leq \rho_{\text{bulk}} \leq 162\,\text{kg/m}^3$.

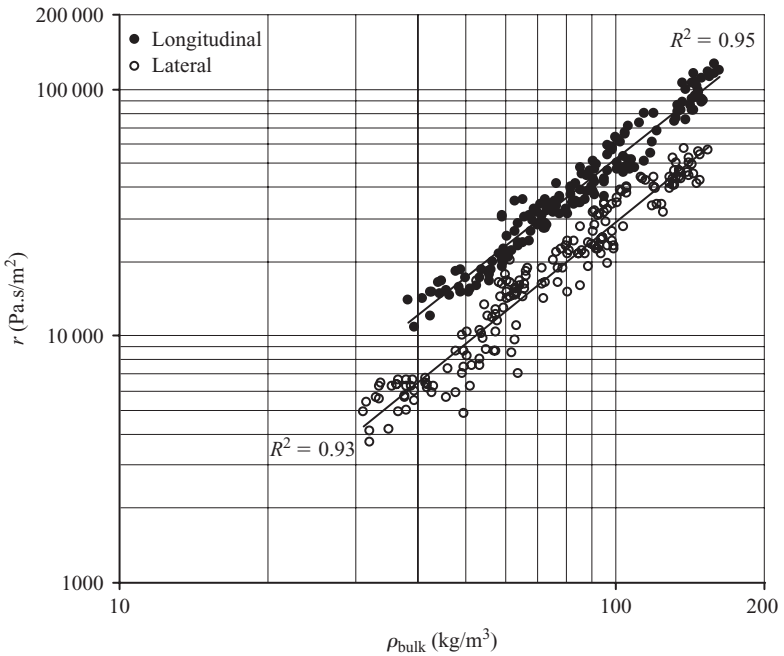

Figure 1.49

Measured airflow resistivity (lateral and longitudinal directions) for rock wool. Individual measurements are shown along with regression lines. Measured data from Hopkins are reproduced with permission from ODPM and BRE.

Measured airflow resistivities and empirical relationships for other porous materials can be found from Bies and Hansen (1980), Mechel and Vér (1992), and Mechel (1995). To cover the full density range for a material it may be necessary to have more than one empirical relationship, this can occur with fibrous materials that can be produced in a wide range of fibre diameters. For materials such as glass wool, the combination of different manufacturing processes and different fibre diameters can lead to empirical relationships that are specific to one manufacturer and/or density range (Bies, 1988).

To determine empirical relationships for materials other than mineral wool, the form of Eq. 1.165 may not be appropriate. For example, with polyester fibre materials it has been shown that better correlation can be found between the airflow resistivity and the number of fibres per unit volume (Narang, 1995).

1.3.2.2 *Propagation theory for an equivalent gas*

General theory for sound propagation in a fluid-saturated porous elastic material requires consideration of two longitudinal waves and one shear wave (Biot, 1956). Modelling these three waves requires knowledge of the fluid density, frame density, porosity, airflow resistivity, tortuosity, complex shear modulus, and Poisson's ratio. In buildings we are usually interested in air-saturated porous materials, rather than liquid-saturated. This simplifies matters because with gases it can often be assumed that the skeletal frame is not elastic, and is sufficiently rigid that it does not move. This allows use of simpler sound propagation models.

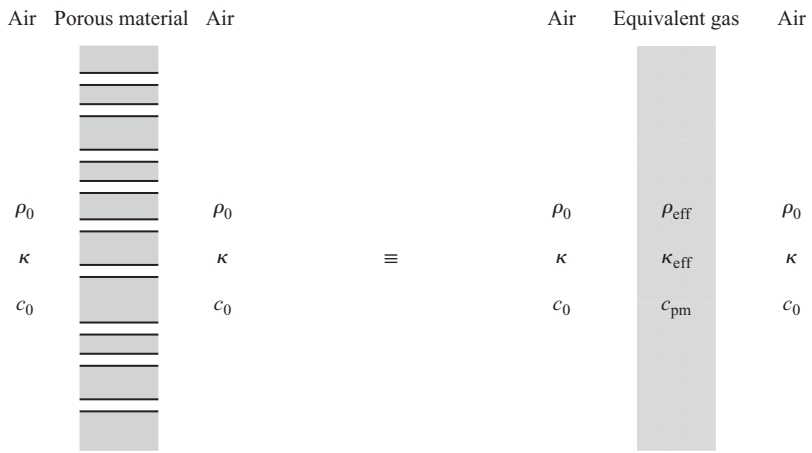

Figure 1.50

Equivalent gas model used for a porous material in air.

For porous materials with a rigid skeletal frame and porosities close to unity, sound propagation can be modelled with a single longitudinal wave by using the concept of an equivalent gas to represent the porous material and the gas (usually air) contained within it (Morse and Ingard, 1968). Within a porous material the compressibility of the gas is altered, and its effective mass is increased because the flow of the gas is impeded by the porous structure. Hence, the equivalent gas is described by using an effective gas compressibility, κ_{eff}, and an effective gas density, ρ_{eff}.

The gas compressibility, κ, equals the reciprocal of the bulk compression modulus of a gas, K, such that

$$\kappa = \frac{1}{K} = \frac{1}{\rho}\frac{\partial \rho}{\partial P} \tag{1.166}$$

where ρ is the gas density.

From this point onwards we will assume that the gas in the porous material is always air. The equivalent gas model is shown in Fig. 1.50. For an infinite medium without internal losses, K takes real values; $K = P_0$ for an isothermal process and $K = 1.4P_0$ for an adiabatic process, where P_0 is the static pressure for air (usually taken as 1.013×10^5 Pa at atmospheric pressure). However, in a porous material it is necessary to use complex values to include the effect of internal damping. For sound propagation in typical rooms, the distances are only usually large enough to require consideration of air absorption in the high-frequency range; this is an internal loss due to the conversion of sound into heat energy. These internal losses occur due to both thermal conduction and viscosity, and result from the molecular constitution of the gas; in an infinite medium the thermal conduction and viscosity contribute almost equally to the internal damping (Morse and Ingard, 1968). In a porous material, sound propagates close to the boundaries of the skeletal frame and the losses due to thermal conduction and viscosity are much larger. Therefore we need to account for these internal losses by using complex values for both the effective gas compressibility and the effective gas density.

The effective gas compressibility varies over the building acoustics frequency range, and depends upon heat transfer between the air and the frame. At 'low' frequencies, the rate of

compression and rarefaction for the longitudinal sound wave in a porous material is sufficiently slow that heat is transferred back and forth between the air and the frame. This means that the temperature remains relatively constant and the process can be assumed to be isothermal. At 'high' frequencies there is insufficient time for this heat transfer to take place, so it becomes an adiabatic process. There is no general definition of 'low' and 'high' frequencies. As a rule-of-thumb for fibrous materials over the building acoustics frequency range, it can be assumed that 'low' corresponds to the low-frequency range, and 'high' corresponds to the high-frequency range, with a transition between isothermal and adiabatic in the mid-frequency range.

The effective gas density also varies with frequency. This can be described in terms of the mass impedance of the skeletal frame, $i\omega m_{\text{frame}}$ (Beranek, 1947). At 'low' frequencies where the mass impedance is small, the compressions and rarefactions of the air particles cause the frame to move too; hence the effective gas density needs to take account of the mass of the frame. At 'high' frequencies where the mass impedance is large, the frame effectively remains motionless.

The concept of an equivalent gas allows sound propagation in porous materials to be described using two parameters, both of which are complex: the complex wavenumber, k_{pm}, and the characteristic impedance, $Z_{0,\text{pm}}$. Assuming harmonic time dependence for a wave using the term $\exp(i\omega t)$, the wave equation for sound propagation in the porous material has the same form as the wave equation for an infinite medium (Eq. 1.14); the difference being that the wavenumber, k, is replaced by k_{pm}.

The complex wavenumber for sound in a porous material, k_{pm}, is

$$k_{\text{pm}} = \text{Re}\{k_{\text{pm}}\} + i\text{Im}\{k_{\text{pm}}\} = \frac{\omega}{c_{\text{pm}}} \tag{1.167}$$

where the phase velocity for sound in the porous material, c_{pm}, is also complex, and equals

$$c_{\text{pm}} = \sqrt{\frac{1}{\phi\rho_{\text{eff}}\kappa_{\text{eff}}}} \tag{1.168}$$

The complex wavenumber is used here to clarify the link between propagation of sound in air and propagation in a porous material via the wave equation. Note that some texts prefer to use the propagation constant, Γ, which is related to the complex wavenumber by

$$\Gamma = ik_{\text{pm}} \tag{1.169}$$

The characteristic impedance for air in a porous material, $Z_{0,\text{pm}}$, is determined in the same way as the characteristic impedance for air in an infinite medium (Eq. 1.18), which gives

$$Z_{0,\text{pm}} = \frac{p}{u} = \rho_{\text{eff}} c_{\text{pm}} = \sqrt{\frac{\rho_{\text{eff}}}{\phi\kappa_{\text{eff}}}} \tag{1.170}$$

The complex wavenumber (Eq. 1.167) and the characteristic impedance (Eq. 1.170) are both calculated from the effective density and the effective gas compressibility. The latter two parameters can be calculated if the structure of the porous material can be represented using idealized geometry. For example, representing all pores by cylindrical tubes at a specified angle to the surface of a sheet of porous material, or representing all the fibres in a sheet of fibrous material by long cylindrical tubes that lie in planes parallel to the surface of the sheet. Microstructural

models that assume idealized geometry can be quite complicated. However, they can give an effective density and gas compressibility that adequately represents real porous materials as well as giving an insight into which parameters are important for sound propagation (e.g. see Allard, 1993). For many porous materials the geometry is not simple and requires a statistical description. However, an alternative, simpler approach can be taken that avoids direct calculation of the effective density and the effective gas compressibility whilst retaining use of the equivalent gas model. This makes use of empirical relationships to determine the complex wavenumber and the characteristic impedance.

The most widely used empirical equations are those of Delany and Bazley (1969, 1970). These form a benchmark against which many other theories are tested, and other empirical equations are compared. They were derived from a large number of measurements on different fibrous materials. The resulting empirical equations for $Z_{0,\mathrm{pm}}$ and k_{pm} only require knowledge of the airflow resistivity which can be measured or determined from other empirical relationships. Although these empirical equations were based upon fibrous materials they can be used to estimate values for porous foams with $r < 10\,000\,\mathrm{Pa.s/m^2}$ (Allard, 1993).

The assumption of a rigid skeletal frame allows empirical laws to be used to calculate sound propagation in isotropic, homogeneous, porous materials. Fibrous materials such as mineral wool can be considered as relatively homogeneous, although they are formed from layers so they are anisotropic. However, by considering propagation through the material in only a single direction, they can be treated as isotropic, homogeneous materials.

Empirical equations are not absolute laws; there are many different materials and there is often more than one way to group or plot the data to carry out regression analysis. Other empirical equations to determine the characteristic impedance and the propagation constant for fibrous materials can be found in the literature (e.g. Mechel and Vér, 1992). A theoretical model for rigid frame fibrous materials from Allard and Champoux (1992) gives similar values to the Delany and Bazley equations in the range of validity but improves the low-frequency trends.

The empirical equations of Delany and Bazley (1969, 1970) are

$$Z_{0,\mathrm{pm}} = \rho_0 c_0 (1 + 0.0571 X^{-0.754} - i0.087 X^{-0.732}) \tag{1.171}$$

and

$$k_{\mathrm{pm}} = \mathrm{Re}\{k_{\mathrm{pm}}\} + i\mathrm{Im}\{k_{\mathrm{pm}}\} = \frac{2\pi f}{c_0}(1 + 0.0978 X^{-0.700} - i0.189 X^{-0.595}) \tag{1.172}$$

where the variable, X, is

$$X = \frac{\rho_0 f}{r} \tag{1.173}$$

The range of validity for Eqs 1.171 and 1.172 is (Delany and Bazley, 1969)

$$0.01 < X < 1.0 \tag{1.174}$$

For the equivalent gas model, the wavelength of sound within the porous material, λ_{pm}, is calculated using

$$\lambda_{\mathrm{pm}} = \frac{2\pi}{\mathrm{Re}\{k_{\mathrm{pm}}\}} \tag{1.175}$$

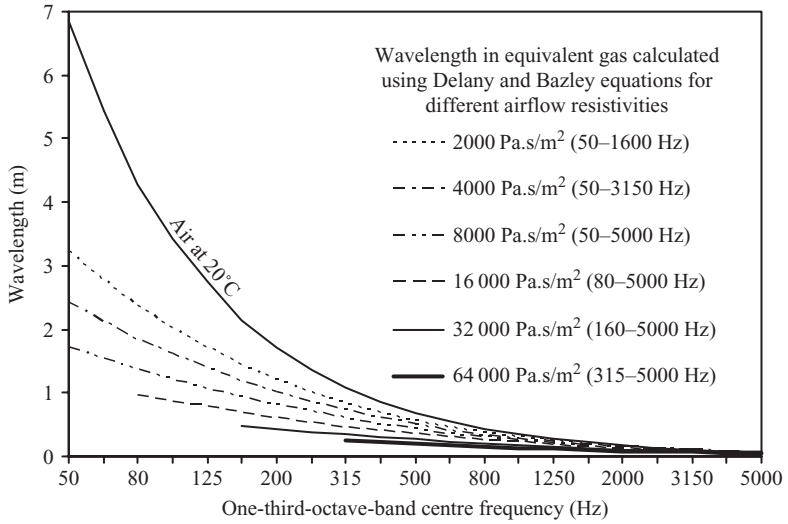

Figure 1.51

Comparison of the wavelength in porous materials using the equivalent gas model with the wavelength in air. The range of validity for the Delany and Bazley equations is shown in brackets in terms of frequency.

In Fig. 1.51 the wavelength in air can be compared with the wavelength for porous materials in air that is calculated using the Delany and Bazley equations. The calculations use a range of airflow resistivities (2000 to 64 000 Pa.s/m^2) that represents porous materials commonly used in buildings. The range of validity for the Delany and Bazley equations (Eq. 1.174) usually allows use of the equivalent gas model for a large part, but not all, of the building acoustics frequency range. The wavelength in the equivalent gas is significantly shorter than air in the low- and mid-frequency ranges, but tends towards the wavelength in air within the high-frequency range.

The sound pressure for a plane wave propagating through a porous material in the positive x-direction is described by

$$p(x,t) = \hat{p}\exp(-ik_{\text{pm}}x)\exp(i\omega t) = \hat{p}\exp(-i\text{Re}\{k_{\text{pm}}\}x)\exp(\text{Im}\{k_{\text{pm}}\}x)\exp(i\omega t) \qquad (1.176)$$

The definition of a complex wavenumber implies attenuation with distance, hence $\text{Im}\{k_{\text{pm}}\}$ is negative; this can be seen in the empirical equation for fibrous materials (Eq. 1.172). Therefore the amplitude of the plane wave decreases with distance according to the decaying exponential term, $\exp(\text{Im}\{k_{\text{pm}}\}x)$. This gives the decrease in sound pressure level in decibels, ΔL_{P}, after propagating a distance, x, through the porous material,

$$\Delta L_{\text{P}} = \frac{20}{\ln 10}|\text{Im}\{k_{\text{pm}}\}|x \qquad (1.177)$$

The installation of porous materials in air spaces means that it is often necessary to account for the reflection that occurs when sound enters the material from air, and when it exits the material into air. This is described in Section 4.3.9 in the calculation of the normal incidence sound reduction index for porous materials.

In some cases there is no air space between the porous material and the plate that forms part of a wall or floor, such as a cavity wall where a porous material fills the cavity. For a plate undergoing bending wave vibration that is immediately next to a porous material, sound transmission from the plate into and through the porous material may need to use Biot theory for the porous material to take account of the shear wave and two longitudinal waves that can propagate within it. In this case, the simplified assumption of an equivalent gas may no longer be appropriate.

1.3.3 Local modes

From Eq. 1.54 the mode frequencies of closed cavities are calculated using

$$f_{p,q,r} = \frac{c}{2}\sqrt{\left(\frac{p}{L_x}\right)^2 + \left(\frac{q}{L_y}\right)^2 + \left(\frac{r}{L_z}\right)^2} \tag{1.178}$$

1.3.3.1 Modal density

To calculate the cavity modal density across the building acoustics frequency range we not only need to consider three-dimensional sound fields like in rooms, but also one-dimensional ($p \neq 0$ and $q = r = 0$), and two-dimensional ($p \neq 0$, $q \neq 0$, and $r = 0$) sound fields. Hence we can represent cavities as a one-dimensional space of length, L_x, a two-dimensional space of surface area, $S = L_x L_y$, and a three-dimensional space of volume, $V = L_x L_y L_z$.

One-, two-, and three-dimensional sound fields can occur in lightweight walls and floors where cavities are formed by a framework of studs or joists. In these cases, the one or two-dimensional modal density can be determined by using Eq. 1.178 to calculate the mode frequencies; the number of modes that fall within each band are then divided by the bandwidth. As with rooms it is simpler to use the following statistical approaches.

For a long (L_x), narrow (L_y), and thin (L_z) cavity at low frequencies there is a one-dimensional sound field consisting purely of axial modes. The modal density is calculated in the same way as for structural waves on beams (Section 2.5.1.4), hence

$$n_{1D}(f) = \frac{2L_x}{c} \tag{1.179}$$

At frequencies at and above $f_{0,1,0}$, but below $f_{0,0,1}$, the cavity acts as a two-dimensional space that supports axial and tangential modes. To count the number of modes the eigenvalues are arranged in a two-dimensional lattice as shown in Fig. 1.52 (Price and Crocker, 1970). Eigenvalues that lie along the x and y-axes represent axial modes; those that lie on the coordinate plane $k_x k_y$ (excluding the eigenvalues on the axes) represent tangential modes. The area associated with each eigenvalue is a rectangle with an area of $\pi^2/L_x L_y$ (which equals π^2/S). The number of modes below a specified wavenumber, k, is equal to the number of eigenvalues that are contained within one-quarter of the area of a circle with radius, k. However, one-half of the area associated with each axial mode falls outside the permissible area in k-space that can only have zero or positive values of k_x and k_y. Therefore calculating the number of modes is a two-step process. The first step is to divide $\pi k^2/4$ by π^2/S to give an estimate for the number of tangential modes that also includes one-half of the axial modes. The second step is to account for the other halves of the axial modes that lie on the x and y-axes by taking one-half

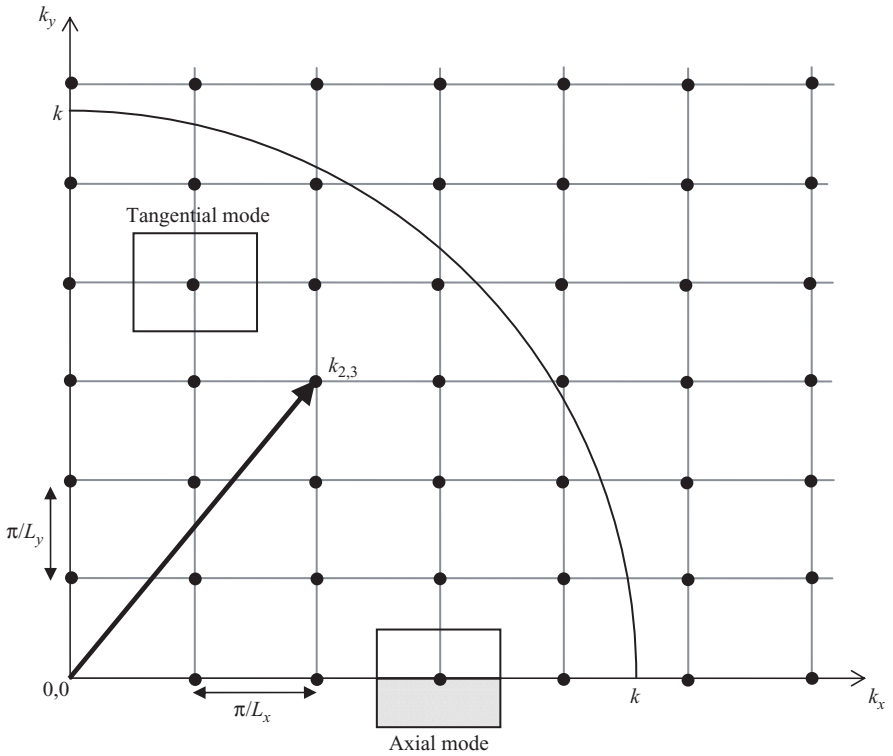

Figure 1.52

Mode lattice for a two-dimensional space. The vector corresponding to eigenvalue, $k_{2,3}$, is shown as an example. The shaded area indicates the fraction of the area associated with axial modes that falls outside the permissible area in k-space. The area enclosed by a circle with radius, k, encloses eigenvalues below wavenumber, k.

of $k/(\pi/(L_x + L_y))$. The sum of these two components gives the number of modes, $N(k)$, below the wavenumber, k, where

$$N(k) = \frac{k^2 S}{4\pi} + \frac{k(L_x + L_y)}{2\pi} \tag{1.180}$$

Hence, from Eq. 1.57 the modal density is

$$n_{2D}(f) = \frac{2\pi f S}{c^2} + \frac{L_x + L_y}{c} \tag{1.181}$$

For cavities that are not box-shaped, and for cavities where there is ambiguity about whether it is reasonable to assume rigid boundaries for one or two of the four boundaries (i.e. those that lie along the planes where $x = 0$, $x = L_x$, $y = 0$, and $y = L_y$), the modal density can be calculated by using only the first term in Eq. 1.181,

$$n_{2D}(f) = \frac{2\pi f S}{c^2} \tag{1.182}$$

The crossover point from a two-dimensional to a three-dimensional sound field occurs at the frequency where there is a half wavelength across the smallest dimension, L_z, which is usually the cavity depth. This corresponds to the axial mode $f_{0,0,1}$, the first cross-cavity mode, where

$$f_{0,0,1} = \frac{c}{2L_z} \tag{1.183}$$

At and above $f_{0,0,1}$ there are axial, tangential, and oblique modes, hence the cavity acts as a three-dimensional space for which the modal density is

$$n_{3D}(f) = \frac{4\pi f^2 V}{c^3} + \frac{\pi f S_T}{2c^2} + \frac{L_T}{8c} \tag{1.184}$$

where S_T is $2(L_xL_y + L_xL_z + L_yL_z)$ and L_T is $4(L_x + L_y + L_z)$.

For cavities that are not box-shaped, and for box-shaped cavities in the high-frequency range, a reasonable estimate of the modal density is found by using only the first term in Eq. 1.184.

The statistical mode count in a frequency band is calculated from the modal density using Eq. 1.63. Mode counts are now used to gain an insight into the distribution of modes for two common cavities, a timber joist floor cavity and a wall cavity (see Fig. 1.53). The timber joist floor cavity is long, narrow, and thin; in the low-frequency range this results in only axial modes along the longest dimension, L_x. Above the first cross-cavity mode in the 800 Hz band there is then a rapid increase in the number of modes with increasing frequency. In contrast, the wall cavity has a two-dimensional sound field over the majority of the building acoustics frequency range with the first cross-cavity mode in the 2500 Hz band.

As with rooms, the distribution of the different mode types is useful in determining which internal cavity surfaces should be lined with absorbent material to reduce the sound level in the cavity. We can take the timber joist floor cavity as an example. To absorb sound in the low-frequency range where there are only axial modes along L_x, absorbent material could be positioned over the surfaces perpendicular to the x-axis at the ends of the cavity where $L_x = 0$ m and $L_x = 4$ m. In practice, floor cavities are often partially or fully filled with absorbent material along their entire length to absorb sound energy stored in axial, tangential, and oblique modes.

1.3.3.2 *Equivalent angles*

Equivalent angles for local modes in rooms were introduced in Section 1.2.5.4. Figure 1.54 shows equivalent angles for the timber joist floor cavity and wall cavity described in Fig. 1.53. These can be compared with the equivalent angles for a 50 m^3 room (refer back to Fig. 1.16). Below the first cross-cavity mode, $\theta_z = 0°$, because the sound field is two-dimensional and there is a limited range of angles. Above the first cross-cavity mode the range of angles tends to cover the full range from 0° to 90°; however, the elongated shape of the timber joist floor cavity means that the distribution of angles between θ_x, θ_y, and θ_z is uneven when compared with the 50 m^3 room.

Compared with rooms, the small volumes and elongated shapes associated with typical cavities means that in the building acoustics range there is often a limited range of angles from which the sound waves will arrive at any point in the space.

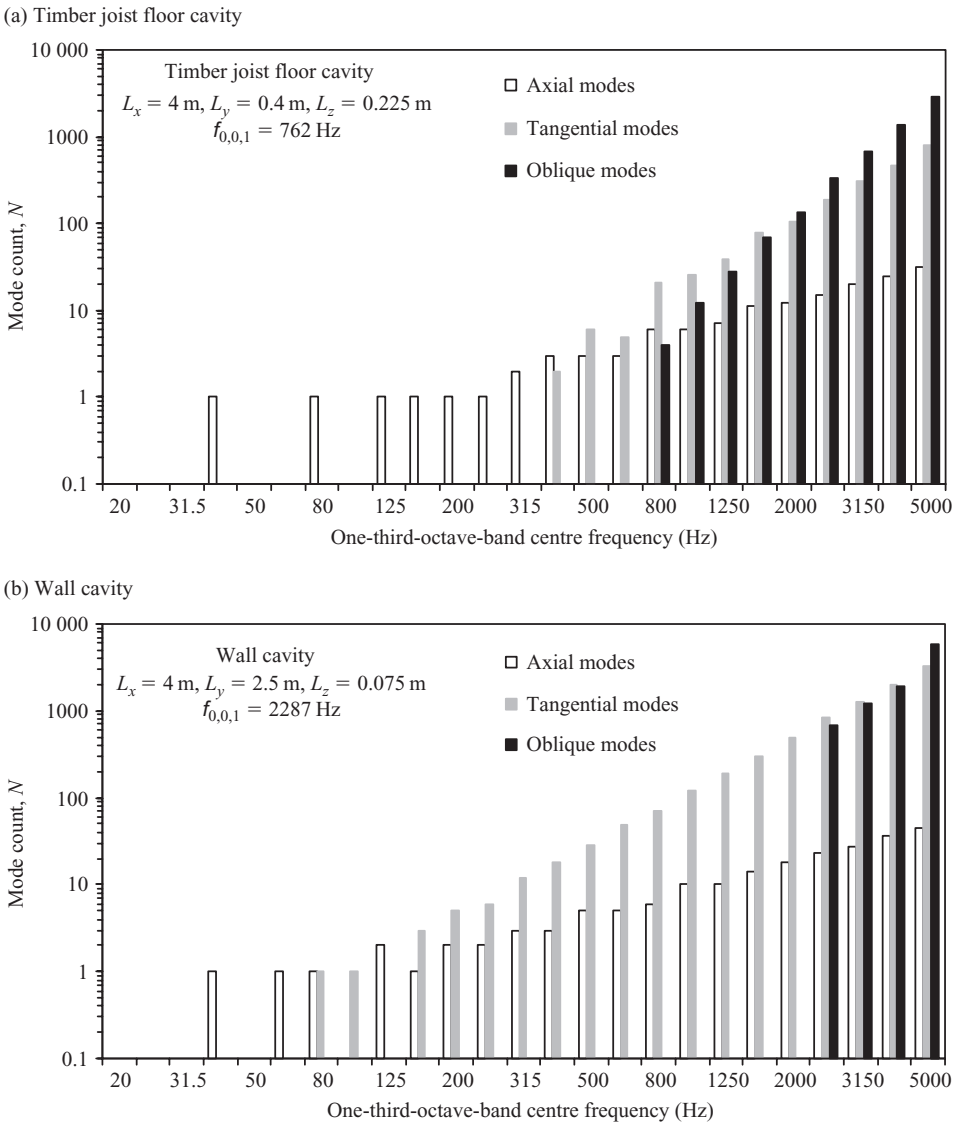

Figure 1.53

Mode count for a timber joist floor cavity and a wall cavity.

1.3.4 Diffuse field

A diffuse field in a cavity is defined in the same way as for rooms. However, when there is a two-dimensional sound field we need to account for the fact that waves can only arrive from directions within one plane rather than from all possible directions in three-dimensional space.

Compared to rooms, cavities have much smaller volumes and the sound field can only usually be considered as diffuse over a narrow part of the building acoustics frequency range.

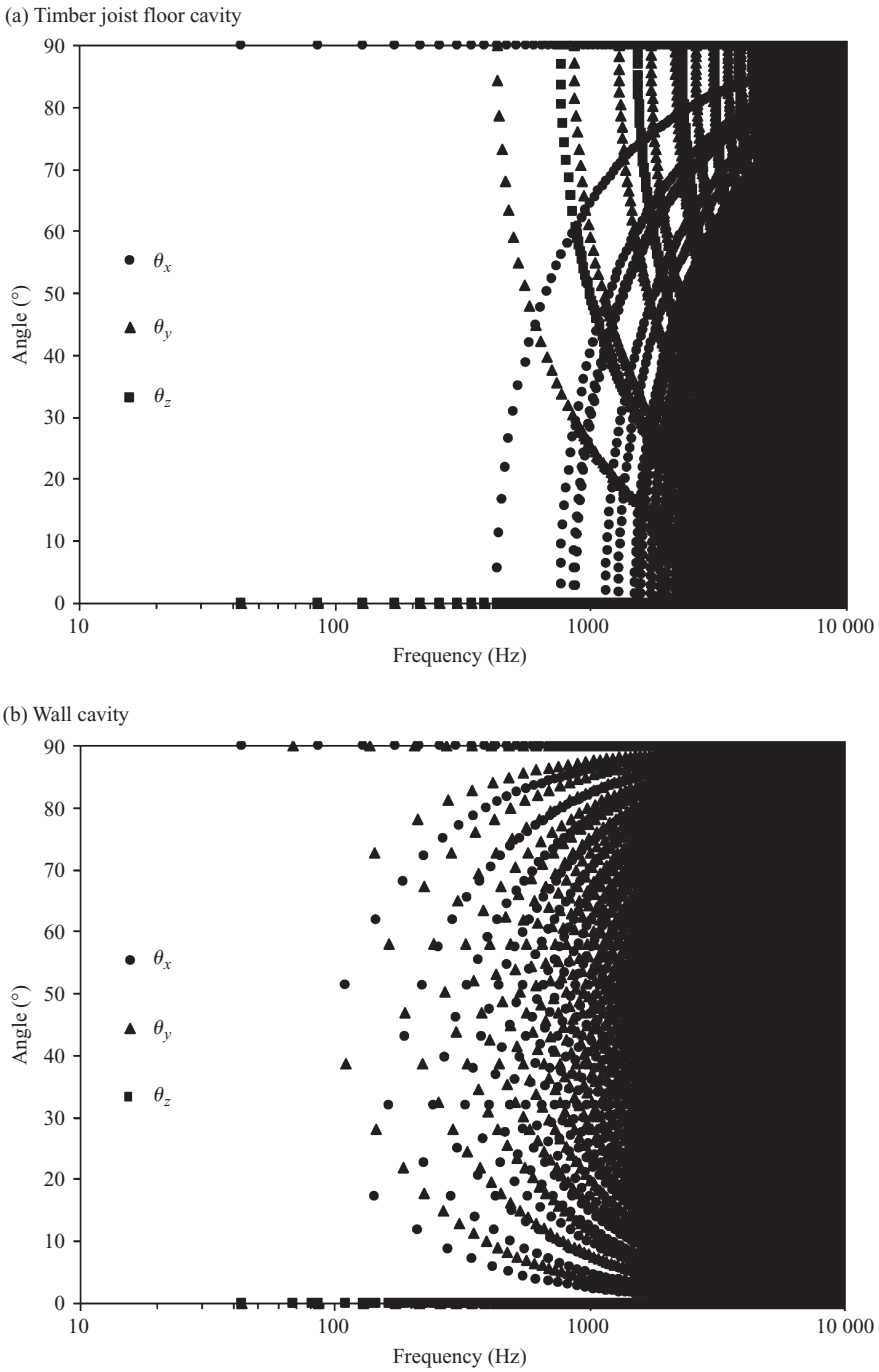

Figure 1.54

Equivalent angles for the modes of a timber joist floor cavity and a wall cavity.

1.3.4.1 Mean free path

As with rooms, the mean free path is only defined for the situation where all reflections from the boundaries are diffuse. When a cavity acts as a three-dimensional space, the mean free path is the same as for rooms and is defined in Eq. 1.47. The mean free path for a two-dimensional space has already been derived in Section 1.2.3.1 and is given by (Kosten, 1960)

$$d_{\text{mfp}} = \frac{\pi S}{U} \tag{1.185}$$

where U is the perimeter of the cavity ($U = 2L_x + 2L_y$ for a rectangular cavity with a depth, L_z).

1.3.5 Damping

In rooms, absorptive material is often distributed in one of two ways: either it is distributed over all the surfaces, or one or two of the room surfaces provide the majority of the absorption area (e.g. highly absorbent tiles that cover the ceiling). In cavities there is more scope to vary the distribution of absorbent material; it can be placed within the cavity volume as well as over the surfaces.

The implications of one, two, and three-dimensional sound fields in cavities becomes apparent when we consider the position of the absorption within the cavity. Below the first cross-cavity mode there are only axial and tangential modes in the cavity, hence sound waves are only incident upon the perimeter of the cavity. To absorb sound in this frequency range, absorptive material needs to be placed around the perimeter of the cavity. In fact, this is sometimes the only practical place to position the absorption. An example of this is high performance windows in music studios, where two or more glazing units are separated by wide cavities. To increase the absorption of sound at and above the first cross-cavity mode the two main surfaces that face into the cavity also need to be absorptive.

Cavities within plasterboard and masonry walls are often filled or partially filled with absorbent porous material. This introduces additional internal losses as sound waves propagate through the porous material.

Cavities tend to have relatively small volumes which often contain additional absorbent material so it is not usually necessary to consider air absorption for the building acoustics frequency range.

1.3.5.1 Reverberation time

Sound fields in cavities rarely approximate a diffuse field in either two or three dimensions, hence the decay curves tend to show various degrees of curvature. The reasons for this are similar to those previously discussed for non-diffuse fields in rooms; normal mode theory indicates that the degree of curvature varies depending upon the combination of axial, tangential, and oblique modes in a frequency band.

Reverberation times in cavities tend to be shorter than those in rooms; examples are shown in Fig. 1.55 which were measured using T_{10}, T_{15}, or T_{20}.

1.3.5.2 Internal losses

Below the frequency of the first cross-cavity mode, the internal loss factor is determined by the absorption of the surface at the cavity perimeter. For locally reacting surfaces, Eq. 1.76

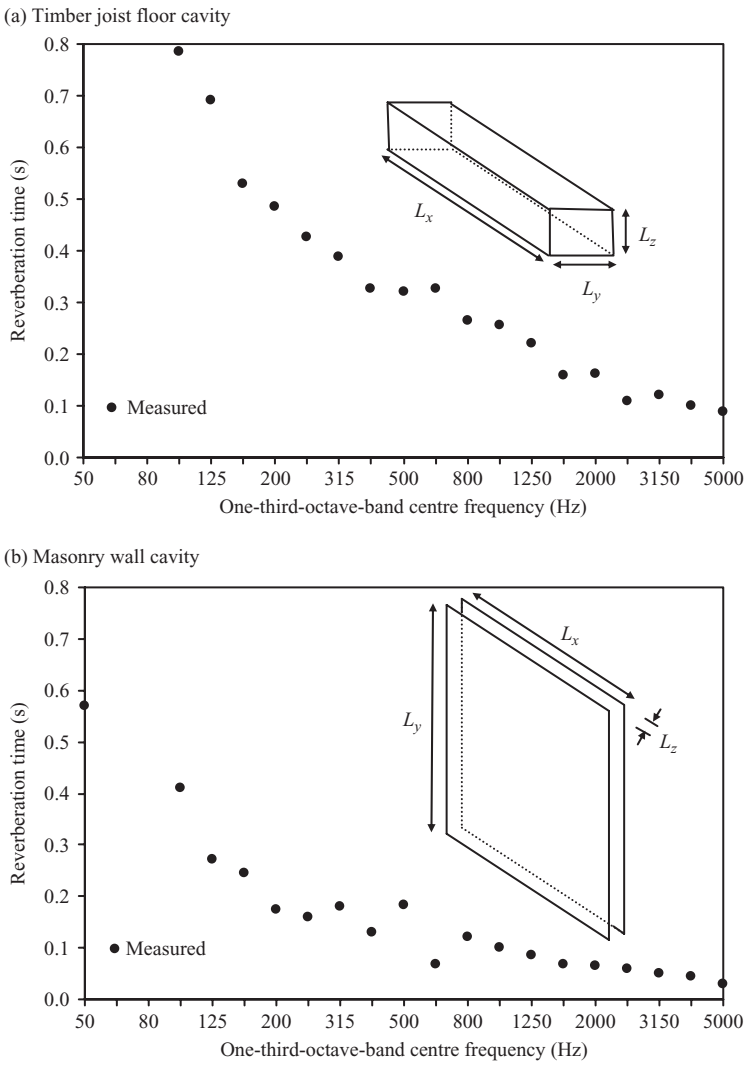

Figure 1.55

Examples of measured reverberation times in cavities. (a) Timber joist floor cavity. $L_x = 4.2\,\text{m}$, $L_y = 0.4\,\text{m}$, and $L_z = 0.225\,\text{m}$. Areas L_yL_z are fair-faced masonry. Areas L_xL_z are timber joists. Area L_xL_y (upper) is chipboard. Area L_xL_y (lower) is plasterboard. (b) Masonry wall cavity. $L_x = 3.6\,\text{m}$, $L_y = 5.0\,\text{m}$, and $L_z = 0.075\,\text{m}$. Areas L_xL_y, L_xL_z and L_yL_z (left side) are fair-faced masonry. Area L_yL_z (right side) is 455 mm, 28 kg/m^3 mineral wool (cavity stop). Measured data from Hopkins are reproduced with permission from ODPM and BRE.

gives the angle-dependent sound absorption coefficient, however, to simplify the calculation it is assumed that $\alpha_\theta = \alpha_0 \cos(\theta)$, which gives (Price and Crocker, 1970)

$$\eta_{ii} = \frac{S_\text{P}\overline{\alpha}_\text{P} c_0}{2\pi^2 f V} \tag{1.186}$$

where S_P is the surface area of the cavity perimeter and $\overline{\alpha}_\text{P}$ is the average statistical sound absorption coefficient for the cavity perimeter. For box-shaped cavities, $S_\text{P} = 2(L_xL_z + L_yL_z)$

and $\overline{\alpha}_P = \sum_{k=1}^{4} S_k \alpha_k / S_P$ where S_k and α_k correspond to the area and statistical absorption coefficient for each side of the cavity perimeter. If the statistical absorption coefficients are not available and the perimeter surface is locally reacting, then $\overline{\alpha}_P$ can be estimated from the normal incidence absorption coefficient, α_0, using (Price and Crocker, 1970)

$$\overline{\alpha}_P = \frac{\pi}{4}\alpha_0 \tag{1.187}$$

At and above the frequency of the first cross-cavity mode, the internal loss factor is

$$\eta_{ii} = \frac{S_T \overline{\alpha} c_0}{8\pi f V} \tag{1.188}$$

where S_T is the total area of all the cavity surfaces and $\overline{\alpha}$ is the average statistical sound absorption coefficient for all the cavity surfaces. For box-shaped cavities, $S_T = 2(L_x L_y + L_x L_z + L_y L_z)$ and $\overline{\alpha} = \sum_{k=1}^{6} S_k \alpha_k / S_T$ where S_k and α_k correspond to each surface of the cavity.

Near the frequency of the first cross-cavity mode an issue arises in using Eqs 1.186 and 1.53 to calculate the internal loss factor. This is because there is often a significant difference between the values for two-dimensional and three-dimensional sound fields. Over the building acoustics frequency range, this causes a sharp transition in the predicted internal loss factor and the predicted reverberation time. In practice, damping measurements inside real cavities indicate a more gradual transition. In the prediction of sound transmission, this is not usually a problem as a sharp transition will not normally occur in the predicted sound insulation because of the existence of many other sound transmission paths.

1.3.5.2.1 *Sound absorption coefficient: Locally reacting porous materials*

Calculation of the internal loss factor requires the normal incidence or statistical sound absorption coefficient for the cavity boundaries. For porous materials the absorption coefficient can be calculated by treating the material as an equivalent gas and using wave theory to calculate the specific acoustic impedance or admittance (e.g. see Allard, 1993). This can make use of equations such as those of Delany and Bazley (Section 1.3.2.2) or Allard and Champoux (1992) to determine $Z_{0,pm}$ and k_{pm} for the equivalent gas.

It is assumed that the porous material is locally reacting with a thickness, h, and is positioned a distance, d, from a rigid non-porous surface that has an infinite impedance (see Fig. 1.56). For this calculation, most masonry/concrete walls and floors can be assumed to be rigid. The calculations in this section are equally applicable to rooms where locally reacting porous materials are placed near masonry/concrete walls or floors.

The normal incidence and statistical absorption coefficients can be calculated using Eqs 1.79 and 1.81 respectively where the specific acoustic admittance is calculated using

$$\beta_{a,s} = \beta_{Re} - i\beta_{Im} = \frac{1}{Z_{a,s}} = \left(\frac{iZ_{0,pm}}{\rho_0 c_0} \frac{\tan(k_{pm}h)\tan\left(\frac{2\pi f d}{c_0}\right) - \frac{\rho_0 c_0}{Z_{0,pm}}}{\tan\left(\frac{2\pi f d}{c_0}\right) + \frac{\rho_0 c_0}{Z_{0,pm}}\tan(k_{pm}h)} \right)^{-1} \tag{1.189}$$

When $d = 0$, the porous layer is next to the rigid surface (often referred to as rigid backing). Equation 1.189 then reduces to

$$\beta_{a,s} = \beta_{Re} - i\beta_{Im} = \frac{1}{Z_{a,s}} = \left(\frac{-iZ_{0,pm}}{\rho_0 c_0} \frac{1}{\tan(k_{pm}h)} \right)^{-1} \tag{1.190}$$

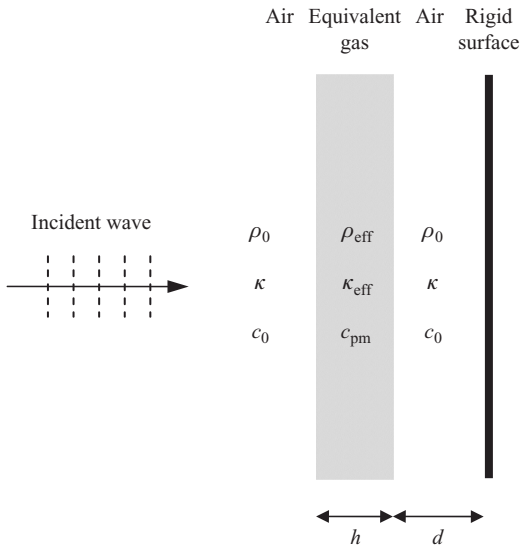

Figure 1.56

Absorber: porous material – air gap – rigid surface. Equivalent gas model used to represent the porous material.

When $d = n\lambda/2$ for $n = 1, 2, 3$, etc., the specific acoustic admittance calculated from Eq. 1.189 is the same as Eq. 1.82, and the porous material can be considered as rigidly backed.

Examples for the statistical absorption coefficient are shown in Fig. 1.57 for a range of airflow resistivities from 2000 to 64 000 Pa.s/m^2. Two thicknesses of porous material are considered, $h = 0.025$ m and $h = 0.1$ m, each of which have air gaps of $d = 0$ m and $d = 0.1$ m. For rigid backing, increasing the thickness of the material from 25 to 100 mm significantly increases the absorption coefficient in the low- and mid-frequency ranges. However, by using a 100 mm air gap with the 25 mm material it is possible to achieve similarly high values to the 100 mm material with rigid backing in the low- and mid-frequency ranges; this is at the expense of lower absorption coefficients in the high-frequency range. With an air gap, the curve for the absorption coefficient has a ripple with troughs that tend to become less pronounced with increasing airflow resistivity. In practice, this ripple is less pronounced due to the use of frequency bands, variation in material properties, and variation in d due to workmanship.

The airflow resistance of porous materials tends to increase with increasing bulk density, but there is no simple rule that porous materials with low or high airflow resistivity will always give the highest absorption coefficients over the building acoustics frequency range. To determine suitable values of r, h, and d, it is necessary to identify which part of the frequency range requires the highest absorption coefficients. There are a large number of permutations for these three variables, and measured absorption coefficients for a specific combination are not always available. In order to assess their effect it is usually sufficient to calculate the absorption coefficient as described in this section. For fibrous materials, a wide range of densities are available (typically 10 to 200 kg/m^3) which gives a wide range of airflow resistivities from which to choose a specific material. However, commonly available materials come in a limited range of thicknesses, which, in combination with the cavity dimensions will limit the choice of h and d.

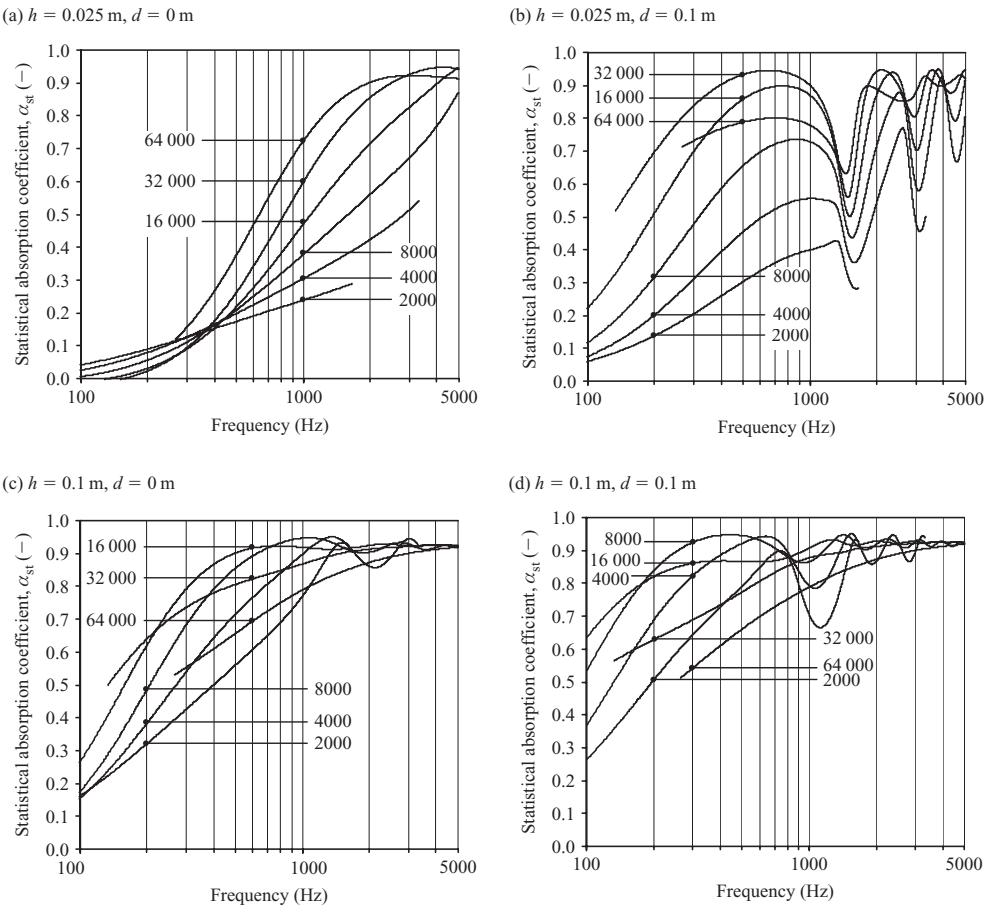

Figure 1.57

Statistical absorption coefficients of porous materials for a range of airflow resistivities in Pa.s/m^2.

1.3.5.3 Coupling losses

Calculation of the coupling loss factors involving the cavity are discussed in Section 4.3.5.3.

1.3.5.4 Total loss factor

The total loss factor equals the sum of the internal and coupling loss factors. For most cavities in walls and floors that have absorptive surfaces, the coupling loss factors are much smaller than the internal loss factor, and the latter provides a reasonable estimate of the total loss factor. As with rooms, Eq. 1.107 can be used to calculate the total loss factor from the reverberation time and vice versa.

1.3.5.5 Modal overlap factor

The modal overlap factor for cavities is calculated using Eq. 1.109.

1.3.6 Energy

Calculation of the sound energy stored in a cavity is calculated using Eq. 1.154 in the same way as for rooms.

1.4 External sound fields near building façades

To assess the airborne sound insulation of the building façade from external sound sources it is necessary to measure the sound pressure levels both inside and outside the building. Having looked at the internal sound field, we will now look at the external sound field near a façade.

The sound pressure level near the façade depends upon: the position of the microphone in relation to the façade and the ground, diffraction effects from the edges of the façade, diffraction effects from protruding or recessed elements on the building façade (e.g. balconies), sound propagation from the source (including the effects of ground impedance, façade impedance, and meteorological conditions), the orientation of the sound source, and the type of sound source outside the building (e.g. point source, line source).

Microphone positions relative to the façade and the ground often differ depending upon whether the primary aim is to measure the façade sound insulation, or measure/predict the environmental noise near the façade. In the latter case, the measurements/predictions are often used at a later point in time to estimate sound transmission into the building via the façade; it is clearly advantageous if the microphone positions are the same or the levels can be accurately converted. For field measurements of façade sound insulation, the microphone is usually attached to the surface of the façade at variable heights that depend upon the building element that is being measured, or positioned 2 m in front of the façade at a height of 1.5 m above the floor of the receiving room (ISO 140 Part 5). Environmental noise measurements are taken at a variety of different positions; often at a height of 1.2, 1.5, or 4 m above floor level, and at distances between 1 and 2 m in front of the façade (ISO 1996 Part 1).

In practice we often need to convert sound pressure levels near the building façade to free-field levels in the absence of the façade and vice versa. This section therefore looks at the difference between the external sound pressure level with the façade to the level without the façade (i.e. the change in level due to the presence of the façade).

1.4.1 Point sources and semi-infinite façades

For façade sound insulation measurements made with a loudspeaker and some environmental noise sources it is appropriate to consider a point source. We therefore start by looking at the sound field generated by a point source in the vicinity of a façade. By creating the image sources for this situation as shown in Fig. 1.58, we see that the sound travels from the source (S) to the receiver (R) via four different paths: the first path is the direct path from the source to the receiver, the second path involves a single reflection from the ground, the third path involves a single reflection from the ground and a single reflection from the façade, and the fourth path involves a single reflection from the façade. The path lengths in terms of the distance, d, from the source, or image source, to the receiver are also indicated in this diagram.

We will assume that: (a) the source emits spherical waves, (b) the ground and façade are perfectly reflecting with no phase change upon reflection (c) all reflections are specular

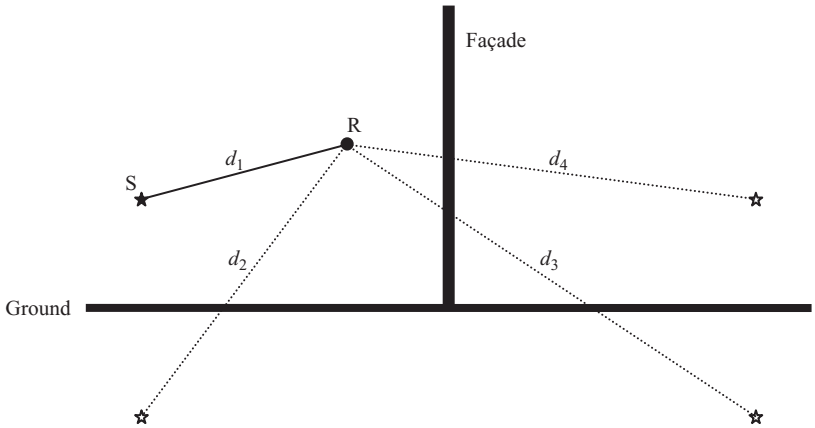

Figure 1.58

External façade sound pressure level measurements. Source (S) and receiver (R) orientation with image sources (☆) for the different propagation paths.

(d) the façade has dimensions that are very large compared to the wavelength (i.e. a semi-infinite plate), and (e) there are no other façades nearby that significantly affect the sound field. Therefore we will not concern ourselves with diffraction from the edges of the wall or with different impedances for the ground and the façade. The assumption of specular reflection is reasonable for this situation, particularly below 1000 Hz; it can generally be assumed that real façades have small scattering coefficients (Ismail and Oldham, 2005).

We are interested in the difference between the sound pressure level in front of the façade and the free-field level without the façade. This requires the ratio of the total mean-square sound pressure, p^2, to the mean-square sound pressure, $(p_1 + p_2)^2$; the latter term corresponds to the combination of the direct path between source and receiver (path length d_1), and the path in which the sound is reflected directly from the ground to the receiver (path length d_2). The sound pressure for spherical waves at single frequencies is taken from Eq. 1.22, hence the required ratio is

$$\frac{\langle p^2 \rangle_t}{\langle (p_1 + p_2)^2 \rangle_t} = \frac{\left| \frac{\exp(-ikd_1)}{d_1} + \frac{\exp(-ikd_2)}{d_2} + \frac{\exp(-ikd_3)}{d_3} + \frac{\exp(-ikd_4)}{d_4} \right|^2}{\left| \frac{\exp(-ikd_1)}{d_1} + \frac{\exp(-ikd_2)}{d_2} \right|^2} \tag{1.191}$$

Now we can calculate the change in level due to the presence of the façade for different distances of the receiver from the façade. For façade sound insulation measurements, the external microphone is usually at a distance of 2 m from the façade or on the surface of the façade (ISO 140 Part 5); hence we will use these to define the minimum and maximum distances for the range of interest. To illustrate the effect of intermediate distances we will look at 300 mm and 1 m.

For measurements on the surface of the façade there are usually physical limitations that determine how close the microphone can be positioned to the surface. For a half-inch microphone (12.7 mm diameter) attached to the façade with the axis of the microphone parallel to the plane of the façade, we can assume that the façade-receiver distance is 6.35 mm (i.e. the distance from the façade surface to the centre of the microphone diaphragm). Figure 1.59 shows the

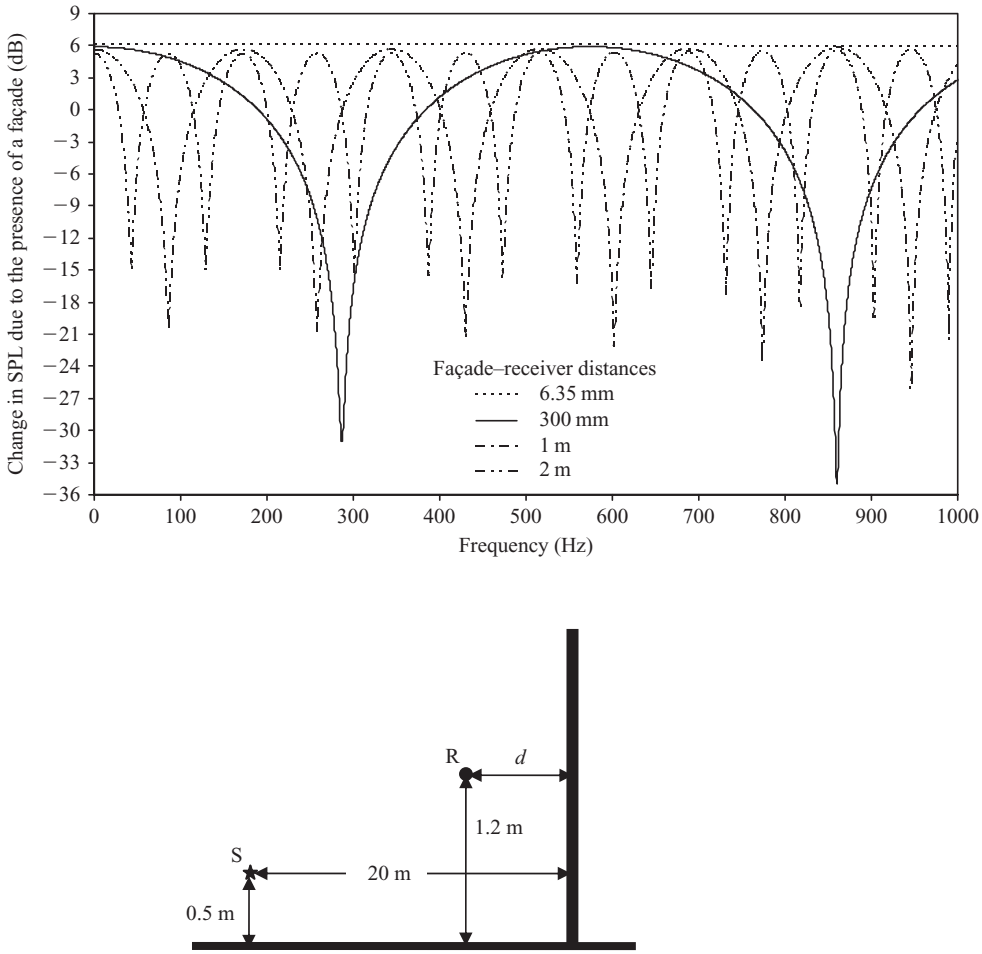

Figure 1.59

Change in the sound pressure level due to the presence of the façade for receiver positions at four different distances, d, from the façade (single frequencies from 0.25 to 1000 Hz). Source-receiver-façade geometry is indicated in the sketch.

calculated level difference for four different façade-receiver distances at frequencies up to 1000 Hz. For a half-inch microphone attached to the surface of a façade there is a constant level difference of 6 dB, this is referred to as pressure doubling. As the microphone is moved further away from the façade we see that there are interference minima in the spectrum due to destructive interference between the different propagation paths. These occur due to the different distances travelled by the sound waves along each of the different paths. For the various combinations of paths, the path difference in metres corresponds to a phase difference in radians. Destructive interference occurs where the path length difference, Δd_{pq}, between paths p and q, corresponds to a phase difference of an odd number of π radians,

$$2\pi \frac{\Delta d_{pq}}{\lambda} = (2n+1)\pi \tag{1.192}$$

where $n = 0, 1, 2, 3$, etc.

The upper frequency shown in this example has been limited to 1000 Hz because at higher frequencies, turbulent air in the outdoor environment tends to reduce the coherence between the waves that travel along the different propagation paths (Attenborough, 1988; Quirt, 1985). As a result, this simple model is no longer appropriate, and sharp minima in the spectrum due to destructive interference are less likely to occur above 1000 Hz.

In practice we usually deal with frequency bands rather than single frequencies. For frequency bands the same ratio can be calculated from the band centre frequency using

$$\frac{\langle p^2\rangle_t}{\langle (p_1+p_2)^2\rangle_t} = \frac{\begin{array}{c} 1+\left(\dfrac{d_1}{d_2}\right)^2+\left(\dfrac{d_1}{d_3}\right)^2+\left(\dfrac{d_1}{d_4}\right)^2 \\ +\dfrac{2d_1}{d_2}R(\Delta d_{12})+\dfrac{2d_1}{d_3}R(\Delta d_{13})+\dfrac{2d_1}{d_4}R(\Delta d_{14}) \\ +\dfrac{2d_1^2}{d_2d_3}R(\Delta d_{23})+\dfrac{2d_1^2}{d_2d_4}R(\Delta d_{24})+\dfrac{2d_1^2}{d_3d_4}R(\Delta d_{34}) \end{array}}{1+\left(\dfrac{d_1}{d_2}\right)^2+\dfrac{2d_1}{d_2}R(\Delta d_{12})} \tag{1.193}$$

where the autocorrelation function, $R(\Delta d_{pq})$ for each path length difference (magnitude), Δd_{pq}, is (Delany *et al*., 1974)

$$R(\Delta d_{pq}) = \frac{\lambda}{2\pi B_{\mathrm{L}}\Delta d_{pq}}\cos\left(\frac{2\pi\Delta d_{pq}}{\lambda}\right)\sin\left(\frac{2\pi B_{\mathrm{L}}\Delta d_{pq}}{\lambda}\right) \tag{1.194}$$

for which λ is the wavelength corresponding to the band centre frequency, and B_{L} is calculated from the lower and upper frequency limits of the band, f_{l} and f_{u}, using $B_{\mathrm{L}} = (f_{\mathrm{u}} - f_{\mathrm{l}})/(f_u + f_l)$. $B_{\mathrm{L}} = 0.115$ for one-third-octave-bands.

For one-third-octave-bands between 50 and 1000 Hz the change in level due to the presence of the façade is shown in Fig. 1.60 (source and receiver positions are the same as in Fig. 1.59). The change in level is 6 dB for a half-inch microphone attached to the surface of the façade. One advantage of using surface measurements is that if the microphone is positioned very close to the surface, we can avoid interference minima in the building acoustics frequency range, although there will be small departures from pressure doubling in the high-frequency range. This allows us to make the convenient assumption of pressure doubling. In contrast, the façade–receiver distance of 300 mm provides an example of the variation that can be introduced when measurements are not made on the surface of the façade. With this particular combination of source–receiver–façade geometry there is an interference dip around the 315 Hz band. If, for example, we were to change the façade-receiver distance from 300 to 200 mm, we would shift the interference dip into a different frequency band. This dependence on the specific geometry of each situation illustrates the importance of well-defined measurement positions for comparative measurements of the sound field near façades. For a façade-receiver distance of 1 or 2 m there are dominant interference minima in the low-frequency range. However the one-third-octave-bands get wider as the frequency increases and the interference effects begin to average out. For façade-receiver distances of 1 or 2 m in the mid-frequency range, the change in level tends towards 3 dB; this is referred to as energy doubling.

For a point sound source, such as a loudspeaker in the low-frequency range, the above discussion indicates that the sound pressure level will also vary over the surface of a façade due to the different interference patterns that occur with different source–receiver–façade geometries. In the mid- and high-frequency ranges, loudspeakers tend to become increasingly directional

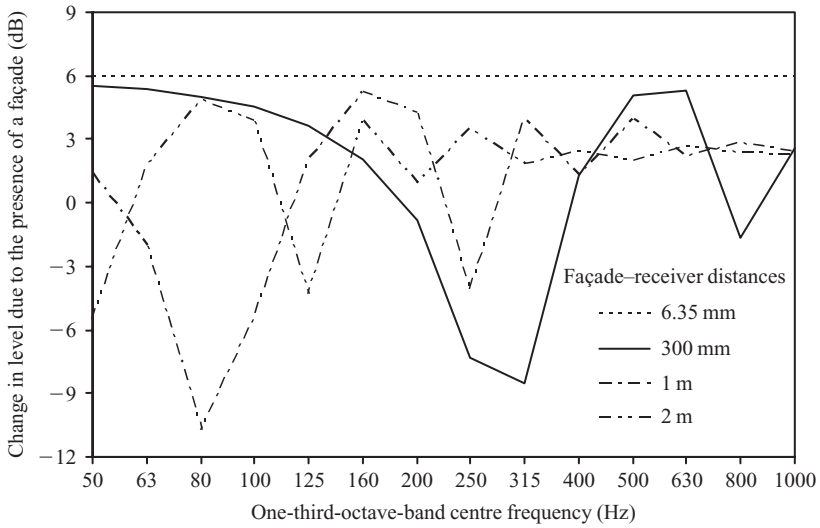

Figure 1.60

Change in the sound pressure level due to the presence of the façade for receiver positions at different distances from the façade.

and no longer act as point sources, hence the variation in sound pressure level over the façade is also affected by the directionality of the loudspeaker.

Although several assumptions have been made in this basic model, it adequately illustrates the general trends. In practice there are other factors that affect the depth and frequency of the interference minima. The finite impedance of the ground causes a phase change upon reflection from the ground, so to improve the model it is necessary to incorporate measurements of the ground impedance (e.g. see Ogren and Jonasson, 1998). Compared to the ground, relatively little information is available on the impedance of façades. However, façade surfaces are rarely highly porous and tend to have low-absorption coefficients (typically less than 0.1 in the low- and mid-frequency ranges). For this reason, the assumption of a perfectly reflecting surface is often reasonable.

1.4.1.1 *Effect of finite reflector size on sound pressure levels near the façade*

As real façades are of finite size, we need to look at the effects of diffraction from the edges of a façade. The sound field in front of finite size reflectors can be considered as the combination of the four geometrical wave paths (as previously considered for the semi-infinite reflector), combined with edge or boundary diffraction waves. To assess diffraction we will look at indoor scale-model measurements because it is awkward to control all the relevant parameters with outdoor measurements near real buildings. Results are taken from scale model experiments in a semi-anechoic chamber with a concrete floor, and a 30 mm thick square reflector (varnished board) to represent the façade. Good agreement between these measurements and predictions using Integral Equation Methods (IEM) allow conclusions to be drawn purely by using measured data (Hopkins and Lam, 2008). A 1:5 scale model was used for the measurements, but all the results shown and discussed in this section are scaled-up to the situation for real façades (i.e. full-size). The source was a small loudspeaker positioned in the vertical plane perpendicular to

the center line of the reflector. The receiver position was offset from this plane by one-twelfth of the reflector dimension to avoid perfect symmetry in the set-up that might be unrepresentative of the situation in practice. Five square reflectors were tested that represented full-size façades with side dimensions of 2, 3, 4, 5, and 6 m.

Figure 1.61 shows the change in level due to two square reflectors (6×6 m and 2×2 m) with a façade–receiver distance of 2 m. Measured data is shown alongside the prediction for a semi-infinite reflector (Eq. 1.191). Compared to the semi-infinite reflector, diffraction from the edges of the finite reflector affects the frequency of the peaks and troughs as well as their values. As one would expect, this is more pronounced for the smaller reflector. For small reflectors, the receiver will be relatively close to the edges and the edge diffracted pressure can significantly change the interference pattern in comparison to the semi-infinite reflector. The 6×6 m reflector can be taken as being representative of the façade of a detached house, and diffraction can be considered to have negligible effect on measured levels above 100 Hz. For the 2×2 m reflector, diffraction can have a significant effect below 1000 Hz; in practice, most façades are much larger than this, but it is used here to represent small square protruding sections of a building (e.g. bay window, entrance hall, enclosed balcony).

For practical purposes we need to assess the difference between finite size reflectors and a semi-infinite reflector in one-third-octave-bands; this is done using the difference between the measured and the predicted (Eq. 1.193) change in level due to the presence of the façade. Figure 1.62 shows this level difference for a façade–receiver distance of 2 m. For square reflectors with side dimensions between 3 and 6 m, the level differences are generally less than 3 dB in the low-frequency range. The differences are larger with the 2×2 m reflector, particularly at 63 Hz, but they are generally less than 3 dB across the low- and mid-frequency ranges. Environmental noise measurements are often taken using a façade–receiver distance between 1 and 2 m. Figure 1.63 shows the level difference for 11 different façade–receiver distances in 0.1 m steps from 1 to 2 m for each of four different square reflectors (side dimensions between 3 and 6 m). In the low-frequency range there are significant differences between the semi-infinite and the finite reflectors due to diffraction. In the mid-frequency range these differences are negligible and these finite reflectors can be treated as semi-infinite. The level differences for the 2×2 m reflector are shown separately in Fig. 1.63; these indicate that it is not appropriate to treat this small reflector as semi-infinite in both the low- and mid-frequency ranges.

In practice there are so many permutations of source–receiver–façade geometry that it is difficult to make a definitive statement about the conditions in which diffraction effects will be negligible. As a rule-of-thumb for a point source near the ground, and façade–receiver distances between 1 and 2 m, diffraction effects are only likely to be significant in the low-frequency range for façades with dimensions <5 m.

1.4.1.2 *Spatial variation of the surface sound pressure level*

Façade elements such as windows or doors often have lower airborne sound insulation than the wall around them. Hence, field measurement of the apparent sound reduction index is often needed for these elements. This requires measurement of the average surface sound pressure level over the element. A spatial average is needed for all elements regardless of the source–receiver–façade geometry; usually between three and ten microphone positions on the surface of the element (ISO 140 Part 5).

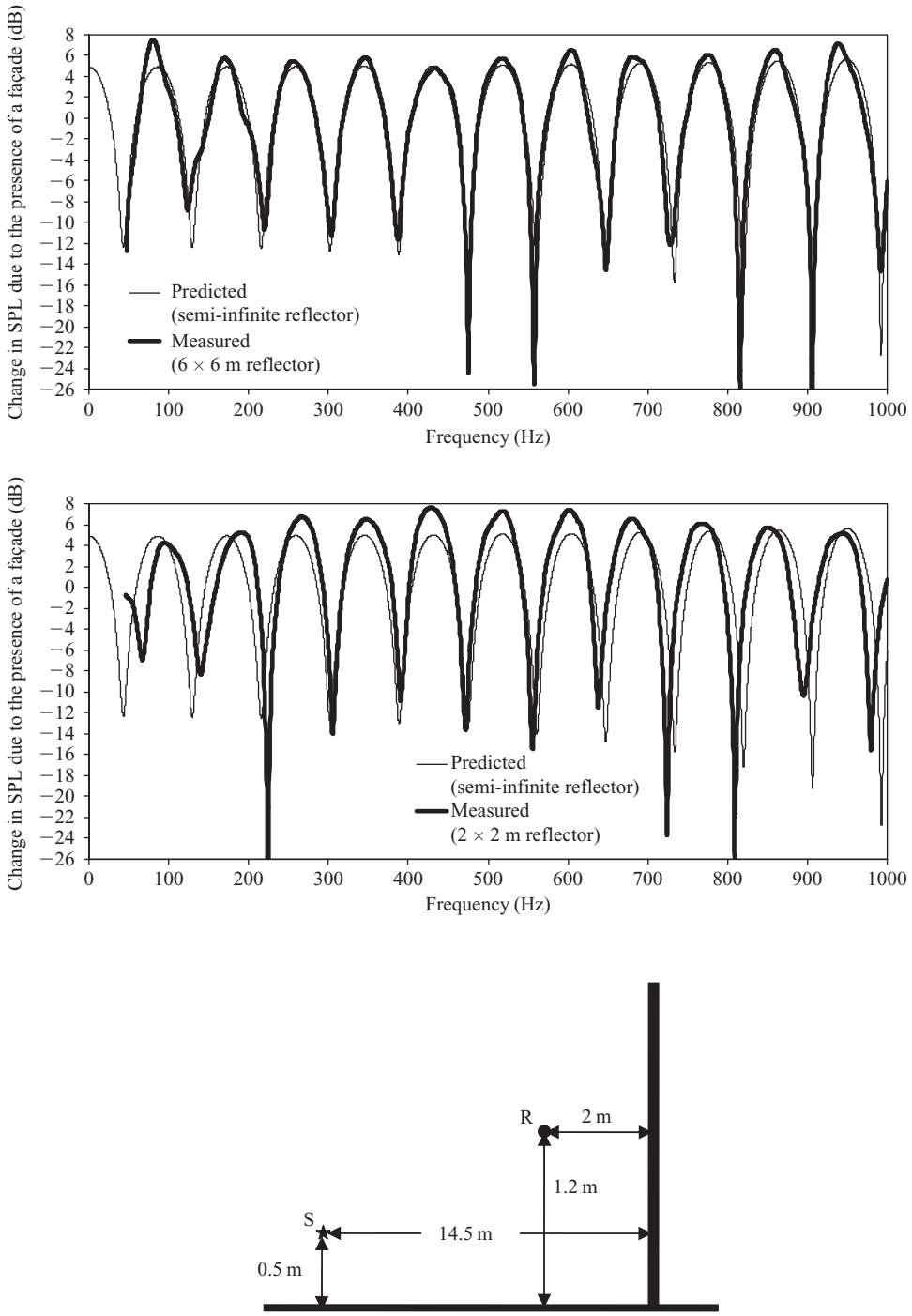

Figure 1.61

Comparison of measured and predicted data for the change in the sound pressure level due to the presence of the façade. Source–receiver–façade geometry is indicated in the sketch. Measured data reproduced with permission from Hopkins and Lam (2008).

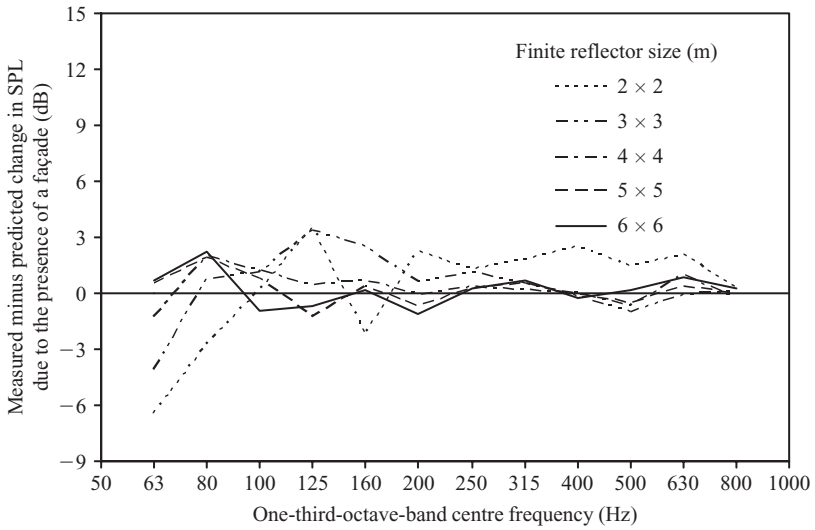

Figure 1.62

Difference between the measured (finite reflector) and predicted (semi-infinite reflector) change in level due to the presence of the façade. Façade–receiver distance of 2 m. Measured data are reproduced with permission from Hopkins and Lam (2008).

For protruding or recessed building elements, the spatial variation over the surface can be affected by a combination of diffraction, shielding, and, within a recess, the existence of a sound field that partly resembles a two-dimensional reverberant field (sometimes referred to as a niche effect). It is quite common for windows to be installed in a recess. Figure 1.64 shows the effect of measuring the surface sound pressure level within a 200 mm deep frame (1 × 1 m) attached to the surface of a masonry façade (Quirt, 1985). A single measurement within the frame is seen to be unrepresentative of the average from eight positions. Measurements on a 1.2 × 1.2 m window with recess depths of 120 and 320 mm indicate that the spatial variation over the surface of a window is larger with a deeper recess (Jonasson and Carlsson, 1986). To get a more accurate estimate of the average surface sound pressure level, more microphone positions may be needed with deep recesses (≈300 mm), than with shallower ones (≈100 mm).

1.4.2 Line sources

Façade sound insulation is often assessed using road traffic noise, which can be represented by a line source. The details of a model for a line source are not discussed here, but the basic principle involves approximating a line source by a line of closely spaced incoherent point sources. For a line source comprising many incoherent point sources, air absorption starts to become significant towards the ends of the line source and therefore needs to be included in the model (ISO 9613 Part 1). An overview of a suitable spherical wave propagation model for each point source which incorporates the ground impedance can be found from Attenborough (1988).

To gain a practical insight into the sound field near façades with a line source it is more useful to look at the statistics of measured data. Hall *et al*. (1984) took measurements at houses on 33 different sites with road traffic as the sound source to assess the level measured at a distance of 2 m from the façade using a microphone on the façade surface (one position

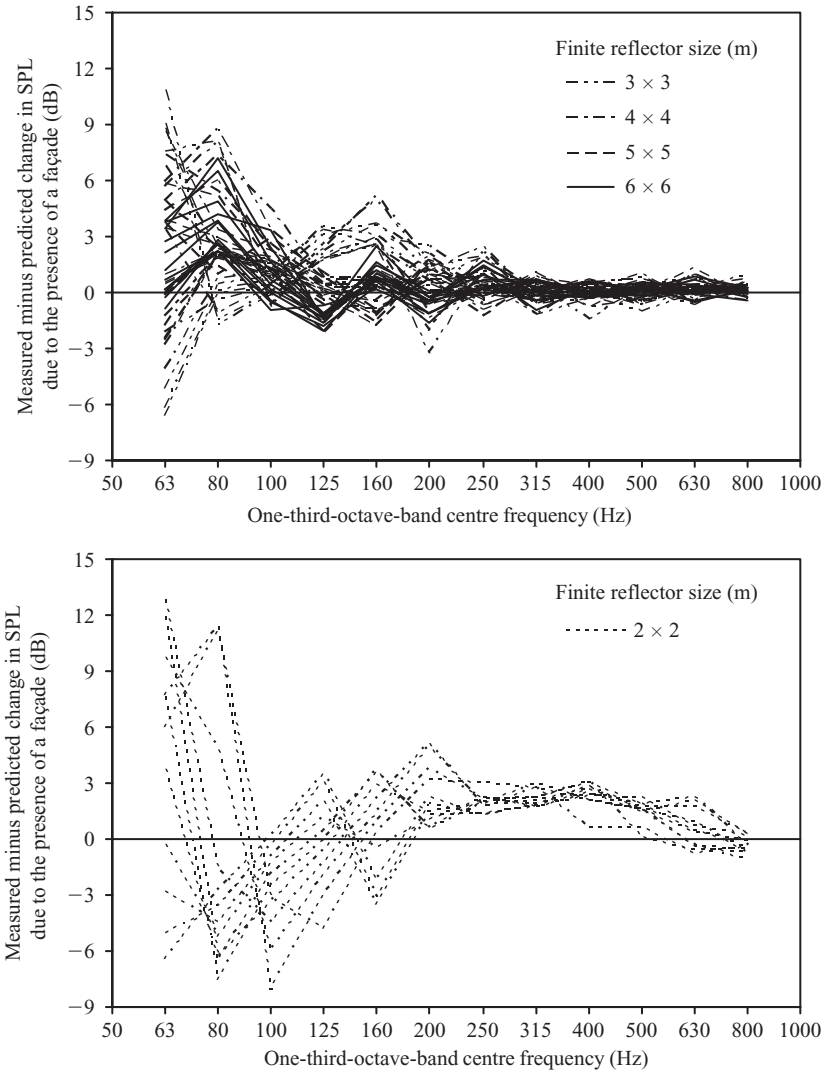

Figure 1.63

Difference between the measured (finite reflector) and predicted (semi-infinite reflector) change in level due to the presence of the façade. For each reflector size the 11 curves correspond to façade–receiver distance in 0.1 m steps from 1 to 2 m inclusive. Measured data are reproduced with permission from Hopkins and Lam (2008).

only). The microphone height above ground level was unspecified although it was the same for both the surface and the 2 m measurement. The results are shown in Fig. 1.65. By assuming pressure doubling (6 dB) for the façade microphone, the assumption of energy doubling (3 dB) for the microphone that is 2 m from the façade can be assessed by comparing the difference between these two microphone positions with a value of 3 dB. In the low-frequency range the assumption of energy doubling is invalid due to large fluctuations caused by the interference pattern. In the mid- and high-frequency ranges the assumption of energy doubling is reasonable when we consider the mean of many measurements; however, from the minimum and maximum values in Fig. 1.65 we see that this assumption is not always valid for an individual

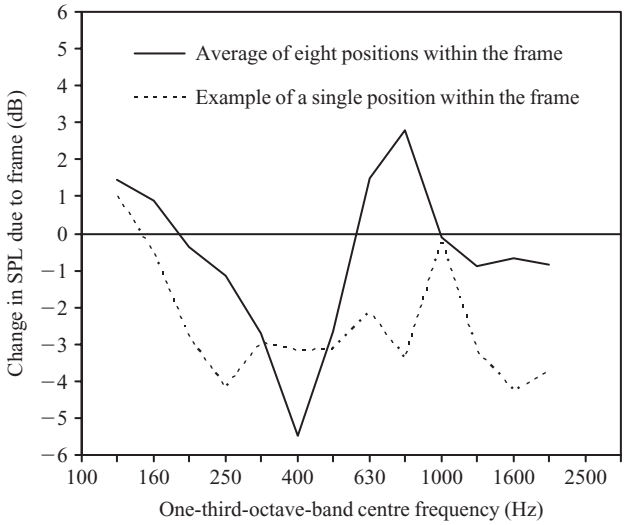

Figure 1.64

Change in the surface sound pressure level on a wall due to the addition of a 200 mm deep frame (1 × 1 m). The loudspeaker was placed on the ground at a distance of 25 m from the mid-point of the frame, with sound incident upon the surface at an angle of 60°. NB: The angle prescribed for façade insulation measurements with a loudspeaker in ISO 140 Part 5 is 45° ± 5° rather than 60°. Measured data are reproduced with permission from Quirt (1985) and the National Research Council of Canada.

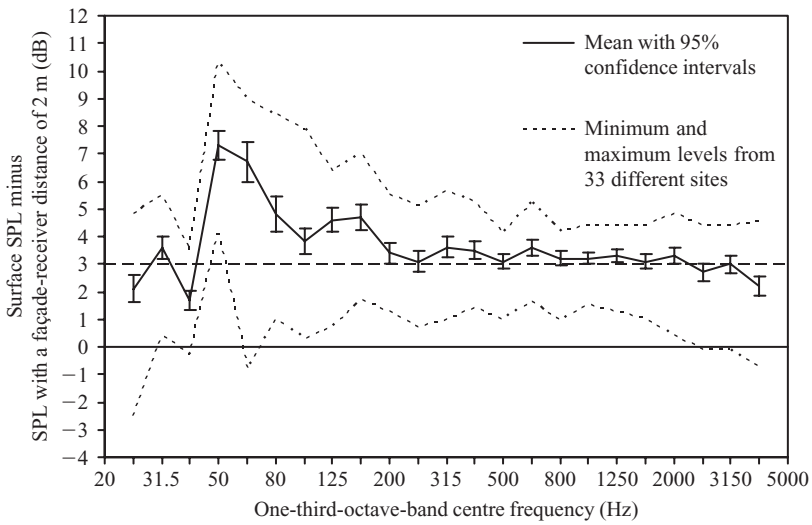

Figure 1.65

Sound pressure levels measured at houses on 33 different sites to assess the level that is measured 2 m from the façade with road traffic as the sound source. Measurements were made with a microphone on the façade surface, and at a distance of 2 m from the façade. Measured data are reproduced with permission from Hall *et al.* (1984).

measurement. This presents a problem if we need to accurately convert individual measurements in frequency bands from the 2 m microphone position to a different microphone position near the façade. This will rarely be possible due to the uncertainty in the many factors that affect the sound propagation paths. Usually we can only make reasonable estimates when we want to convert the mean value of many measurements for either frequency bands, or an A-weighted level.

References

Allard, J.F. (1993). *Propagation of sound in porous media: modelling sound absorbing materials*, Elsevier Science Publishers Ltd, London and New York. ISBN: 185166887X.

Allard, J.F. and Champoux, Y. (1992). New empirical equations for sound propagation in rigid frame fibrous materials, *Journal of the Acoustical Society of America*, **91** (6), 3346–3353.

Arau-Puchades, H. (1988). An improved reverberation formula, *Acustica*, **65**, 163–180.

Attenborough, K. (1988). Review of ground effects on outdoor sound propagation from continuous broadband sources, *Applied Acoustics*, **24**, 289–319.

Barron, M. (1973). Growth and decay of sound intensity in rooms according to some formulae of geometric acoustics theory, *Journal of Sound and Vibration*, **27** (2), 183–196.

Beranek, L.L. (1947). Acoustical properties of homogeneous, isotropic rigid tiles and flexible blankets, *Journal of the Acoustical Society of America*, **19** (4), 556–568.

Bies, D.A. (1988). Acoustical properties of porous materials. In Beranek, L.L (ed.), *Noise and vibration control*, Washington, DC. Institute of Noise Control Engineering, 245–269. ISBN: 0962207209.

Bies, D.A. and Hansen, C.H. (1980). Flow resistance information for acoustical design, *Applied Acoustics*, **13**, 357–391.

Biot, M.A. (1956). Theory of propagation of elastic waves in a fluid-saturated porous solid. I. Low-frequency range. II. Higher frequency range, *Journal of the Acoustical Society of America*, **28** (2), 168–191.

Bodlund, K. (1976). Statistical characteristics of some standard reverberant sound field measurements, *Journal of Sound and Vibration*, **45** (4), 539–557.

Bodlund, K. (1980). Monotonic curvature of low frequency decay records in reverberation chambers, *Journal of Sound and Vibration*, **73** (1), 19–29.

Craik, R.J.M. (1990). On the accuracy of sound pressure level measurements in rooms, *Applied Acoustics*, **29**, 25–33.

Delany, M.E. and Bazley, E.N. (1969). Acoustical characteristics of fibrous absorbent materials. *NPL AERO Report Ac37 March 1969*, National Physical Laboratory, UK.

Delany, M.E. and Bazley, E.N. (1970). Acoustical properties of fibrous absorbent materials, *Applied Acoustics*, **3**, 105–116.

Delany, M.E., Rennie, A.J. and Collins, K.M. (1974). Model evaluation of the noise shielding of aircraft ground-running pens. *NPL Report Ac67 April 1974*, National Physical Laboratory, UK.

Eyring, C.F. (1930). Reverberation time in dead rooms, *Journal of the Acoustical Society of America*, **1**, 217–241.

Fahy, F. (2001). *Foundations of engineering acoustics*, Elsevier Ltd, Oxford. ISBN: 0122476654.

Fitzroy, D. (1959). Reverberation formulae which seems to be more accurate with non-uniform distribution of absorption, *Journal of the Acoustical Society of America*, **31**, 893–897.

Hall, F.L., Papakyriakou, M.J. and Quirt, J.D. (1984). Comparison of outdoor microphone locations for measuring sound insulation of building façades, *Journal of Sound and Vibration*, **92** (4), 559–567.

Hodgson, M. (1993). Experimental evaluation of the accuracy of the Sabine and Eyring theories in the case of non-low surface absorption, *Journal of the Acoustical Society of America*, **94** (2), 835–840.

Hodgson, M. (1996). When is diffuse-field theory applicable?, *Applied Acoustics*, **49** (3), 197–207.

Hopkins, C. and Turner, P. (2005). Field measurement of airborne sound insulation between rooms with non-diffuse sound fields at low frequencies, *Applied Acoustics*, **66** (12), 1339–1382.

Hopkins, C. and Lam, Y. (2008). Sound fields near building façades – comparision of finite and semi-infinite reflectors on a rigid ground plane, *Applied Acoustics*. (Submitted)

Ismail, M.R. and Oldham, D.J. (2005). A scale model investigation of sound reflection from building façades, *Applied Acoustics*, **66**, 123–147.

Jacobsen, F. (1982). Decay rates and wall absorption at low frequencies, *Journal of Sound and Vibration*, **81** (3), 405–412.

Jonasson, H. and Carlsson, C. (1986). Measurement of sound insulation of windows in the field. *Nordtest Project 556–85*, *Technical Report SP-RAPP 1986:37*, Swedish National Testing Institute SP.
Kang, J. (2002). *Acoustics of long spaces: Theory and design practice*, Thomas Telford, London. ISBN: 0727730134.
Kosten, C.W. (1960). The mean free path in room acoustics, *Acustica*, **10**, 245–250.
Kuttruff, H. (1979). *Room acoustics*, Second Edition, Applied Science Publishers Ltd, Barking, England. ISBN: 0853348138.
Larsen, H. (1978). *Technical review No.4: Reverberation at low frequencies*, Bruel & Kjaer. (Refer to the paper by Bodlund (1980) for corrections.)
Lubman, D. (1968). Fluctuations of sound with position in a reverberant room, *Journal of the Acoustical Society of America*, **44**, 1491–1502.
Lubman, D. (1974). Precision of reverberant sound power measurements, *Journal of the Acoustical Society of America*, **56** (2), 523–533.
Lyon, R.H. and DeJong, R.G. (1995). *Theory and application of statistical energy analysis*, Butterworth-Heinemann, MA, USA. ISBN: 0750691115.
Mechel, F.P. (1989/1995/1998). *Schallabsorber Band I, II and III,* S. Hirzel Verlag, Stuttgart. ISBN: 3777604259/ISBN: 3777605727/ISBN: 3777608092.
Mechel, F.P. and Vér, I.L. (1992). Sound-absorbing materials and sound absorbers. In Beranek, L.L. and Vér, I.L. (eds.), *Noise and vibration control engineering: principles and applications*, John Wiley & Sons, 203–243. ISBN: 0471617512.
Mechel, F.P. (1995). Absorberparameter, *Schallabsorber Band II: Innere Schallfelder*, *Strukturen*, *Kennwerte*, S. Hirzel, Verlag, Stuttgart, 103–123. ISBN: 3777605727.
Michelsen, N. (1982). Repeatability of sound insulation measurements. *Technical Report No. 36*, Danish Acoustical Laboratory (now DELTA Acoustics), Denmark.
Morse, P.M. and Ingard, K.U. (1968). *Theoretical acoustics*, McGraw-Hill, New York. ISBN: 0691084254.
Munro, T.J. (1982). Alternative models of the sound field in a reverberation room, M.Eng thesis, Department of Mechanical Engineering, University of Adelaide, Adelaide, South Australia.
Narang, P.P. (1995). Material parameter selection in polyester fibre insulation for sound transmission and absorption, *Applied Acoustics*, **45**, 335–358.
Neubauer, R.O. (2001). Estimation of reverberation time in rectangular rooms with non-uniformly distributed absorption using a modified Fitzroy equation, *Building Acoustics*, **8** (2), 115–137.
Nichols, R.H. (1947). Flow-resistance characteristics of fibrous acoustical materials, *Journal of the Acoustical Society of America*, **19** (5), 866–871.
Nilsson, E. (2004). Decay processes in rooms with non-diffuse sound fields. Part I: Ceiling treatment with absorbing material, *Building Acoustics*, **11** (1), 39–60.
Ogren, M. and Jonasson, H. (1998). Measurement of the acoustic impedance of ground. *SP Report 1998:28*, *Swedish National Testing and Research Institute SP.*
Olesen, H.S. (1992). Measurements of the acoustical properties of buildings – additional guidelines. Nordtest Technical Report No. 203 (www.nordtest.org). ISSN: 0283–7234.
Pan, J. and Bies, D.A. (1988). An experimental investigation into the interaction between a sound field and its boundaries, *Journal of the Acoustical Society of America*, **83** (4), 1436–1444.
Pan, J. and Bies, D.A. (1990). The effect of fluid-structural coupling on sound waves in an enclosure – Theoretical part, *Journal of the Acoustical Society of America*, **87** (2), 691–707.
Pan, J. and Bies, D.A. (1990). The effect of fluid-structural coupling on sound waves in an enclosure – Experimental part, *Journal of the Acoustical Society of America*, **87** (2), 708–717.
Price, A.J. and Crocker, M.J. (1970). Sound transmission through double panels using statistical energy analysis, *Journal of the Acoustical Society of America*, **47** (3), 683–693.
Quirt, J.D. (1985). Sound fields near exterior building surfaces, *Journal of the Acoustical Society of America*, **77** (2), 557–566.
Redmore, T.L. (1982). A method to predict the transmission of sound through corridors, *Applied Acoustics*, **15**, 133–146.
Redmore, T.L. and Flockton, S.J. (1977). A design formula for predicting the attenuation of sound along a corridor, *Acoustic Letters*, **1**, 21–24.
Sabine, C. (1932) *Collected papers on acoustics*, (1964 Edition) Dover Publications, New York.
Schroeder, M.R. (1962). Frequency-correlation functions of frequency responses in rooms, *Journal of the Acoustical Society of America*, **34** (12), 1819–1823.

Schroeder, M.R. (1969). Effect of frequency and space averaging on the transmission responses of multimode media, *Journal of the Acoustical Society of America*, **46** (1), (2), 277–283.

Simmons, C. (1996). Measurement of low frequency sound in rooms. *SP Report 1996:10*, Swedish National Testing and Research Institute SP.

Vian, J.P., Danner, W.F. and Bauer, J.W. (1983). Assessment of significant acoustical parameters for rating sound insulation of party walls, *Journal of the Acoustical Society of America*, **73** (4), 1236–1243.

Vorländer, M. (1995). Revised relation between the sound power and the average sound pressure level in rooms and consequences for acoustic measurements, *Acustica*, **81**, 332–343.

Waterhouse, R.V. (1955). Interference patterns in reverberant sound fields, *Journal of the Acoustical Society of America*, **27** (2), 247–258.

Waterhouse, R.V. (1968). Statistical properties of reverberant sound fields, *Journal of the Acoustical Society of America*, **43**, 1436–1444.